放送大学審査学位論文（博士）

Landau Level Spectroscopy by Optical Angular Momentum

by

Hirohisa Takahashi

to

The Graduate School of Arts and Sciences

The Open University of Japan

in partial fulfillment of the requirements

for the degree of

Doctor of Philosophy

in the subject of

Arts and Sciences

March, 2020

Contents

Abstract

The optical vortex beam carries the orbital angular momentum ℓ in addition to the spin angular momentum σ. We propose that the existence of finite ℓ is demonstrated through modified selection rules for absorption processes of the optical vortex by the Landau-quantized two-dimensional electron gas. We show that the lowest LL electrons absorb the optical vortex beams with $\sigma = 1$ (positive helicity) and $\ell = 0$ or $\sigma = -1$ (negative helicity) and $\ell = 2$. This means that the intrinsic spin (helicity) and the orbital angular momentum of the optical vortex are tied to each other in the absorption processes. It is also shown that the electric currents induced by the optical vortex are distributed along the edge of the sample due to cancellation of the bulk currents. Reflecting the spatial profile of the optical vortex beam, the induced current disappears when the dark rings of the beam coincide with the circular edge. This scheme may provide a helicity-dependent absorption using the optical vortex beam.

Thus, the magnetization can be induced by only the edge current. It is shown that the induced orbital magnetization also disappears when the dark ring of the beam coincides with the disk edge.

Acknowledgments

I would like to express my appreciation to Professor Jun-ichiro Kishine, my supervisor, for providing great advice and patient guidance, and constant support in my dissertation study. His expertise in a broad range of condensed matter physics helps me solve problems and eventually bring the study to a positive conclusion. His passion and honesty for science was a constant source of my enthusiasm. I have had this great experience and pleasure to work in his group which provides inspirational discussions and great opportunities for me to improve my academic experience. He is also a kind and generous person who is willing to teach and share his knowledge and experience.

I would also like to give my very special thanks to Dr. Igor Proskurin. He is a great person to work with and to learn from. I was helped by the enlightening discussions with him.

Great thanks to my dissertation committees Professors Katsuya Ishizaki, Yoshiaki Hada, Masahiro Sato for making time to be in my committees and discuss to make this research accurate, Professors Kenichi Oto, Yasuhiro Yamada, Dr. Shun Hashiyada, Dr. Yuya Sawada for valuable discussion to give me experimental knowledge. I am grateful to Professors Tomokazu Yasuike, Tetsuo Matsui, Katsuya Inoue, Yoshihiko Togawa, Eiko Torikai, Jun Akimitsu, Dr. Hiroyasu Matsuura, and Dr. Yusuke Kousaka for valuable discussion and encouraging me in many moments. In addition, I am grateful for the friendly help and support of faculty and staff members in Department of Arts and Sciences of The Open University of Japan.

Finally, I want to thank my parents, Ryoichi Tsujimoto and Kazuko Tsujimoto for depthless love and support, my beloved dogs, Chum and A-nan for encouraging me via their comfort, and my wife Kaoru for her limitless love, care and support. In particular, my father, Ryoichi, passed away during preparing this dissertation. I would like to dedicate this dissertation to my father.

Chapter 1

Introduction

Originally, it was suggested by Poynting that circularly polarized light carries spin angular momentum (SAM) equal to $\pm\hbar$ per photon, which can be transferred to medium and produce a mechanical torque in light-matter interactions[1]. Later, Beth experimentally confirmed that the angular momentum transfers from a light in 1935[2, 3]. After about a century, it was suggested that lights can also carry an orbital angular momentum (OAM) in addition to SAM by Allen *et al.*[4]. This part of angular momentum appears as a modulation of a phase front, so it was dubbed an optical vortex (OV) or twisted light. It was experimentally demonstrated that a single photon is able to carry quantized OAM[5]. Theoretical and experimental techniques were developed to generate OVs in various forms such as the Laguerre-Gaussian (LG) and the Bessel light beams[4, 6, 7, 8]. These unique forms of light beams have triggered much interest on the transfer of optical OAM to material particles and atoms via light-matter interactions[9, 10].

Mathematically, OV is described by a constant phase profile given by $\exp(i\ell\phi + ikz)$, where ϕ is the azimuthal angle in the cylindrical coordinate system for a light beam propagating in the z direction with the wavenumber k. It carries an intrinsic OAM equal to $\ell\hbar$ per photon ($\ell = 0, \pm1, \pm2, \ldots$), which is independent of the polarization state of light[4]. Geometrically the phase front of OV is a helix with the winding number determined by ℓ. The radial dependence of the beam amplitude is typically given in terms of either Laguerre-Gaussian or Bessel modes. The former has the property of gradually expanding as the beam propagates, while the latter is diffraction free, or propagation invariant[6, 11]. Experimentally, the zero-order Bessel beams ($\ell = 0$) can be created in the back focal plane of a convergent lens by a plane wave[11], by an axicon lens from a Gaussian beam[12], by the use of computer-generated holograms[13], or by a Fabry-Perot resonator[14]. The higher-order Bessel beam ($\ell > 0$) can also created by using axicon-type

computer-generated holograms[15], in back of an axicon lens illuminated with a Laguerre-Gaussian beam[16, 17], or by passing an input zero-order Bessel beam through biaxial crystals[18].

From the point of view of classical mechanics, exerting a torque by transferring angular momentum from OV has been actively studied, for example, with particles rotating in an optical tweezers[19, 20, 21, 22], and the laser ablation technique[23]. In recent years, couplings of the OV beam with condensed matter also saw a considerable development, including such topics as the generation of atomic vortex states by coherent transfer of OAM from photons to the Bose-Einstein condensate[24], photocurrents excited by the OV beam-absorption in semiconductors and graphene[25, 26, 27], excitation of multipole plasmons in metal nanodisks[28], spin and charge transport on a surface of topological insulator[29], and the generation of skyrmionic defects in chiral magnets[30] among other things.

However, whether OAM affects any spectroscopic selection rules via optically induced electronic transitions is still an open question. In 2002, Babiker *et al.* stated that an exchange of the optical orbital angular momentum does not occur in an electric dipole transition in atoms and molecules[31, 32]. Their statement has been considered an interaction of two-particle system with an optical vortex as

$$H_{\text{int}} = -\int d^3\mathbf{r}\ \mathbf{P}\left(\mathbf{r}\right) \cdot \mathbf{E}_{k\ell}, \tag{1.1}$$

where $\mathbf{P}\left(\mathbf{r}\right)$ is an electric polarization and an electric field of OV in the cylindrical coordinates $(r_\perp, \phi, z)$ is $\mathbf{E}_{k\ell} = \boldsymbol{\varepsilon} F\left(r_\perp\right) \mathrm{e}^{i\ell\phi} \mathrm{e}^{ik_z z - i\omega t}$. When the center of mass cylindrical coordinate $\mathbf{R} = (R_\perp, \Phi_R, R_z)$ and relative cylindrical coordinate $\mathbf{q} = \left(q_\perp, \phi_q, q_z\right)$ are defined, it is shown that the interaction Hamiltonian in a dipole approximation reduces to

$$H_{\text{int}}^{\text{dipole}} = e\boldsymbol{\varepsilon} \cdot \mathbf{q} F\left(R_\perp\right) \mathrm{e}^{i\ell\Phi_R} \mathrm{e}^{ik_z R_z - i\omega t}. \tag{1.2}$$

The important point is that the interaction Hamiltonian in the dipole approximation $H_{\text{int}}^{\text{dipole}}$ is independent of the relative coordinate. Concerning the transition via this Hamiltonian, this signifies that the optical orbital angular momentum can be transferred only to the center-of-mass motion of the atoms but not to the relative motion or the internal motion of atoms.

In fact, it is known that, although transferring of the OAM to atomic electrons from the OV beam via the electric quadrupole transition was reported[33, 34, 35], the electric dipole transition has not been reported. Similar in the coupling of OV with the exciton, the optical OAM can be transferred only to the exciton center-of-mass motion[36]. These phenomena are analogous to

the fact that the cyclotron resonance frequency is independent of short-range electron-electron interactions[37]. Thus the electric dipole selection rules in OV-absorption remain unchanged.

Therefore, it naively seems that a free electron is a good candidate of OV absorption. However, it is shown that a photon cannot be absorbed by a free electron because the linear momentum conservation condition contradicts the energy conservation condition[38]. This can be shown as follows. In the absorption process, the linear momentum conservation and energy one are written as

$$p_i - p_f + p = 0, \tag{1.3}$$

and

$$E_f - E_i - cp = 0, \tag{1.4}$$

where p_i and $E_i = p_i^2/2m_e$ are the initial momentum and energy of the electron, p_f and $E_f = p_f^2/2m_e$ are its final momentum and energy, and p and cp are the linear momentum and energy of the absorbed photon. Since we have $p_i = 0$ and $E_i = 0$ in the rest frame of the initial electron, (1.3) and (1.4) give $p_f = p$ and $E_f = cp$, respectively. Plugging these into $E_f = p_f^2/2m_e$, we obtain $p_f^2/2m_e = cp_f$ or $p_f = 2m_e c$. This suggests that the speed of the photon would be zero, $c = 0$, or that the final velocity of the electron $v_f = 2c$. Of course, these are impossible. Thus, it is shown that a free electron cannot absorb a photon.

To avoid these two bottlenecks, so far as concerning OV absorption processes in an electronic dipole transition, a bounded electron must be considered. In this case, it is interesting to see whether these concepts are applicable to a degenerated two-dimensional electron gas (2DEG) in magnetic field. To our best knowledge, such a system has not been considered. In this dissertation, we will discuss the optical conductivity and the selection rules in 2DEG irradiated with OV carrying OAM. By applying the magnetic field, 2DEG is characterized by discrete energy levels with localized semi-classical electron orbits. It is demonstrated that the bulk current induced by OV disappears, and only the edge current survives when the 2DEG is irradiated with a Bessel beam[39]. This situation is similar to the picture of orbital magnetization[40], which is known to appear due to the existence of the edge currents. Therefore, in 2DEG we can anticipate an orbital Edelstein effect[41] where additional magnetization is induced by the OV, which is one of the central issues of this dissertation.

This dissertation is organized as follows. We will briefly review the derivation of the vector potential of circularly polarized Bessel-mode optical vortex

beams and demonstrate the physical properties of vortex beams in Chapter 2. Also, the optical vortex under the paraxial approximation is studied there.

In Chapter 3, we devote the review of electron in two dimension system under the magnetic field. In particular, we construct the wavefunction and eigenenergy in symmetric gauge. In addition, the coherent states in symmetric gauge is introduced to show the disappearing the bulk current.

Chapter 4 is a central thesis of this dissertation. First, we investigate the induced photocurrent and the selection rules by irradiation of circularly polarized Bessel-mode optical vortex. Then it is shown that the selection rule by optical orbital angular momentum is modified. After that, we give the result of the magnetic field dependence of the induced photocurrent. We also mention that the magnetization by irradiation of optical vortex.

We devote Chapter 5 to propose the experimental scheme for consequence of our theory. We will first overview the generation of light beam carrying orbital angular momentum. Then, we discuss the influence of a electron spin and a disorder in samples to the experiments to measure our consequence. After that, the concept of experimental setup for the measurement will be described.

We recapitulate the major conclusion of this dissertation in Chapter 6.

Chapter 2

Optical Vortex

2.1 Circularly Polarized Bessel-mode Optical Vortex

In 1992, Allen *et al.* showed that the light beams with an azimuthal phase term $\exp(i\ell\phi)$ carries an angular momentum independent of the polarization state[4]. ℓ is a topological charge which can be taken an integer value. Such light beams are called optical vortex (OV) beams. The orbital angular momentum carried by OV has a value $L_z = \ell\hbar$ per photon. When the topological charge ℓ is given, the wavefronts of the beams form ℓ intertwined helical wavefronts as shown in Fig. 2.1. The sign of orbital angular momentum ℓ corresponds to the handedness of helical wavefronts with respect to the beam propagation direction. The optical vortex beam has a remarkable feature that the helical wavefronts produce the phase singularity on the beam axis, that is, zero intensity on the axis. Then, the radial profile of OV beam forms an annular distribution. The several radial modes having such features of OV beams are known: e.g. a Laguerre-Gaussian (LG) mode[4] and Bessel one[6] among other things.

One of the major phenomena in optics is a diffraction. The diffraction is a phenomenon that, when a wave encounters the obstacle, the parts of the wavefront usually interfere in some manner and occur a diffraction pattern. For a Gaussian light beams, the output laser has a very low divergence but the diffraction causes the light to spread. It is important to manipulate the Gaussian beam to produce a tight focusing beam or collimated one. However, as one of the features of Bessel mode beams, it is known that the Bessel beams can overcome the diffraction, that is, they are non-diffracting beams or propagation-invariant beams[11]. Therefore, the Bessel beams are manageable tools which can be used without an accurately focusing.

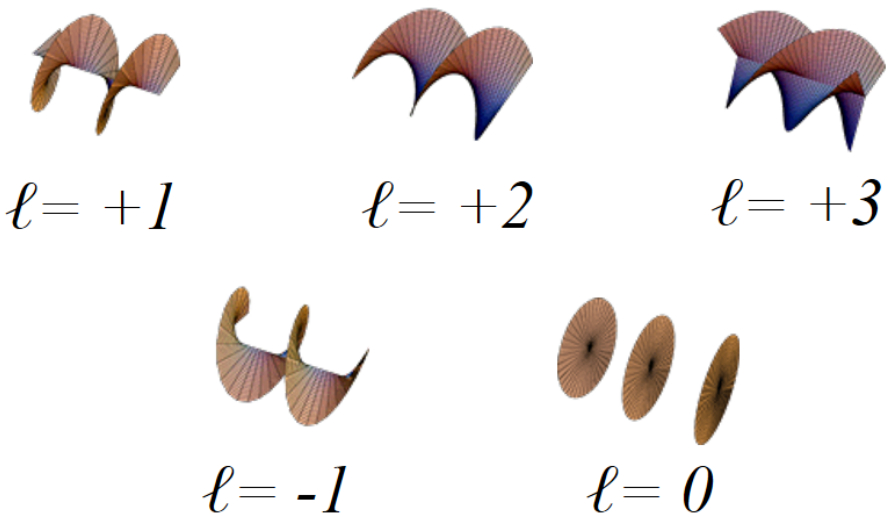

Figure 2.1: Illustrations of wavefronts of ℓ-th order helical beams. The number of ℓ corresponds to the number of the spiral arms. The sign of ℓ indicates the handedness of wavefronts with respect to the beam direction.

Another feature of Bessel beams is that they can naturally be generalized to non-paraxial one because they are exact solutions of a Helmholtz equation, whereas Gaussian beams including LG-mode ones are essentially paraxial beam (As we mention in Appendix G, Gaussian beams are derived from a Helmholtz equation after applying a paraxial approximation $k \gg k_\perp$ with the total wavenumber k and transverse wavenumber $k_\perp$). A paraxial approximation is crucial for studying quantum mechanical properties of light to separate a total angular momentum (TAM) into the spin and orbital parts, since they can be conserved separately for light interacting with particles. In the paraxial approximation, this separation can be done explicitly, and the light beam has a well-defined spin angular momentum (SAM) related to its polarization state and OAM determined by the phase modulation. Therefore, the Bessel beam is expected naturally to generalize a theory built in the paraxial region to the theory under the non-paraxial region[42, 43].

In consideration of such features, in this dissertation, we adopt the Bessel mode vortex beam in the paraxial approximation. In this Chapter, as preparation to discuss the coupling of the Bessel beam with an electron, we review the derivation and properties of the circularly polarized Bessel mode optical vortex beam.

2.1.1 The Helmholtz Equation

We first derive a Helmholtz equation, which represents a time-independent the wave equation, from Maxwell equations. Maxwell equations in vacuum ($\epsilon = \epsilon_0, \mu = \mu_0, \rho(\mathbf{r}, t) = 0, \mathbf{j}(\mathbf{r}, t) = 0$) in SI units are given by

$$\boldsymbol{\nabla} \cdot \mathbf{E}(\mathbf{r}, t) = 0, \tag{2.1}$$

$$\boldsymbol{\nabla} \cdot \mathbf{B}(\mathbf{r}, t) = 0, \tag{2.2}$$

$$\boldsymbol{\nabla} \times \mathbf{E}(\mathbf{r}, t) = -\frac{\partial \mathbf{B}(\mathbf{r}, t)}{\partial t}, \tag{2.3}$$

$$\boldsymbol{\nabla} \times \mathbf{B}(\mathbf{r}, t) = \frac{1}{c^2}\frac{\partial \mathbf{E}(\mathbf{r}, t)}{\partial t}, \tag{2.4}$$

where the first equation is Gauss law for electricity, the second is Gauss law for magnetism, the third is Faraday's law of electromagnetic induction, and the last one is Ampere-Maxwell law. Plugging the magnetic and electric fields described by the vector potential in Coulomb gauge ($\phi(\mathbf{r}, t) = 0$, $\boldsymbol{\nabla} \cdot \mathbf{A}(\mathbf{r}, t) = 0$),

$$\mathbf{B}(\mathbf{r}, t) = \boldsymbol{\nabla} \times \mathbf{A}(\mathbf{r}, t), \tag{2.5}$$

$$\mathbf{E}(\mathbf{r}, t) = -\frac{\partial \mathbf{A}(\mathbf{r}, t)}{\partial t}, \tag{2.6}$$

into Ampere-Maxwell law, we obtain the wave equation for the vector potential,

$$\boldsymbol{\nabla} \times [\boldsymbol{\nabla} \times \mathbf{A}(\mathbf{r}, t)] = -\frac{1}{c^2}\frac{\partial^2 \mathbf{A}(\mathbf{r}, t)}{\partial t^2},$$

$$\Delta \mathbf{A}(\mathbf{r}, t) = \frac{1}{c^2}\frac{\partial^2 \mathbf{A}(\mathbf{r}, t)}{\partial t^2}, \tag{2.7}$$

where Δ is the Laplace operator and c is the speed of light in a vacuum. If we assume the monochromatic state of light with the frequency ω, $\mathbf{A}(\mathbf{r}, t) = \mathbf{A}(\mathbf{r})\, \mathrm{e}^{-i\omega t}$, it leads to the Helmholtz equation:

$$\Delta \mathbf{A}(\mathbf{r}) + k^2 \mathbf{A}(\mathbf{r}) = 0 \tag{2.8}$$

with the square of the wavenumber of light, $k^2 = \omega^2/c^2$.

In order to obtain twisted solutions, we have to take account of two additional requirements. The first is that $\mathbf{A}(\mathbf{r})$ is a propagating wave along z-axis, so it is the eigenvector of the linear momentum operator $p_z = -i\hbar\nabla_z$, and $\hat{p}_z \mathbf{A}(\mathbf{r}) = \hbar k_z \mathbf{A}(\mathbf{r})$. The second is that $\mathbf{A}(\mathbf{r})$ should also be the eigenvector of z-component of the TAM operator

$$\hat{J}_z \mathbf{A}(\mathbf{r}) = J \mathbf{A}(\mathbf{r}), \tag{2.9}$$

where the operator $\hat{J}_z = \hat{L}_z + \hat{S}_z$ is given by the corresponding components of the orbital and spin angular momentum operators:

$$\hat{L}_z = -i\hbar\frac{\partial}{\partial\phi}, \quad \hat{S}_z = -i\hbar \begin{pmatrix} 0 & 1 & 0 \\ -1 & 0 & 0 \\ 0 & 0 & 0 \end{pmatrix}. \tag{2.10}$$

2.1.2 Scalar Solutions of the Helmholtz Equation

At first, we construct the scalar solutions of the Helmholtz equation which are eigenfunctions of $\hat{p}_z$ and $\hat{L}_z$ with periodic boundary conditions. We note that the Laplace operator in cylindrical coordinates is written by

$$\Delta f = \frac{1}{r_\perp}\frac{\partial}{\partial r_\perp}\left(r_\perp\frac{\partial f}{\partial r_\perp}\right) + \frac{1}{r_\perp^2}\frac{\partial^2 f}{\partial\phi^2} + \frac{\partial^2 f}{\partial z^2} \tag{2.11}$$

and assume the scalar function,

$$\psi(\mathbf{r}) = \psi(r_\perp)\,\mathrm{e}^{i\ell\phi}\mathrm{e}^{ik_z z}, \tag{2.12}$$

where ℓ is an integer and $r_\perp$ is transverse to the propagation direction z. By plugging the scalar function (2.12) into the Helmholtz equation (2.8), the radial part of (2.12), $\psi(r_\perp)$, satisfies the equation

$$\frac{1}{r_\perp}\frac{\partial}{\partial r_\perp}\left(r_\perp\frac{\partial\psi(r_\perp)}{\partial r_\perp}\right) - \frac{\ell^2}{r_\perp^2}\psi(r_\perp) + \left(k^2 - k_z^2\right)\psi(r_\perp) = 0. \tag{2.13}$$

Introducing a transverse linear momentum $k_\perp = |\mathbf{k}_\perp| = \sqrt{k^2 - k_z^2}$ as shown in Fig. 2.2, we then obtain the Bessel equation for $\psi(r_\perp)$

$$\frac{\partial^2\psi(r_\perp)}{\partial r_\perp^2} + \frac{1}{r_\perp}\frac{\partial\psi(r_\perp)}{\partial r_\perp} + \left(k_\perp^2 - \frac{\ell^2}{r_\perp^2}\right)\psi(r_\perp) = 0 \tag{2.14}$$

with $k_\perp^2 > 0$. Therefore, we obtain the bounded solution as

$$\psi(r_\perp) = NJ_\ell(k_\perp r_\perp), \tag{2.15}$$

or

$$\psi(\mathbf{r}) = \psi(\mathbf{r}|k_\perp, k_z, \ell) = NJ_\ell(k_\perp r_\perp)\,\mathrm{e}^{i\ell\phi}\mathrm{e}^{ik_z z}, \tag{2.16}$$

where ℓ is the orbital angular momentum of light which is the eigenvalue of the orbital angular momentum operator (2.10) and $J_n(x)$ is the n-th order Bessel function of the first kind. Imposing the normalization condition,

$$\int \psi_{\ell'}^*(\mathbf{r}'|k_\perp', k_z')\,\psi_\ell(\mathbf{r}|k_\perp, k_z)\,d^3r = 2\pi\delta(k_\perp - k_\perp')\,\delta(k_z - k_z')\,\delta_{\ell,\ell'}, \tag{2.17}$$

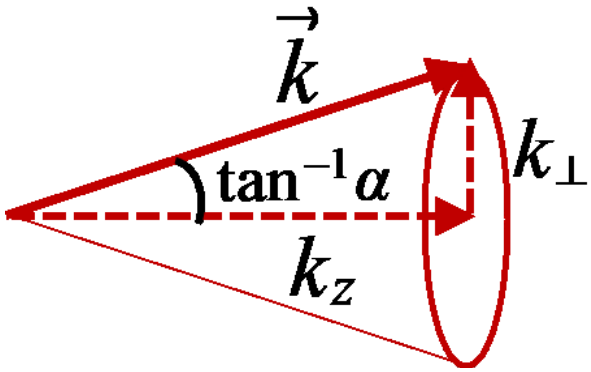

Figure 2.2: Relation between wavenumber vector $\mathbf{k}$ and the cone angle $\theta_k = \tan^{-1}\alpha$ with $\alpha = k_\perp/k_z$. k_z is the light traveling component of $\mathbf{k}$ and $k_\perp$ is its perpendicular component to k_z. The Bessel mode optical vortex can be viewed as a superposition of plane waves traveling on the cone with the cone angle θ_k.

we obtain the normalized scalar solution of the Helmholtz equation (2.8) in cylindrical coordinates $(r_\perp, \phi, z)$ can be written in the form

$$\psi_\ell\left(\mathbf{r}|k_\perp, k_z\right) = \sqrt{\frac{k_\perp}{2\pi}} J_\ell\left(k_\perp r_\perp\right) \mathrm{e}^{i\ell\phi} \mathrm{e}^{ik_z z}, \tag{2.18}$$

where we used a formula

$$\int_0^\infty z J_n\left(az\right) J_n\left(bz\right) dz = \frac{\delta\left(a-b\right)}{a}. \tag{2.19}$$

Expansion over plane waves of the scalar function $\psi_\ell\left(\mathbf{r}|k_\perp, k_z\right)$ leads to

$$\begin{aligned} \psi_\ell\left(\mathbf{r}|k_\perp, k_z\right) &= \int \frac{d^2\mathbf{k}''_\perp}{\left(2\pi\right)^2} a_{k_\perp,\ell}(\mathbf{k}''_\perp) \mathrm{e}^{i\mathbf{k}''\cdot\mathbf{r}} \\ &= \int \frac{d^2\mathbf{k}''_\perp}{\left(2\pi\right)^2} a_{k_\perp,\ell}(\mathbf{k}''_\perp) \mathrm{e}^{i\mathbf{k}''_\perp\cdot\mathbf{r}_\perp + ik''_z z} \end{aligned} \tag{2.20}$$

with $\mathbf{k}''_\perp = (k''_\perp \cos\phi_k, k''_\perp \sin\phi_k, 0)$ and $\mathbf{r}_\perp = (\cos\phi, \sin\phi, 0)$. Each plane wave component is written by

$$a_{k_\perp,\ell}(\mathbf{k}''_\perp) = \sqrt{\frac{2\pi}{k_\perp}} \left(-i\right)^\ell \mathrm{e}^{i\ell\phi_k} \delta\left(k''_\perp - k_\perp\right). \tag{2.21}$$

These expressions show that $\psi_\ell\left(\mathbf{r}|k_\perp, k_z\right)$ can be viewed as a superposition of plane waves with fixed $k = |\mathbf{k}| = \sqrt{k''^2_\perp + k_z^2}$ whose direction belongs to the cone with the cone angle $\theta_k = \tan^{-1} k''_\perp/k_z$ as shown in Fig. 2.2.

We prove this as follows. By plugging Eq. (2.21) into Eq. (2.20), we can calculate

$$\begin{aligned}\psi_\ell\left(\mathbf{r}|k_\perp,k_z\right) &= \sqrt{\frac{2\pi}{k_\perp}}\frac{(-i)^\ell\,\mathrm{e}^{ik_z z}}{(2\pi)^2}\int_0^{2\pi} d\phi_k \mathrm{e}^{i\ell\phi_k} \\ &\times \int_0^\infty dk''_\perp k''_\perp \delta\left(k''_\perp - k_\perp\right)\mathrm{e}^{ik''_\perp r_\perp\cos(\phi_k-\phi)} \\ &= \sqrt{\frac{k_\perp}{2\pi}}(-i)^\ell\frac{\mathrm{e}^{ik_z z}}{2\pi}\int_0^{2\pi} d\phi_k \mathrm{e}^{i\ell\phi_k}\mathrm{e}^{ik_\perp r_\perp\cos(\phi_k-\phi)}. \end{aligned} \tag{2.22}$$

Changing the variable as $\varphi = \phi_k - \phi$, we proceed the proof as

$$\begin{aligned}\psi_\ell\left(\mathbf{r}|k_\perp,k_z\right) &= \sqrt{\frac{k_\perp}{2\pi}}(-i)^\ell\frac{\mathrm{e}^{ik_z z}}{2\pi}\mathrm{e}^{i\ell\phi}\int_{-\phi}^{2\pi-\phi} d\varphi \mathrm{e}^{i\ell\varphi}\mathrm{e}^{ik_\perp r_\perp\cos\varphi} \\ &= \sqrt{\frac{k_\perp}{2\pi}}(-i)^\ell\frac{\mathrm{e}^{ik_z z}}{2\pi}\mathrm{e}^{i\ell\phi}\int_0^{2\pi} d\varphi \mathrm{e}^{i\ell\varphi}\mathrm{e}^{ik_\perp r_\perp\cos\varphi}. \end{aligned} \tag{2.23}$$

As the $\varphi-$integral gives a Bessel function

$$\int_0^{2\pi} d\varphi \mathrm{e}^{in\varphi}\mathrm{e}^{ia\cos\varphi} = 2\pi i^n J_n\left(a\right), \tag{2.24}$$

we can reproduce

$$\psi_\ell\left(\mathbf{r}|k_\perp,k_z\right) = \sqrt{\frac{k_\perp}{2\pi}}J_\ell\left(k_\perp r_\perp\right)\mathrm{e}^{i\ell\phi}\mathrm{e}^{ik_z z}. \tag{2.25}$$

2.1.3 Vector Solutions of the Helmholtz Equation

When the scalar solution of the Helmholtz equation is considered as a superposition of plane waves, it is important to study the polarization structure of the plane wave with the propagation vector $\mathbf{k}$. The vector potential of the plane wave has to be an eigenvector of the SAM operator, $\hat{S}_z\mathbf{A}^{\mathrm{pl}}\left(\mathbf{r}\right) = \hbar S\mathbf{A}^{\mathrm{pl}}\left(\mathbf{r}\right)$. For the plane wave traveling along $\mathbf{k} = (0,0,k_z)$, the spin angular momentum operators $\hat{S}_z$ has the following eigenvectors:

$$\begin{aligned}\boldsymbol{\eta}_0 &= \begin{pmatrix}0\\0\\1\end{pmatrix} \quad \text{for } S=0, \\ \boldsymbol{\eta}_\pm &= \mp\frac{1}{\sqrt{2}}\begin{pmatrix}1\\\pm i\\0\end{pmatrix} \quad \text{for } S=\pm 1, \end{aligned} \tag{2.26}$$

and the vector potential is then given by $\mathbf{A}^{\mathrm{pl}}(\mathbf{r}) = \boldsymbol{\eta}_\sigma A_0 \mathrm{e}^{ik_z z}$, where A_0 is a constant.

When the plane wave travels in arbitrary direction $\mathbf{k}$, which does not necessary coincide with the z-axis, $\mathbf{k} = k(\cos\phi_k \sin\theta_k, \sin\phi_k \sin\theta_k, \cos\theta_k)$, its polarization vector $\boldsymbol{\varepsilon}_{k,\sigma}$ can be found from original polarization vectors $\boldsymbol{\eta}_\sigma$ by rotating them with rotation matrix

$$\begin{aligned}\hat{R}_k &= \hat{R}_{\phi_k}\hat{R}_{\theta_k} \\ &= \begin{pmatrix} \cos\phi_k & -\sin\phi_k & 0 \\ \sin\phi_k & \cos\phi_k & 0 \\ 0 & 0 & 1 \end{pmatrix} \begin{pmatrix} \cos\theta_k & 0 & \sin\theta_k \\ 0 & 1 & 0 \\ -\sin\theta_k & 0 & \cos\theta_k \end{pmatrix} \\ &= \begin{pmatrix} \cos\phi_k\cos\theta_k & -\sin\phi_k & \cos\phi_k\sin\theta_k \\ \sin\phi_k\cos\theta_k & \cos\phi_k & \sin\phi_k\sin\theta_k \\ -\sin\theta_k & 0 & \cos\theta_k \end{pmatrix}, \end{aligned} \tag{2.27}$$

which gives

$$\boldsymbol{\varepsilon}_{k,\sigma} = \hat{R}_k \boldsymbol{\eta}_\sigma = -\frac{\sigma}{\sqrt{2}} \begin{pmatrix} \cos\phi_k\cos\theta_k - i\sigma\sin\phi_k \\ \sin\phi_k\cos\theta_k + i\sigma\cos\phi_k \\ -\sin\theta_k \end{pmatrix}. \tag{2.28}$$

Then the vector potential for the plane wave traveling along $\mathbf{k}$ is given by

$$\mathbf{A}^{\mathrm{pl}}(\mathbf{r}) = \boldsymbol{\varepsilon}_{k,\sigma} A_0 \mathrm{e}^{i\mathbf{k}\cdot\mathbf{r}},\ \boldsymbol{\varepsilon}_{k,\sigma}\cdot\mathbf{k} = 0, \tag{2.29}$$

where the Coulomb gauge is used. The polarization vector $\boldsymbol{\varepsilon}_{k,\sigma}$ then describes photon carrying a helicity $\sigma = \pm 1$. We can expand $\boldsymbol{\varepsilon}_{k,\sigma}$ over the orthonormal basis $\{\boldsymbol{\eta}_S\}_{S=0,\pm1}$ of the eigenvectors of the SAM operator $\hat{S}_z$:

$$\begin{aligned}\boldsymbol{\varepsilon}_{k,\sigma} &= \frac{1}{\sqrt{2}} \begin{pmatrix} -\frac{1}{2}(1+\sigma\cos\theta_k)\mathrm{e}^{-i\phi_k} + \frac{1}{2}(1-\sigma\cos\theta_k)\mathrm{e}^{i\phi_k} \\ -\frac{i}{2}(1+\sigma\cos\theta_k)\mathrm{e}^{-i\phi_k} - \frac{i}{2}(1-\sigma\cos\theta_k)\mathrm{e}^{i\phi_k} \\ \sigma\sin\theta_k \end{pmatrix} \\ &= \frac{1}{\sqrt{2}} \begin{pmatrix} -c_{+1,\sigma}\mathrm{e}^{-i\phi_k} + c_{-1,\sigma}\mathrm{e}^{i\phi_k} \\ -ic_{+1,\sigma}\mathrm{e}^{-i\phi_k} - ic_{-1,\sigma}\mathrm{e}^{i\phi_k} \\ \sqrt{2}c_{0,\sigma} \end{pmatrix} \\ &= \sum_{S=0,\pm1} c_{S,\sigma}\mathrm{e}^{-iS\varphi_k}\boldsymbol{\eta}_S, \end{aligned} \tag{2.30}$$

where the expansion coefficients are given by

$$c_{0,\sigma} = \frac{\sigma}{\sqrt{2}} \sin\theta_k = \frac{\sigma}{\sqrt{2}} \frac{k_\perp}{\sqrt{k_\perp^2 + k_z^2}}, \tag{2.31}$$

$$c_{+1,\sigma} = \frac{1}{2}\left(1 + \sigma\cos\theta_k\right) = \frac{1}{2}\left(1 + \frac{\sigma k_z}{\sqrt{k_\perp^2 + k_z^2}}\right), \tag{2.32}$$

$$c_{-1,\sigma} = \frac{1}{2}\left(1 - \sigma\cos\theta_k\right) = \frac{1}{2}\left(1 - \frac{\sigma k_z}{\sqrt{k_\perp^2 + k_z^2}}\right). \tag{2.33}$$

and we used $\sigma^2 = 1$.

Now we can find the expression for the vector potential for OV based on the expansion over the plane waves in Eq. (2.20) and taking into account that each plane wave is characterized by its own polarization vector $\boldsymbol{\varepsilon}_{k,\sigma}$:

$$\begin{aligned}\mathbf{A}^{\mathrm{OV}}(\mathbf{r}) &= \mathbf{A}^{\mathrm{OV}}(\mathbf{r}|k_\perp, k_z, J, \sigma) \\ &= A_0 \int \frac{d^2\mathbf{k}''_\perp}{(2\pi)^2} a_{k_\perp,J}(\mathbf{k}''_\perp)\boldsymbol{\varepsilon}_{k,\sigma} \mathrm{e}^{i\mathbf{k}''_\perp\cdot\mathbf{r}_\perp + ik''_z z},\end{aligned} \tag{2.34}$$

where we introduced J as the eigenvalue of the TAM operator $\hat{J}_z = \hat{L}_z + \hat{S}_z$. Integrating over $\mathbf{k}''_\perp$, we finally obtain the vector potential of the Bessel mode OV[42, 43],

$$\mathbf{A}^{\mathrm{OV}}(\mathbf{r}|k_\perp, k_z, J, \boldsymbol{\sigma}) = A_0\sqrt{\frac{k_\perp}{2\pi}} \sum_{S=0,\pm1} \boldsymbol{\eta}_S (-i)^S c_{S,\sigma} J_{J-S}(k_\perp r_\perp) \mathrm{e}^{i(J-S)\phi} \mathrm{e}^{ik_z z}. \tag{2.35}$$

2.1.4 Paraxial Approximation

In general, it is not always true that an optical ray propagates along the optical axis of the optics system. However, in a geometric optics, if the ray propagates almost along the optical axis, so-called the paraxial approximation, it is known that such a ray will simplify the calculation of the ray path. The paraxial approximation allows three approximations, $\sin\theta \approx \theta$, $\cos\theta \approx 1$, and $\tan\theta \approx \theta$ for the first order approximation, where θ is an angle between the ray propagation and optical axis[44]. The tangent in the first-order approximation is accurate within about 1% for angles under about 10°. Also in our case, the paraxial approximation is crucial. In the non-paraxial region, the spin angular momentum and orbital one are mixed and the total angular momentum is only conserved as shown in the previous subsections.

To conserve the spin and orbital angular momentum separately, we need to apply a paraxial approximation.

The degree of the paraxial approximation can be characterized by a parameter

$$\alpha = k_\perp / k_z = \tan\theta_k. \tag{2.36}$$

If we choose the angle $\theta_k = 10^\circ$ to the tangent accuracy within 1% in the first order, the parameter α gives about 0.17. Consequently, we will employ $\alpha = 0.1$ for the numerical calculation in many cases.

To obtain the expression of vector potential of optical vortex in paraxial approximation, we assume that the longitudinal momentum of the photon is much greater than its transverse momentum, $k_z \gg k_\perp$. Then, the expansion coefficients become $c_{S,\sigma} \approx \delta_{S,\sigma}$, and we obtain the vector potential in the form:

$$\begin{aligned}\mathbf{A}^{\mathrm{OV}}(\mathbf{r}|k_\perp, k_z, \ell+\sigma, \sigma) &\sim \boldsymbol{\eta}_\sigma A_0 \sqrt{\frac{k_\perp}{2\pi}} (-i)^\sigma J_\ell(k_\perp r_\perp) \mathrm{e}^{i\ell\phi} \mathrm{e}^{ik_z z} \\ &\equiv \boldsymbol{A}^{\mathrm{OV}}_{\ell,\sigma}(\boldsymbol{r}),\end{aligned} \tag{2.37}$$

where we introduced a OAM quantum number, $\ell = J - \sigma$. Moreover, if we take the limit $k_\perp \to 0$ with $r_\perp$ being fixed, then the Bessel function gives $J_\ell(k_\perp r_\perp) \to \delta_{\ell,0}$, and we recover a plane wave solution with $J = \sigma$ propagating along the z-axis.

The Bessel-mode OV exhibits a feature of being diffraction free and has a phase singularity. The first feature can easily be seen by using Eq. (2.37). The intensity of the vector potential, $I \propto |\mathbf{A}|^2$, is independent of z. The second feature, the phase singularity, is located on the beam axis where the intensity becomes zero. To demonstrate a transfer of OAM, the target particles are usually located in non-zero intensity region off the beam axis and dark rings. The radius of i-th dark ring of the higher-order Bessel beam is given by

$$r_\perp^{\ell,i} = \frac{(\text{the } i\text{-th zeros of } \ell\text{-th order Bessel function})}{k_\perp}, \tag{2.38}$$

which is determined by $J_\ell(k_\perp r_\perp^{\ell,i}) = 0$. For example, the central core size of the zero-order Bessel beam is given by $r_\perp^{0,1} = 2.404/k_\perp$. We exhibit some examples of the intensity distribution of the Bessel-mode OV, and the definition of the dark ring radius and the central core spot size in Fig. 2.3. We note that the Bessel-mode OV even with $\ell = 0$ has the dark rings or the annular distribution, This feature is also the crucial difference with the plane wave.

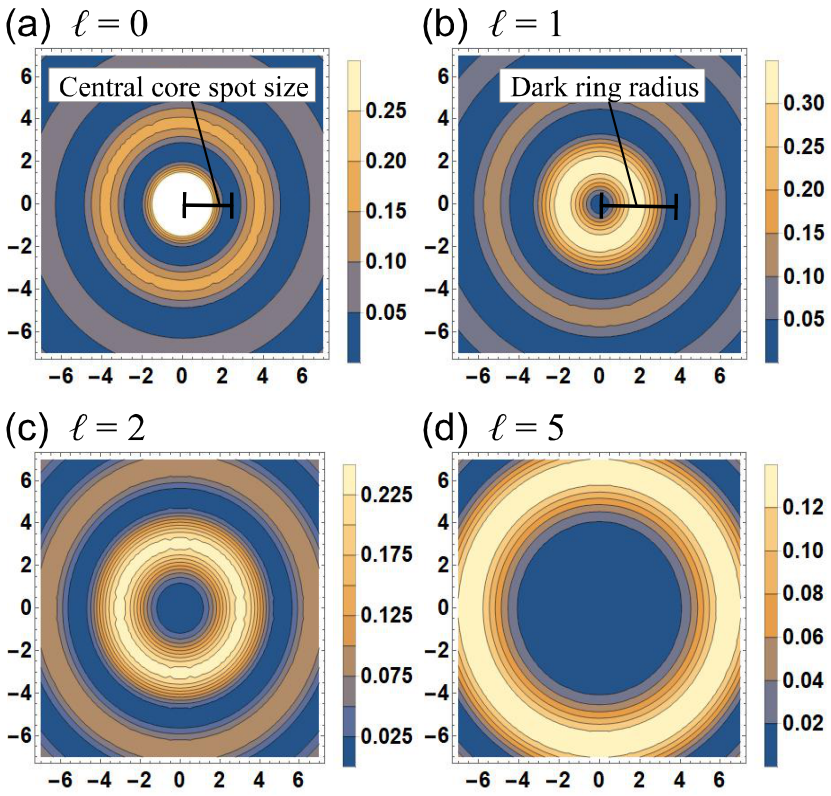

Figure 2.3: Some examples of the intensity distribution of the Bessel-mode optical vortex, $|J_\ell(x)|^2$. (a) $\ell = 0$. The central core spot size is given by the first zeros of $J_0(x)$. (b) $\ell = 1$. The dark ring radius is given by i-th zeros of $J_\ell(x)$. (c) $\ell = 2$, (d) $\ell = 5$.

2.2 Physical Properties of Optical Vortex

We have seen that optical vortices have characteristic features, e.g. the phase singularity, bright and the dark rings, etc. Since the electric field, magnetic one, Poynting vector, and energy density are fundamental physical quantities, it is important to see their physical properties of OV. It is useful to describe such a helical wavefront by a cylindrical coordinates. In the cylindrical coordinates, the vector potential of the circularly polarized optical vortex in

non-paraxial region is given by

$$\begin{aligned}
&A_{r_\perp}^{\mathrm{OV}}(\mathbf{r},t|k_\perp,k_z,J,\sigma)\\
&=\frac{i}{\sqrt{2}}A_0\sqrt{\frac{k_\perp}{2\pi}}\left(c_{+1,\sigma}J_{J-1}(k_\perp r_\perp)+c_{-1,\sigma}J_{J+1}(k_\perp r_\perp)\right)\mathrm{e}^{i(J\phi+k_z z-\omega t)},\\
&A_{\phi}^{\mathrm{OV}}(\mathbf{r},t|k_\perp,k_z,J,\sigma)\\
&=-\frac{1}{\sqrt{2}}A_0\sqrt{\frac{k_\perp}{2\pi}}\left(c_{+1,\sigma}J_{J-1}(k_\perp r_\perp)-c_{-1,\sigma}J_{J+1}(k_\perp r_\perp)\right)\mathrm{e}^{i(J\phi+k_z z-\omega t)},\\
&A_{z}^{\mathrm{OV}}(\mathbf{r},t|k_\perp,k_z,J,\sigma)\\
&=A_0\sqrt{\frac{k_\perp}{2\pi}}c_{0,\sigma}J_J(k_\perp r_\perp)\mathrm{e}^{i(J\phi+k_z z-\omega t)}.
\end{aligned}\tag{2.39}$$

The physical electric field, $\mathbf{E}=-\operatorname{Re}\dot{\mathbf{A}}=\operatorname{Re}[i\omega\mathbf{A}]$, is obtained as

$$\begin{aligned}
&E_{r_\perp}^{\mathrm{OV}}(\mathbf{r},t|k_\perp,k_z,J,\sigma)\\
&=-\frac{1}{\sqrt{2}}A_0\omega\sqrt{\frac{k_\perp}{2\pi}}\left(c_{+1,\sigma}J_{J-1}(k_\perp r_\perp)+c_{-1,\sigma}J_{J+1}(k_\perp r_\perp)\right)\cos(J\phi+k_z z-\omega t),\\
&E_{\phi}^{\mathrm{OV}}(\mathbf{r},t|k_\perp,k_z,J,\sigma)\\
&=\frac{1}{\sqrt{2}}A_0\omega\sqrt{\frac{k_\perp}{2\pi}}\left(c_{+1,\sigma}J_{J-1}(k_\perp r_\perp)-c_{-1,\sigma}J_{J+1}(k_\perp r_\perp)\right)\sin(J\phi+k_z z-\omega t),\\
&E_{z}^{\mathrm{OV}}(\mathbf{r},t|k_\perp,k_z,J,\sigma)\\
&=-A_0\omega\sqrt{\frac{k_\perp}{2\pi}}c_{0,\sigma}J_J(k_\perp r_\perp)\sin(J\phi+k_z z-\omega t).
\end{aligned}\tag{2.40}$$

By using the formula of vector rotation,

$$\begin{aligned}
&\boldsymbol{\nabla}\times\mathbf{C}\\
&=\left(\frac{1}{r_\perp}\frac{\partial C_z}{\partial\phi}-\frac{\partial C_\phi}{\partial z}\right)\hat{\mathbf{e}}_r+\left(\frac{\partial C_{r_\perp}}{\partial z}-\frac{\partial C_z}{\partial r_\perp}\right)\hat{\mathbf{e}}_\phi+\left(\frac{1}{r_\perp}\frac{\partial\left[r_\perp C_\phi\right]}{\partial r_\perp}-\frac{1}{r_\perp}\frac{\partial C_{r_\perp}}{\partial\phi}\right)\hat{\mathbf{e}}_z,
\end{aligned}\tag{2.41}$$

we can easily show,

$$\boldsymbol{\nabla}\times\mathbf{A}^{\mathrm{OV}}=\sigma k\mathbf{A}^{\mathrm{OV}}(\mathbf{r},t).\tag{2.42}$$

We thus obtain the physical magnetic field, $\mathbf{B} = \mathrm{Re}\left[\boldsymbol{\nabla} \times \mathbf{A}\right]$, as

$$
\begin{aligned}
&B_{r_\perp}^{\mathrm{OV}}\left(\mathbf{r}, t | k_\perp, k_z, J, \sigma\right) \\
&= -\frac{1}{\sqrt{2}} A_0 \sigma k \sqrt{\frac{k_\perp}{2\pi}} \left(c_{+1,\sigma} J_{J-1}\left(k_\perp r_\perp\right) + c_{-1,\sigma} J_{J+1}\left(k_\perp r_\perp\right)\right) \sin\left(J\phi + k_z z - \omega t\right), \\
&B_{\phi}^{\mathrm{OV}}\left(\mathbf{r}, t | k_\perp, k_z, J, \sigma\right) \\
&= -\frac{1}{\sqrt{2}} A_0 \sigma k \sqrt{\frac{k_\perp}{2\pi}} \left(c_{+1,\sigma} J_{J-1}\left(k_\perp r_\perp\right) - c_{-1,\sigma} J_{J+1}\left(k_\perp r_\perp\right)\right) \cos\left(J\phi + k_z z - \omega t\right), \\
&B_{z}^{\mathrm{OV}}\left(\mathbf{r}, t | k_\perp, k_z, J, \sigma\right) \\
&= A_0 \sigma k \sqrt{\frac{k_\perp}{2\pi}} c_{0,\sigma} J_J\left(k_\perp r_\perp\right) \cos\left(J\phi + k_z z - \omega t\right),
\end{aligned}
\tag{2.43}
$$

where we used the formula of Bessel functions,

$$
z \frac{d}{dz} J_\nu\left(z\right) \pm \nu J_\nu\left(z\right) = \pm z J_{\nu \mp 1}\left(z\right). \tag{2.44}
$$

Because the Poynting vector is defined by

$$
\begin{aligned}
\mathbf{P} &= \frac{1}{\mu_0} \mathbf{E} \times \mathbf{B} \\
&= \frac{1}{\mu_0} \mathrm{Re}\left[i\omega \mathbf{A}\right] \times \mathrm{Re}\left[\boldsymbol{\nabla} \times \mathbf{A}\right],
\end{aligned}
\tag{2.45}
$$

we obtain its explicit form as

$$
\begin{aligned}
P_{r_\perp} &= \frac{1}{\mu_0}\left(E_\phi^{\mathrm{OV}} B_z^{\mathrm{OV}} - E_z^{\mathrm{OV}} B_\phi^{\mathrm{OV}}\right) \\
&= 0, \\
P_\phi &= \frac{1}{\mu_0}\left(E_z^{\mathrm{OV}} B_r^{\mathrm{OV}} - E_r^{\mathrm{OV}} B_z^{\mathrm{OV}}\right) \\
&= \frac{\sigma}{\sqrt{2}} \frac{A_0^2 c k^2 k_\perp}{2\pi\mu_0} c_{0,\sigma} J_J\left(k_\perp r_\perp\right) \left[c_{+1,\sigma} J_{J-1}\left(k_\perp r_\perp\right) + c_{-1,\sigma} J_{J+1}\left(k_\perp r_\perp\right)\right], \\
P_z &= \frac{1}{\mu_0}\left(E_r^{\mathrm{OV}} B_\phi^{\mathrm{OV}} - E_\phi^{\mathrm{OV}} B_r^{\mathrm{OV}}\right) \\
&= \sigma \frac{A_0^2 c k^2 k_\perp}{4\pi\mu_0} \left[\left(c_{+1,\sigma}\right)^2 J_{J-1}^2\left(k_\perp r_\perp\right) - \left(c_{-1,\sigma}\right)^2 J_{J+1}^2\left(k_\perp r_\perp\right)\right],
\end{aligned}
\tag{2.46}
$$

where we note that the wavenumber vector $\mathbf{k}$ is related to Poynting vector as $\hbar\mathbf{k} = \mathbf{P}/c^2$. On the other hands, because the energy density is defined by

$$
u = \frac{1}{2}\left(\varepsilon_0 \mathbf{E}^2 + \frac{1}{\mu_0}\mathbf{B}^2\right), \tag{2.47}
$$

we obtain its explicit form as

$$u = \frac{A_0^2 \omega^2 k_\perp}{4\pi\mu_0 c^2} \left[(c_{+1,\sigma})^2 J_{J-1}^2 (k_\perp r_\perp) + (c_{-1,\sigma})^2 J_{J+1}^2 (k_\perp r_\perp) + (c_{0,\sigma})^2 J_J^2 (k_\perp r_\perp) \right]. \tag{2.48}$$

2.2.1 Paraxial Approximation

In the paraxial region, because the expansion coefficient reduces to $c_{S,\sigma} = \delta_{S,\sigma}$ with $\sigma = \pm 1$, we can easily show the expressions of the physical electric and magnetic fields from Eqs. (2.40) and (2.43). First, the vector potential in paraxial approximation in cylindrical coordinates can be expressed by

$$\begin{aligned} A^{\mathrm{OV}}_{r_\perp,\ell,\sigma}(\mathbf{r},t) &= A_0 \frac{i}{\sqrt{2}} \sqrt{\frac{k_\perp}{2\pi}} J_\ell(k_\perp r_\perp) \mathrm{e}^{i[(\ell+\sigma)\phi + k_z z - \omega t]}, \\ A^{\mathrm{OV}}_{\phi,\ell,\sigma}(\mathbf{r},t) &= -\sigma A_0 \frac{1}{\sqrt{2}} \sqrt{\frac{k_\perp}{2\pi}} J_\ell(k_\perp r_\perp) \mathrm{e}^{i[(\ell+\sigma)\phi + k_z z - \omega t]}, \\ A^{\mathrm{OV}}_{z,\ell,\sigma}(\mathbf{r},t) &= 0. \end{aligned} \tag{2.49}$$

The physical electric field is then obtained as

$$\begin{aligned} E^{r_\perp}_{\ell,\sigma}(\mathbf{r},t) &= -A_0 \frac{\omega}{\sqrt{2}} \sqrt{\frac{k_\perp}{2\pi}} J_\ell(k_\perp r_\perp) \cos\left[k_z z + (\ell+\sigma)\phi - \omega t\right], \\ E^{\phi}_{\ell,\sigma}(\mathbf{r},t) &= \sigma A_0 \frac{\omega}{\sqrt{2}} \sqrt{\frac{k_\perp}{2\pi}} J_\ell(k_\perp r_\perp) \sin\left[k_z z + (\ell+\sigma)\phi - \omega t\right], \\ E^{z}_{\ell,\sigma}(\mathbf{r},t) &= 0. \end{aligned} \tag{2.50}$$

The physical magnetic field is also obtained as

$$\begin{aligned} B^{r_\perp}_{\ell,\sigma}(\mathbf{r},t) &= -\sigma A_0 \frac{k_z}{\sqrt{2}} \sqrt{\frac{k_\perp}{2\pi}} J_\ell(k_\perp r_\perp) \sin\left[k_z z + (\ell+\sigma)\phi - \omega t\right], \\ B^{\phi}_{\ell,\sigma}(\mathbf{r},t) &= -A_0 \frac{k_z}{\sqrt{2}} \sqrt{\frac{k_\perp}{2\pi}} J_\ell(k_\perp r_\perp) \cos\left[k_z z + (\ell+\sigma)\phi - \omega t\right], \\ B^{z}_{\ell,\sigma}(\mathbf{r},t) &= 0. \end{aligned} \tag{2.51}$$

The Poynting vector thus has almost z component as

$$\begin{aligned} P^{r_\perp}_{\ell,\sigma}(\mathbf{r},t) &= 0, \\ P^{\phi}_{\ell,\sigma}(\mathbf{r},t) &= 0, \\ P^{z}_{\ell,\sigma}(\mathbf{r},t) &= A_0^2 \frac{\omega k_\perp k_z}{4\pi\mu_0} J_\ell^2(k_\perp r_\perp). \end{aligned} \tag{2.52}$$

The energy density is obtained as

$$u^{\pm} = A_0^2 \frac{k_\perp k_z^2}{4\pi\mu_0} J_\ell^2 \left(k_\perp r_\perp\right). \tag{2.53}$$

Noting that $\omega = ck \approx ck_z$ in paraxial approximation, we can see that the equation of continuity for energy is satisfied.

Figs. 2.4 - 2.9 show the snapshots of electric field of the optical vortex under the paraxial approximation $\mathbf{E}_{\ell,\sigma}(\mathbf{r}, t)$. We graphically see that the helicity of the optical vortex corresponds to the rotation direction at each point, whereas the orbital angular momentum manifests the winding number around the phase singularity $(x, y) = (0, 0)$.

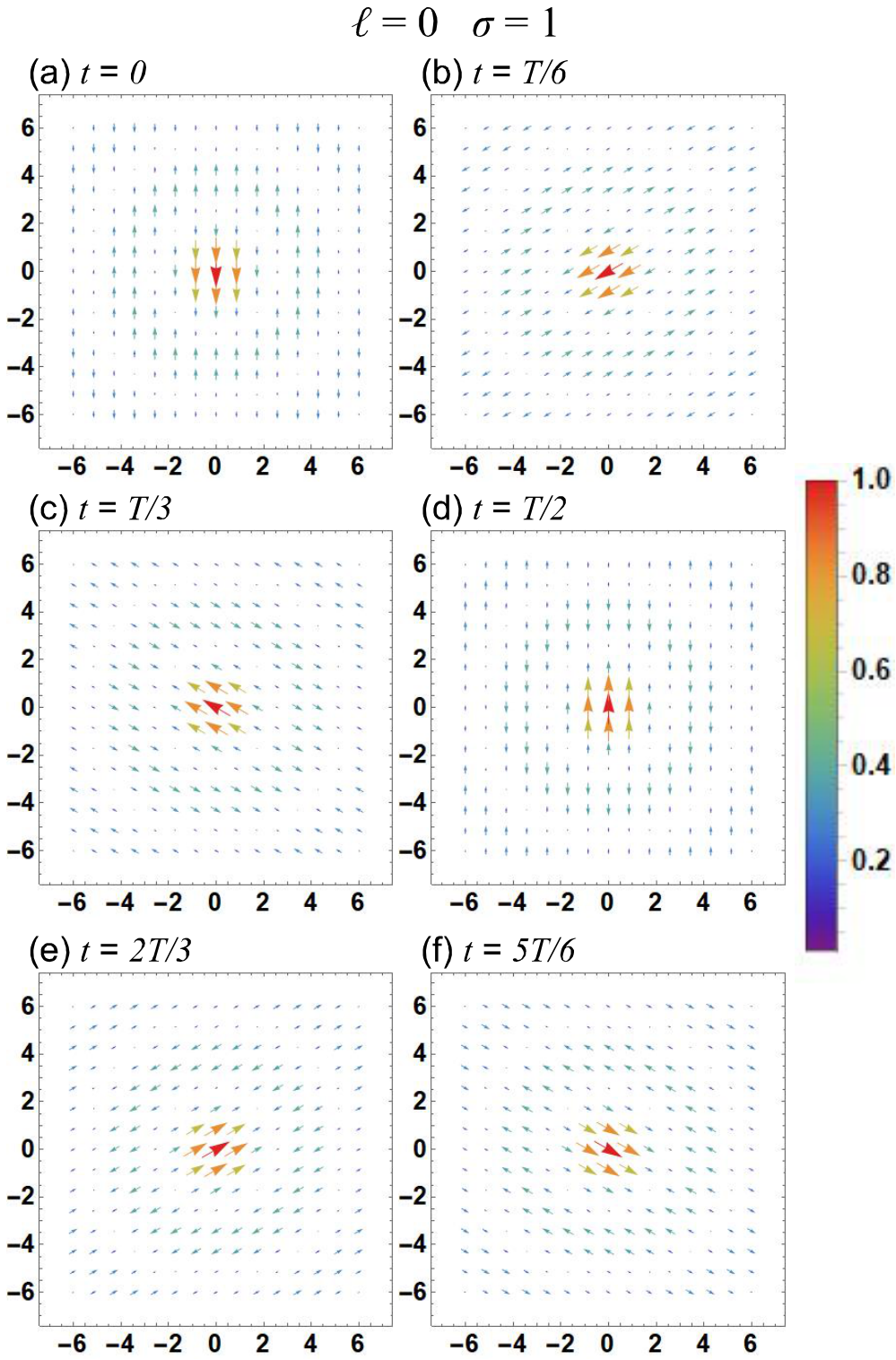

Figure 2.4: Snapshots of the electric field of the optical vortex with $\ell = 0$ and $\sigma = 1$. (a) for $t = 0$, (b) $t = \frac{1}{6}T$, (c) $t = \frac{1}{3}T$, (d) $t = \frac{1}{2}T$, (e) $t = \frac{2}{3}T$, and (f) $t = \frac{5}{6}T$, where $T = 2\pi/\omega$ is a period.

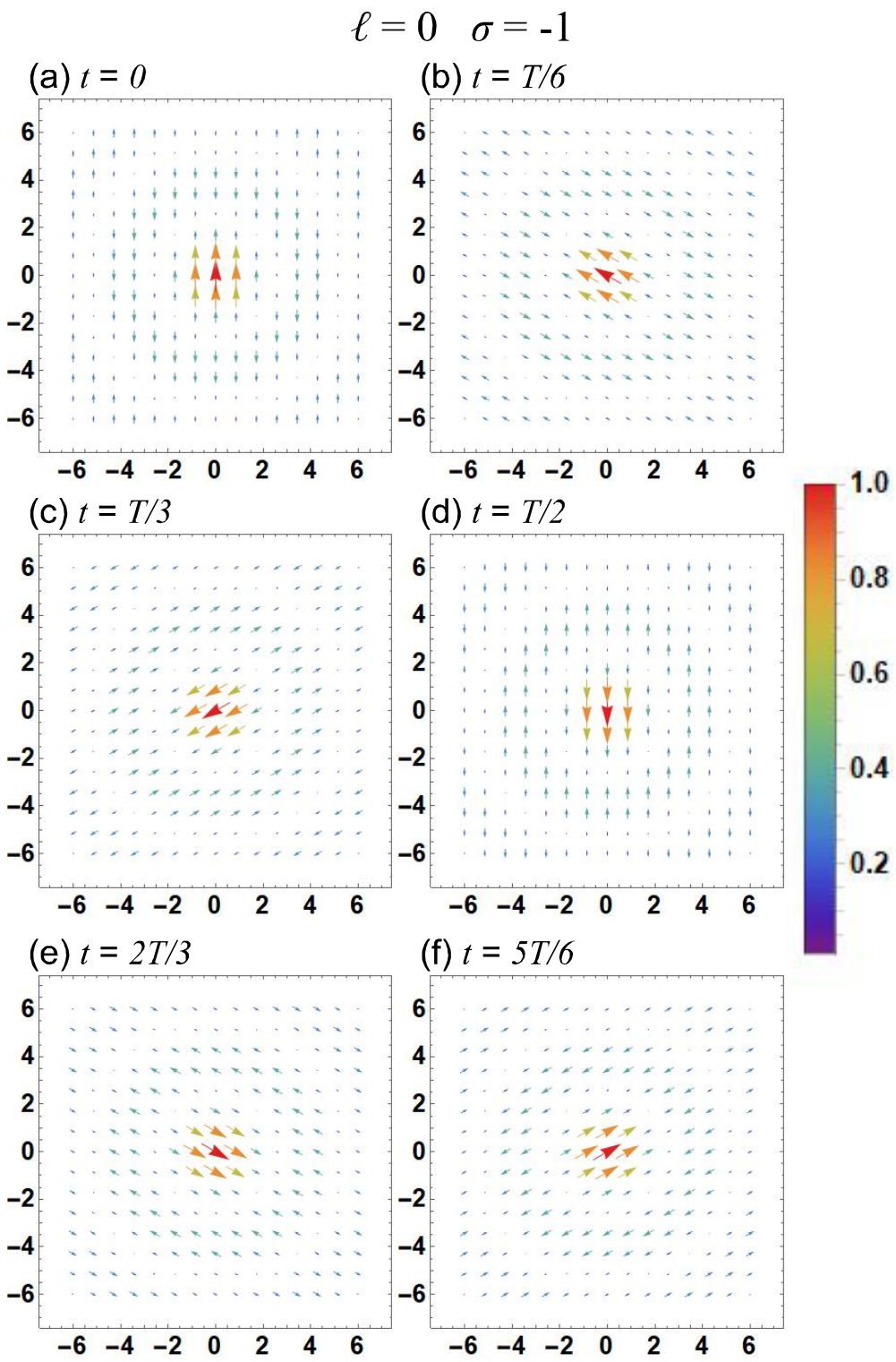

Figure 2.5: Snapshots of the electric field of the optical vortex with $\ell = 0$ and $\sigma = -1$. (a) for $t = 0$, (b) $t = \frac{1}{6}T$, (c) $t = \frac{1}{3}T$, (d) $t = \frac{1}{2}T$, (e) $t = \frac{2}{3}T$, and (f) $t = \frac{5}{6}T$, where $T = 2\pi/\omega$ is a period.

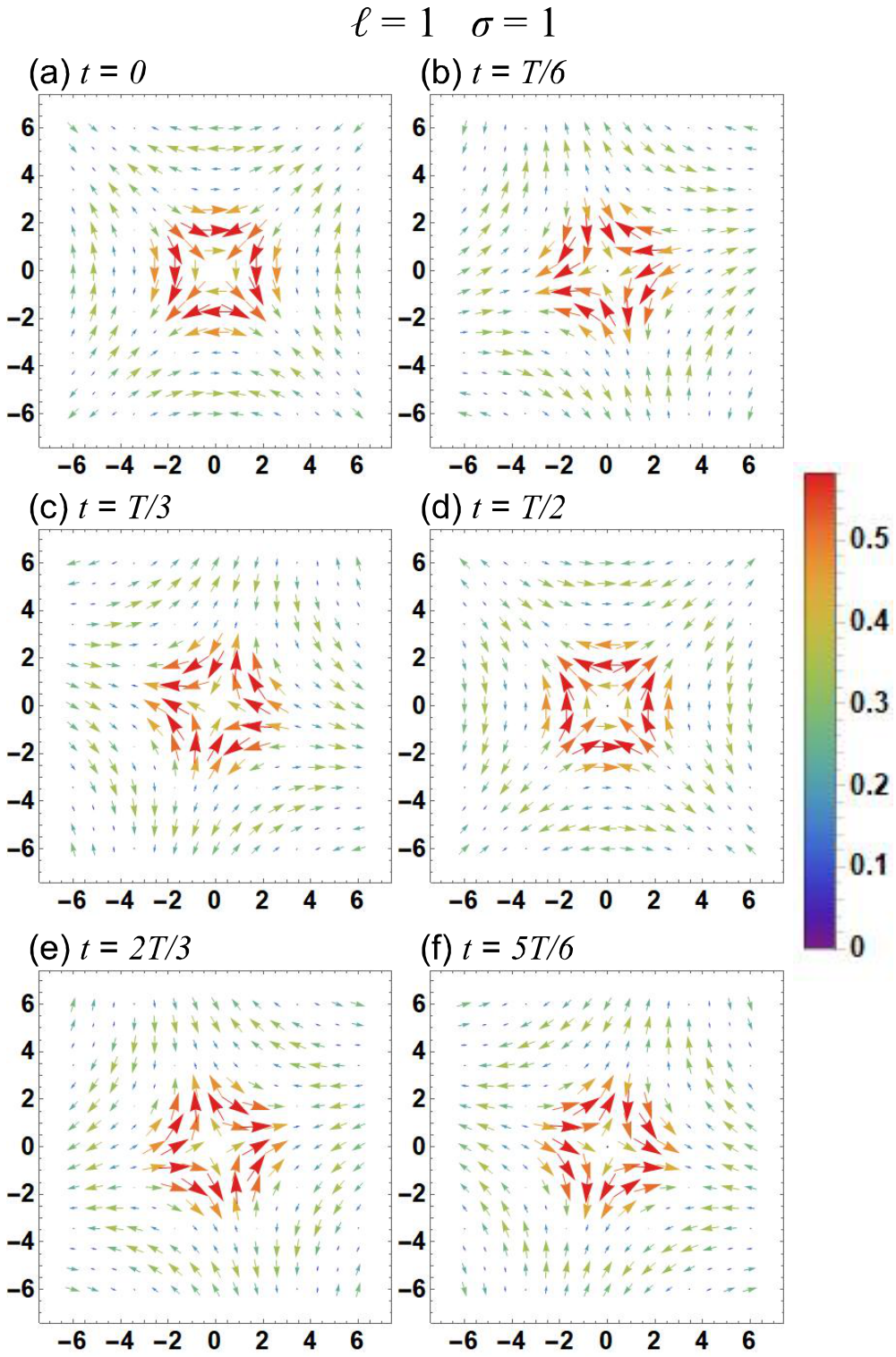

Figure 2.6: Snapshots of the electric field of the optical vortex with $\ell = 1$ and $\sigma = 1$. (a) for $t = 0$, (b) $t = \frac{1}{6}T$, (c) $t = \frac{1}{3}T$, (d) $t = \frac{1}{2}T$, (e) $t = \frac{2}{3}T$, and (f) $t = \frac{5}{6}T$, where $T = 2\pi/\omega$ is a period.

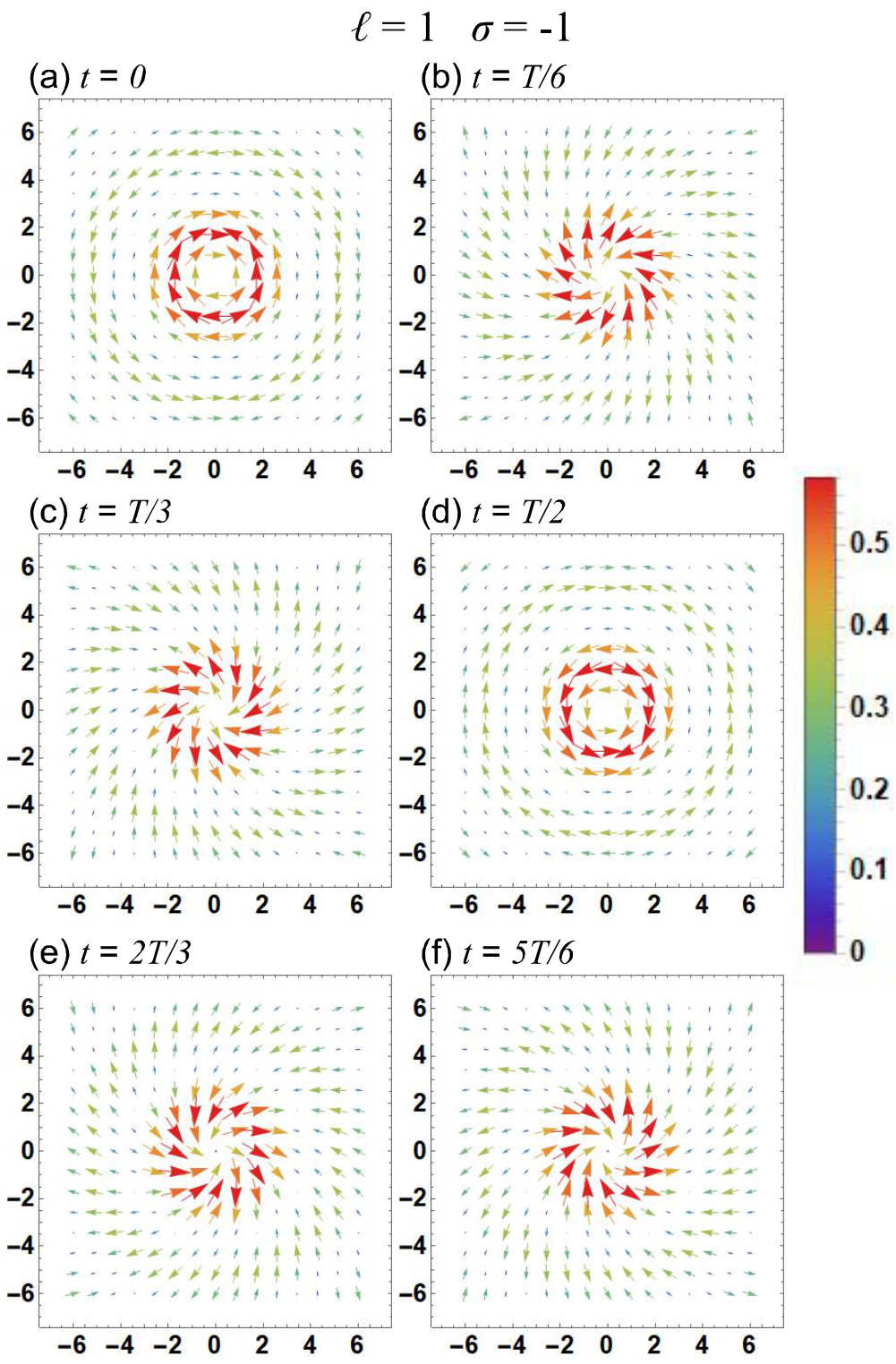

Figure 2.7: Snapshots of the electric field of optical vortex with $\ell = 1$ and $\sigma = -1$. (a) for $t = 0$, (b) $t = \frac{1}{6}T$, (c) $t = \frac{1}{3}T$, (d) $t = \frac{1}{2}T$, (e) $t = \frac{2}{3}T$, and (f) $t = \frac{5}{6}T$, where $T = 2\pi/\omega$ is a period.

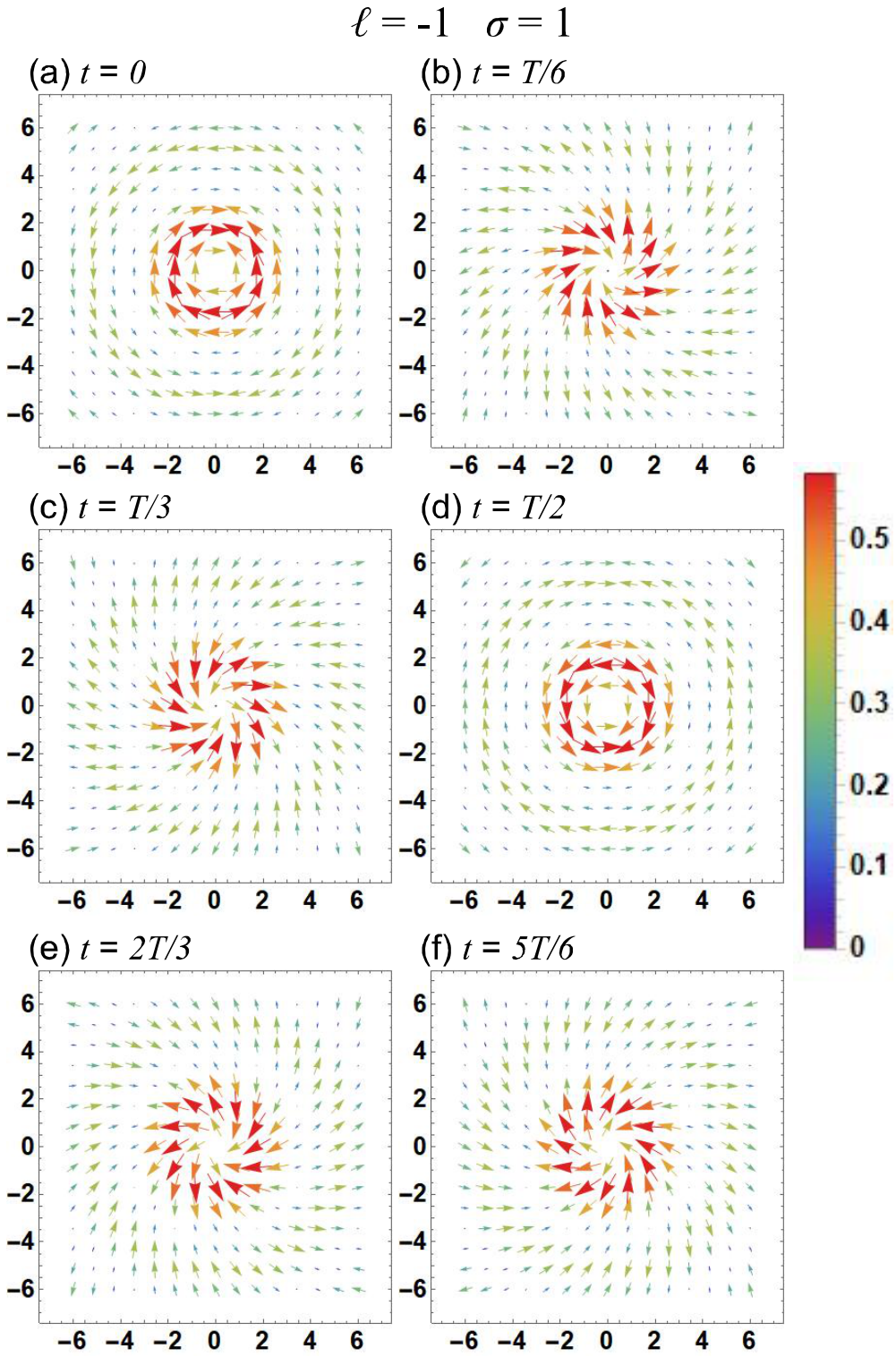

Figure 2.8: Snapshots of the electric field of the optical vortex with $\ell = -1$ and $\sigma = 1$. (a) for $t = 0$, (b) $t = \frac{1}{6}T$, (c) $t = \frac{1}{3}T$, (d) $t = \frac{1}{2}T$, (e) $t = \frac{2}{3}T$, and (f) $t = \frac{5}{6}T$, where $T = 2\pi/\omega$ is a period.

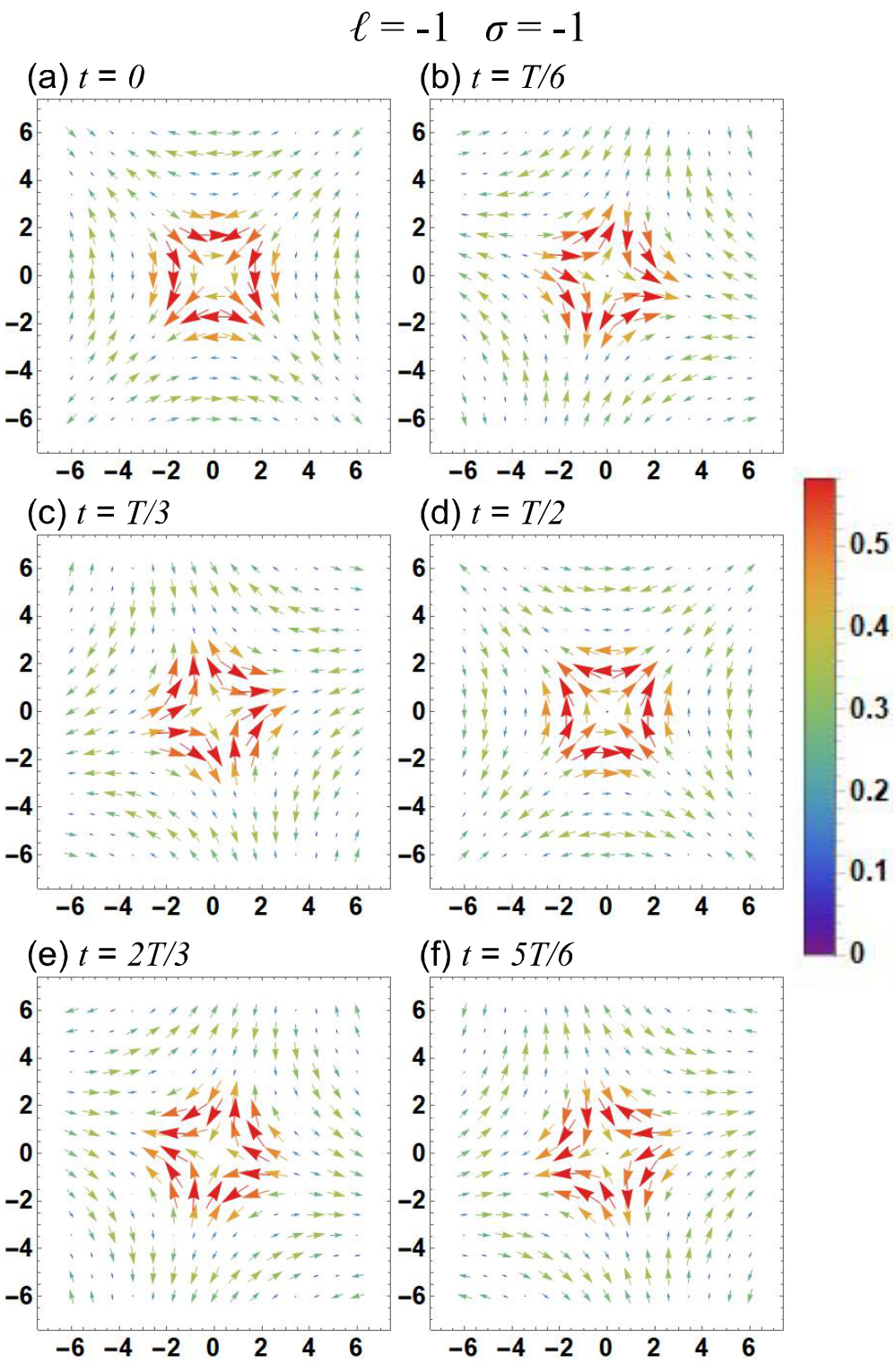

Figure 2.9: Snapshots of the electric field of the optical vortex with $\ell = -1$ and $\sigma = -1$. (a) for $t = 0$, (b) $t = \frac{1}{6}T$, (c) $t = \frac{1}{3}T$, (d) $t = \frac{1}{2}T$, (e) $t = \frac{2}{3}T$, and (f) $t = \frac{5}{6}T$, where $T = 2\pi/\omega$ is a period.

Chapter 3

Two Dimensional Electron Gas

The two dimensional electron gas (2DEG) is a mightily simple system but generates curious phenomena. When a magnetic field is applied perpendicular to the surface, whereas, in a classical picture, the magnetic field causes an orbital motion of the electron due to the Lorentz force perpendicular to their direction of motion (cyclotron motion), in a quantum mechanical picture, the energy spectrum for its orbit is quantized (so-called Landau level, LL). In consequence, the 2DEG at low temperatures (< 4 K) in a strong perpendicular magnetic field (typically, $B > 1$ T) occurs a quantum Hall effect. In 1980, von Klitzing, Dorda and Pepper [45] observed an integer quantum Hall effect which is a Hall conductance of such a system (which is the conductance transverse to an external electric field applied to the conductor and to an applied magnetic field perpendicular to the electric field) is an integer multiple of e^2/h, where e is the elementary charge and h is the Planck constant. It is also known that Tsui, Stormer and Gossard discovered that the Hall conductance at lower temperatures and in clean samples can be a rational fraction of e^2/h in 1982 [46].

The 2DEG comes to realization at the interface between two semiconductors or between a semiconductor and an insulator. That is to say, it exists in the semiconductor with the lower-energy conduction band, but is confined in a narrow potential well near the interface. Such a confinement is caused by the electrostatic attraction to a positively charged layer away from the interface (see Fig. 3.1). The electrons in the 2DEG typically move freely in the plane of the interface. Especially, GaAs/AlGaAs heterostructures are more widely used because of higher mobilities (or very long mean free paths of electron).

In this Chapter, we review the physics of the 2DEG under the magnetic field at such interfaces. First, we introduce the classical motion of the electrons under the magnetic field before the quantum treatment. To treat it in

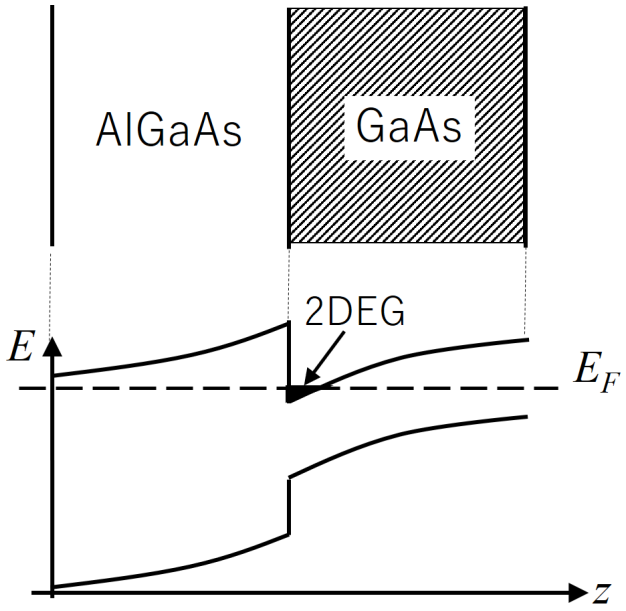

Figure 3.1: Schematics of GaAs/AlGaAs heterostructure. The upper half shows the real space structure of the GaAs/AlGaAs layers. The lower half shows the corresponding structure of the energy levels. 2DEG exists at the interface painted in black.

quantum mechanics, we describe it in Lagrangian formalism and Hamilton one. Then, we give the review of quantum treatment of the 2DEG under the magnetic field. Through seeing the semi-classical states of it, so-called coherent states, we see that, because circular currents formed by coherent states are canceled out at contact points, the current flowing in the bulk does not exist. As a result, we see that the current flowing on the system should survive.

3.1 Electron in Magnetic Field (Classical Treatment)

Before a quantum treatment of the motion of a charged particle (e.g. electron) in a magnetic field, we review classical treatment of the motion.

3.1.1 Cyclotron Motion

Because the charged particle in a magnetic field, $\mathbf{B} = B\hat{\mathbf{e}}_z$, experiences the Lorentz force $\mathbf{F} = -e\dot{\mathbf{r}} \times \mathbf{B}$, the particle moves on a circle (Larmor motion). Since the Lorentz force is given by the cross product, the equation of motion is then given by

$$\begin{aligned} \ddot{x} &= -\omega_c \dot{y}, \\ \ddot{y} &= \omega_c \dot{x}, \end{aligned} \tag{3.1}$$

where $\omega_c = eB/m_e$ is a cyclotron frequency with charge $-e\,(e > 0)$ and an electron mass m_e. The integral of this equation is given by

$$\begin{aligned} \dot{x} &= -\omega_c \left(y - y_0\right), \\ \dot{y} &= \omega_c \left(x - x_0\right), \end{aligned} \tag{3.2}$$

where $\mathbf{r}_0 = (x_0, y_0)$ is a constant of motion. By introducing a variable $\boldsymbol{\eta} = \left(\eta_x, \eta_y\right) = \mathbf{r} - \mathbf{r}_0$, we can separate Eq. (3.2) into each component. By plugging $\boldsymbol{\eta}$ into (3.2),

$$\begin{aligned} \ddot{\eta}_x &= -\omega_c^2 \eta_x, \\ \ddot{\eta}_y &= -\omega_c^2 \eta_y, \end{aligned} \tag{3.3}$$

we then obtain the solution as

$$\begin{aligned} \eta_x &= \eta \cos\left(\omega_c t + \gamma\right), \\ \eta_y &= \eta \sin\left(\omega_c t + \gamma\right), \end{aligned} \tag{3.4}$$

that is,

$$\begin{aligned} x\left(t\right) &= x_0 + \eta \cos\left(\omega_c t + \gamma\right), \\ y\left(t\right) &= y_0 + \eta \sin\left(\omega_c t + \gamma\right), \end{aligned} \tag{3.5}$$

where η is the Larmor radius (cyclotron radius) and γ is an arbitrary angle (a constant of motion). We find that the constant of motion $\mathbf{r}_0$ previously introduced means the guiding center. Therefore, the electron moves on a circle of radius $\boldsymbol{\eta}$ around the guiding center $\mathbf{r}_0$ as shown in Fig. 3.2.

3.1.2 Lagrangian Formalism

Lagrangian of the electron system under the magnetic field is described by

$$L = \frac{1}{2} m_e \dot{\mathbf{r}}^2 - e\mathbf{A}\left(\mathbf{r}\right) \cdot \dot{\mathbf{r}}, \tag{3.6}$$

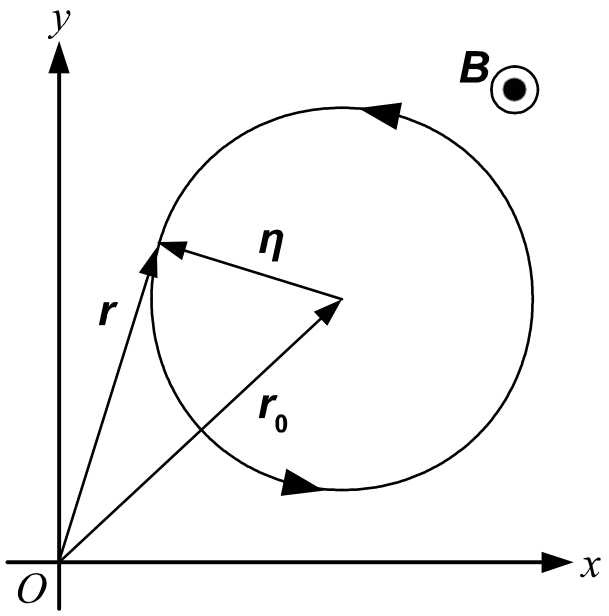

Figure 3.2: The trajectory of cyclotron motion with radius $\boldsymbol{\eta}$ around the guiding center $\mathbf{r}_0$, governed by the equation of motion (3.1)

where $\mathbf{A}(\mathbf{r})$ is a time-independent vector potential describing the external magnetic field. The equation of motion is obtained from Euler-Lagrange equation:

$$\begin{aligned}
&\frac{d}{dt}\frac{\partial L}{d\dot{\mathbf{r}}} - \frac{\partial L}{\partial \mathbf{r}} = 0 \\
&m_e\ddot{\mathbf{r}} + e\dot{r}_j \frac{\partial}{\partial \mathbf{r}} A_j(\mathbf{r}) = 0 \\
&\left[m_e\ddot{x} + e\left\{\dot{x}\nabla\cdot\mathbf{A}(\mathbf{r}) - \left(\dot{x}\frac{\partial}{\partial y} + \dot{y}\frac{\partial}{\partial x}\right)A_y(\mathbf{r}) + \left(\dot{z}\frac{\partial}{\partial x} - \dot{x}\frac{\partial}{\partial z}\right)A_z(\mathbf{r})\right\}\right]\hat{\mathbf{e}}_x \\
&+ (\hat{\mathbf{e}}_y \text{ term}) + (\hat{\mathbf{e}}_z \text{ term}) = 0. \qquad (3.7)
\end{aligned}$$

We here assume the Coulomb gauge, $\nabla\cdot\mathbf{A}(\mathbf{r}) = 0$. Then we can proceed to calculate this equation as the following,

$$\begin{aligned}
&\left\{m_e\ddot{x} - e(\dot{\mathbf{r}}\times\boldsymbol{\nabla})_z A_y(\mathbf{r}) + e(\dot{\mathbf{r}}\times\boldsymbol{\nabla})_y A_z(\mathbf{r})\right\}\hat{\mathbf{e}}_x + (\hat{\mathbf{e}}_y \text{ term}) + (\hat{\mathbf{e}}_z \text{ term}) = 0 \\
&\left[m_e\ddot{x} + e\{(\dot{\mathbf{r}}\times\boldsymbol{\nabla})\times\mathbf{A}(\mathbf{r})\}_x\right]\hat{\mathbf{e}}_x + (\hat{\mathbf{e}}_y \text{ term}) + (\hat{\mathbf{e}}_z \text{ term}) = 0 \\
&m_e\ddot{\mathbf{r}} + e\dot{\mathbf{r}}\times(\boldsymbol{\nabla}\times\mathbf{A}(\mathbf{r})) = 0. \qquad (3.8)
\end{aligned}$$

Since the magnetic field $\mathbf{B}$ can be represented by vector potential $\mathbf{A}(\mathbf{r})$ as $\mathbf{B}(\mathbf{r}) = \boldsymbol{\nabla} \times \mathbf{A}(\mathbf{r})$, we can reproduce the motion of equation with the Lorentz force,

$$m_e \ddot{\mathbf{r}} + e\dot{\mathbf{r}} \times \mathbf{B}(\mathbf{r}) = 0. \tag{3.9}$$

We can describe the canonical (gauge-dependent) momentum as

$$\begin{aligned} \mathbf{p} &= \frac{\partial L}{\partial \dot{\mathbf{r}}} \\ &= m_e \dot{\mathbf{r}} - e\mathbf{A}(\mathbf{r}). \end{aligned} \tag{3.10}$$

3.1.3 Gauge Invariance

From the requirement that observables (e.g. magnetic field) are independent of gauge choice (so-called gauge invariant), we can define a gauge transformation of the vector potential as $\mathbf{A}' = \mathbf{A} + \boldsymbol{\nabla}\chi$, where χ is an arbitrary (gauge) function satisfying $\boldsymbol{\nabla} \times \boldsymbol{\nabla}\chi = 0$. Although the choice of the gauge function can arbitrarily be defined, it is useful to adopt the Coulomb gauge $\boldsymbol{\nabla} \cdot \mathbf{A} = 0$ in non-relativistic physics. However, we note that this gauge condition can not completely determine the gauge function.

It is known that two gauge choices are especially useful in quantum treatment of 2D-electron in the magnetic field. The first is the Landau gauge (e.g. for a rectangular sample),

$$\mathbf{A}_L = B(-y, 0, 0), \tag{3.11}$$

and another is the symmetric gauge (e.g. for a circular disk sample),

$$\mathbf{A}_S = \frac{B}{2}(-y, x, 0). \tag{3.12}$$

The gauge function which transforms between the two gauges is then obtained by

$$\begin{aligned} \boldsymbol{\nabla}\chi &= \mathbf{A}_S - \mathbf{A}_L \\ &= \frac{B}{2}(y, x, 0), \end{aligned} \tag{3.13}$$

that is

$$\chi = \frac{B}{2}xy. \tag{3.14}$$

The canonical momenta in equation (3.10) are not clearly gauge invariant. In contrast, the velocity $\dot{\mathbf{r}}$ must be gauge invariant. The gauge invariant momentum (or mechanical momenta) are thus given by

$$\boldsymbol{\Pi} \equiv m_e \dot{\mathbf{r}} = \mathbf{p} + e\mathbf{A}. \tag{3.15}$$

In particular, we can explicitly write it by components, $\boldsymbol{\eta} = \left(\eta_x, \eta_y\right) = \mathbf{r} - \mathbf{r}_0$,

$$\begin{aligned} \Pi_x &= -m_e\omega_c\eta_y, \\ \Pi_y &= m_e\omega_c\eta_x. \end{aligned} \tag{3.16}$$

3.1.4 Hamiltonian Formalism

The Hamiltonian for the electron gas under the magnetic field is derived from the Lagrangian (3.6) by a Legendre transformation,

$$\begin{aligned} H &= \mathbf{p}\cdot\dot{\mathbf{r}} - L \\ &= \frac{1}{2m_e}\left[\mathbf{p}+e\mathbf{A}\left(\mathbf{r}\right)\right]^2. \end{aligned} \tag{3.17}$$

When we use the relative variable (Larmor radius vector) $\boldsymbol{\eta}$, we can rewrite the Hamiltonian as

$$H = \frac{1}{2}m_e\omega_c^2\left(\eta_x^2+\eta_y^2\right), \tag{3.18}$$

where we note that the variable $\boldsymbol{\eta}$ is written by the variables in phase space $(\mathbf{r}, \mathbf{p})$ as

$$\begin{aligned} \eta_x &= \frac{1}{m_e\omega_c}\left[p_y + eA_y\left(\mathbf{r}\right)\right], \\ \eta_y &= -\frac{1}{m_e\omega_c}\left[p_x + eA_x\left(\mathbf{r}\right)\right], \end{aligned} \tag{3.19}$$

3.2 Landau-Quantized-Electron in Symmetric Gauge

As well-known, in quantum mechanics, the energy spectrum of an electron in two dimension under the magnetic field is quantized[47]. The quantized energy levels of two dimensional electron gas are given by $E_N = \hbar\omega_c\left(N+1/2\right)$, which usually appear by solving the Schrödinger equation in the Landau's gauge ($\mathbf{A}_L = B\left(-y,0,0\right)$), where $N = 0, 1, 2, \ldots$ is the LL index. However, to see the quantum selection rule of interaction of electron with optical vortex beam carrying the orbital angular momentum, the symmetric gauge in the cylindrical system becomes a natural choice. Then the electron angular momentum becomes good quantum number. We thus adopt the symmetric gauge,

$$\mathbf{A}^{\text{ext}}(\mathbf{r}) = \mathbf{A}_S = \left(-\frac{By}{2}, \frac{Bx}{2}, 0\right), \tag{3.20}$$

which gives the external magnetic field along z direction,

$$\begin{aligned}\mathbf{B}(\mathbf{r}) &= \boldsymbol{\nabla} \times \mathbf{A}^{\text{ext}}(\mathbf{r}) \\ &= \left(\frac{\partial A_y^{\text{ext}}}{\partial x} - \frac{\partial A_x^{\text{ext}}}{\partial y}\right)\hat{\mathbf{e}}_z \\ &= B. \end{aligned} \tag{3.21}$$

As discussed the previous section, the Hamiltonian of electron in the magnetic field along z direction is given by

$$H_0 = \frac{1}{2m_e}\left[-i\hbar\boldsymbol{\nabla} + e\mathbf{A}^{\text{ext}}(\mathbf{r})\right]^2 \quad (e > 0). \tag{3.22}$$

Here, we derive the commutation relation of the Hamiltonian H_0 with position operator $\mathbf{r}$,

$$\begin{aligned}[H_0, \mathbf{r}] &= H_0\mathbf{r} - \mathbf{r}H_0 \\ &= -\frac{i\hbar}{m_e}\left(-i\hbar\boldsymbol{\nabla} + e\mathbf{A}^{\text{ext}}(\mathbf{r})\right). \end{aligned} \tag{3.23}$$

This commutation relation is used for calculation of the matrix elements of interaction with optical vortex.

Before solving the Schrödinger equation, $H_0\Psi = E\Psi$, we describe the Hamiltonian (3.22) by Cartesian coordinates,

$$H_0 = \frac{\hbar^2}{2m_e}\left[\left(-i\frac{\partial}{\partial x} - \frac{eB}{2\hbar}y\right)^2 + \left(-i\frac{\partial}{\partial y} + \frac{eB}{2\hbar}x\right)^2 + \frac{\partial^2}{\partial z^2}\right]. \tag{3.24}$$

We can separate this Hamiltonian into 2D part, H_0^{2D}, and a plane wave part, H_0^{plane}, that is,

$$\begin{aligned} H_0 &= H_0^{\text{2D}} + H_0^{\text{plane}}, \\ H_0^{\text{2D}} &= \frac{\hbar^2}{2m_e}\left[\left(-i\frac{\partial}{\partial x} - \frac{eB}{2\hbar}y\right)^2 + \left(-i\frac{\partial}{\partial y} + \frac{eB}{2\hbar}x\right)^2\right], \\ H_0^{\text{plane}} &= \frac{\hbar^2}{2m_e}\frac{\partial^2}{\partial z^2}. \end{aligned} \tag{3.25}$$

By focusing on the 2D part H_0^{2D}, we can obtain the solution of two dimensional electron gas (2DEG) under the magnetic field, that is, that of Landau-quantized electrons. We will derive the eigenenergy and wavefunction step-by-step. We first introduce the magnetic length $l_B = \sqrt{\hbar/eB}$ and the cyclotron frequency $\omega_c = eB/m_e$,

$$H_0^{\text{2D}} = \frac{\hbar\omega_c}{2}\left[\left(-il_B\frac{\partial}{\partial x} - \frac{1}{2l_B}y\right)^2 + \left(-il_B\frac{\partial}{\partial y} + \frac{1}{2l_B}x\right)^2\right]. \tag{3.26}$$

We further introduce the dimensionless variables $\overline{x} = x/l_B$ and $\overline{y} = y/l_B$,

$$H_0^{\rm 2D} = \frac{\hbar\omega_c}{2}\left[-\left(\frac{\partial^2}{\partial\overline{x}^2}+\frac{\partial^2}{\partial\overline{y}^2}\right)+i\left(\overline{y}\frac{\partial}{\partial\overline{x}}-\overline{x}\frac{\partial}{\partial\overline{y}}\right)+\frac{1}{4}\left(\overline{x}^2+\overline{y}^2\right)\right]. \quad (3.27)$$

To derive the wavefunction and eigenenergy in cylindrical coordinates, we describe $\overline{x}$ and $\overline{y}$ by cylindrical coordinates,

$$\begin{aligned}\overline{x} &= \bar{\rho}\cos\phi,\\ \overline{y} &= \bar{\rho}\sin\phi,\end{aligned} \quad (3.28)$$

respectively, where $\bar{\rho} = \left(\overline{x}^2+\overline{y}^2\right)^{1/2}$ and $\phi = \arctan\left(\overline{y}/\overline{x}\right)$. Then the differential operators are written in the cylindrical coordinates as

$$\begin{aligned}\frac{\partial}{\partial\overline{x}} &= \cos\phi\frac{\partial}{\partial\bar{\rho}}-\frac{\sin\phi}{\bar{\rho}}\frac{\partial}{\partial\phi},\\ \frac{\partial}{\partial\overline{y}} &= \sin\phi\frac{\partial}{\partial\bar{\rho}}+\frac{\cos\phi}{\bar{\rho}}\frac{\partial}{\partial\phi},\\ \frac{\partial^2}{\partial\overline{x}^2}+\frac{\partial^2}{\partial\overline{y}^2} &= \frac{\partial^2}{\partial\bar{\rho}^2}+\frac{1}{\bar{\rho}}\frac{\partial}{\partial\bar{\rho}}+\frac{1}{\bar{\rho}^2}\frac{\partial^2}{\partial\phi^2},\\ \overline{y}\frac{\partial}{\partial\overline{x}}-\overline{x}\frac{\partial}{\partial\overline{y}} &= -\frac{\partial}{\partial\phi}.\end{aligned} \quad (3.29)$$

We can check these expressions as the followings. The variable transformations are given by

$$\begin{aligned}\frac{\partial\bar{\rho}}{\partial\overline{x}} &= \frac{\partial}{\partial\overline{x}}\left(\overline{x}^2+\overline{y}^2\right)^{1/2} = \frac{\overline{x}}{\bar{\rho}} = \cos\phi,\\ \frac{\partial\bar{\rho}}{\partial\overline{y}} &= \frac{\overline{y}}{\bar{\rho}} = \sin\phi,\\ \frac{\partial\phi}{\partial\overline{x}} &= \frac{\partial}{\partial\overline{x}}\left(\arctan\frac{\overline{y}}{\overline{x}}\right) = \frac{-\overline{y}}{\overline{x}^2+\overline{y}^2} = -\frac{\sin\phi}{\bar{\rho}},\\ \frac{\partial\phi}{\partial\overline{y}} &= \frac{\partial}{\partial\overline{y}}\left(\arctan\frac{\overline{y}}{\overline{x}}\right) = \frac{\overline{x}}{\overline{x}^2+\overline{y}^2} = \frac{\cos\phi}{\bar{\rho}}.\end{aligned} \quad (3.30)$$

The first two differential operators in Eq. (3.29) can be derived by

$$\begin{aligned}\frac{\partial}{\partial\overline{x}} &= \frac{\partial\bar{\rho}}{\partial\overline{x}}\frac{\partial}{\partial\bar{\rho}}+\frac{\partial\phi}{\partial\overline{x}}\frac{\partial}{\partial\phi}\\ &= \cos\phi\frac{\partial}{\partial\bar{\rho}}-\frac{\sin\phi}{\bar{\rho}}\frac{\partial}{\partial\phi},\\ \frac{\partial}{\partial\overline{y}} &= \frac{\partial\bar{\rho}}{\partial\overline{y}}\frac{\partial}{\partial\bar{\rho}}+\frac{\partial\bar{\rho}}{\partial\overline{y}}\frac{\partial}{\partial\phi}\\ &= \sin\phi\frac{\partial}{\partial\bar{\rho}}+\frac{\cos\phi}{\bar{\rho}}\frac{\partial}{\partial\phi}.\end{aligned} \quad (3.31)$$

And the last two differential operators in Eq. (3.29) can also be derived by

$$\begin{aligned}\frac{\partial^2}{\partial\overline{x}^2}+\frac{\partial^2}{\partial\overline{y}^2} &= \left(\cos\phi\frac{\partial}{\partial\bar{\rho}}-\frac{\sin\phi}{\bar{\rho}}\frac{\partial}{\partial\phi}\right)^2+\left(\sin\phi\frac{\partial}{\partial\bar{\rho}}+\frac{\cos\phi}{\bar{\rho}}\frac{\partial}{\partial\phi}\right)^2 \\ &= \frac{\partial^2}{\partial\bar{\rho}^2}+\frac{1}{\bar{\rho}}\frac{\partial}{\partial\bar{\rho}}+\frac{1}{\bar{\rho}^2}\frac{\partial^2}{\partial\phi^2},\end{aligned} \tag{3.32}$$

and

$$\begin{aligned}\overline{y}\frac{\partial}{\partial\overline{x}}-\overline{x}\frac{\partial}{\partial\overline{y}} &= \bar{\rho}\sin\phi\left(\cos\phi\frac{\partial}{\partial\bar{\rho}}-\frac{\sin\phi}{\bar{\rho}}\frac{\partial}{\partial\phi}\right)-\bar{\rho}\cos\phi\left(\sin\phi\frac{\partial}{\partial\bar{\rho}}+\frac{\cos\phi}{\bar{\rho}}\frac{\partial}{\partial\phi}\right) \\ &= -\frac{\partial}{\partial\phi}.\end{aligned} \tag{3.33}$$

We thus obtain the 2D part of Hamiltonian in the cylindrical coordinates,

$$H_0^{\mathrm{2D}}=\frac{\hbar\omega_c}{2}\left(-\frac{\partial^2}{\partial\bar{\rho}^2}-\frac{1}{\bar{\rho}}\frac{\partial}{\partial\bar{\rho}}-\frac{1}{\bar{\rho}^2}\frac{\partial^2}{\partial\phi^2}-i\frac{\partial}{\partial\phi}+\frac{1}{4}\bar{\rho}^2\right). \tag{3.34}$$

We will look for the solutions of the Schrödinger equation, $H_0^{\mathrm{2D}}\Psi\left(\bar{\rho},\phi\right)=E\Psi\left(\bar{\rho},\phi\right)$. For the angular part of Ψ, we use the 2π-periodic boundary condition,

$$\Psi(\bar{\rho},\phi)=\frac{1}{\sqrt{2\pi}}\mathrm{e}^{im\phi}R(\bar{\rho}),\ m=0,\pm1,\pm2,\cdots. \tag{3.35}$$

Then, we explicitly write the Schrödinger equation as a differential equation:

$$\frac{\partial^2R(\bar{\rho})}{\partial\bar{\rho}^2}+\frac{1}{\bar{\rho}}\frac{\partial R(\bar{\rho})}{\partial\bar{\rho}}+\left(2\varepsilon-\frac{m^2}{\bar{\rho}^2}-m-\frac{\bar{\rho}^2}{4}\right)R(\bar{\rho})=0, \tag{3.36}$$

where we denoted $\varepsilon=E/\hbar\omega_c$ for simplicity.

We should choice the natural boundary conditions for this equation:

1. $R(0)$ is finite.
2. $R(\bar{\rho})$ is continuous and smooth.
3. $R(\infty)$ is finite.

When we change the variable as $z=\bar{\rho}^2$, that is, $\bar{\rho}=\sqrt{z}$, we then have

$$\begin{aligned}R(\bar{\rho}) &= R(\sqrt{z})\equiv\widetilde{R}(z), \\ \frac{\partial R(\bar{\rho})}{\partial\bar{\rho}} &= \frac{\partial\widetilde{R}(z)}{\partial\bar{\rho}}=\frac{\partial\widetilde{R}(z)}{\partial z}\frac{\partial z}{\partial\bar{\rho}}=2\sqrt{z}\frac{\partial\widetilde{R}(z)}{\partial z}, \\ \frac{\partial^2R(\bar{\rho})}{\partial\bar{\rho}^2} &= \frac{\partial}{\partial\bar{\rho}}\left(2\bar{\rho}\frac{\partial\widetilde{R}(z)}{\partial z}\right)=4z\frac{\partial^2\widetilde{R}(z)}{\partial z^2}+2\frac{\partial\widetilde{R}(z)}{\partial z}.\end{aligned} \tag{3.37}$$

Thus, Eq. (3.36) can be rewritten by the variable change as

$$\frac{\partial^2 \widetilde{R}(z)}{\partial z^2} + \frac{1}{z}\frac{\partial \widetilde{R}(z)}{\partial z} + \left(\frac{\varepsilon}{2z} - \frac{m^2}{4z^2} - \frac{m}{4z} - \frac{1}{16}\right)\widetilde{R}(z) = 0. \tag{3.38}$$

Now, we consider the asymptotic behavior at $z = \infty$. In the limit $z \to \infty$, because of the condition 3, we have

$$\frac{\partial^2 \widetilde{R}(z)}{\partial z^2} - \frac{1}{16}\widetilde{R}(z) = 0. \tag{3.39}$$

Therefore, this equation has the solution like

$$\widetilde{R}(z) = C\mathrm{e}^{-\frac{z}{4}}, \tag{3.40}$$

where we introduced the constant of integration as C. Next, let us find the solution in the form $\widetilde{R}(z) = \mathrm{e}^{-\frac{z}{4}}\widetilde{w}(z)$. Then it satisfies

$$\begin{aligned}
\frac{\partial \widetilde{R}(z)}{\partial z} &= \mathrm{e}^{-\frac{z}{4}}\frac{\partial \widetilde{w}(z)}{\partial z} - \frac{1}{4}\mathrm{e}^{-\frac{z}{4}}\widetilde{w}(z), \\
\frac{\partial^2 \widetilde{R}(z)}{\partial z^2} &= \mathrm{e}^{-\frac{z}{4}}\frac{\partial^2 \widetilde{w}(z)}{\partial z^2} - \frac{1}{2}\mathrm{e}^{-\frac{z}{4}}\frac{\partial \widetilde{w}(z)}{\partial z} + \frac{1}{16}\mathrm{e}^{-\frac{z}{4}}\widetilde{w}(z).
\end{aligned} \tag{3.41}$$

Then, plugging these expressions into Eq. (3.38), we obtain a differential equation for $\widetilde{w}(z)$,

$$4z\frac{\partial^2 \widetilde{w}(z)}{\partial z^2} + (4 - 2z)\frac{\partial \widetilde{w}(z)}{\partial z} + \left(2\varepsilon - \frac{m^2}{z} - m - 1\right)\widetilde{w}(z) = 0. \tag{3.42}$$

Next, we consider $z \to 0$ case. Because of condition 1, choosing dominant factors in each term in Eq. (3.42), we obtain an equation as

$$4z^2\frac{\partial^2 \widetilde{w}(z)}{\partial z^2} + 4z\frac{\partial \widetilde{w}(z)}{\partial z} - m^2\widetilde{w}(z) = 0. \tag{3.43}$$

To solve Eq. (3.43), we take the solution in the form $\widetilde{w}(z) = z^\alpha$. Then, since it satisfies

$$\begin{aligned}
\frac{\partial \widetilde{w}(z)}{\partial z} &= \alpha z^{\alpha-1}, \\
\frac{\partial^2 \widetilde{w}(z)}{\partial z^2} &= \alpha(\alpha-1)z^{\alpha-2},
\end{aligned} \tag{3.44}$$

we obtain the solution α by plugging these expressions into Eq. (3.43) as the following:

$$4\alpha^2 - m^2 = 0,$$

which gives

$$\alpha = \pm\frac{|m|}{2}. \tag{3.45}$$

Since the solution $\alpha = -|m|/2$ diverges in the limit $z \to 0$, we must adopt the solution $\alpha = +|m|/2$.

Finally, let us find the solution in the form $\widetilde{w}(z) = z^{\frac{|m|}{2}} w(z)$, then it satisfies

$$\begin{aligned}
\frac{\partial \widetilde{w}(z)}{\partial z} &= \frac{|m|}{2} z^{\frac{|m|}{2}-1} w(z) + z^{\frac{|m|}{2}} \frac{\partial w(z)}{\partial z}, \\
\frac{\partial^2 \widetilde{w}(z)}{\partial z^2} &= z^{\frac{|m|}{2}} \frac{\partial^2 w(z)}{\partial z^2} + |m| z^{\frac{|m|}{2}-1} \frac{\partial w(z)}{\partial z} + \frac{|m|}{2}\left(\frac{|m|}{2} - 1\right) z^{\frac{|m|}{2}-2} w(z).
\end{aligned} \tag{3.46}$$

Plugging these expressions into Eq. (3.42), we then obtain

$$z\frac{\partial^2 w(z)}{\partial z^2} + \left(|m| + 1 - \frac{z}{2}\right)\frac{\partial w(z)}{\partial z} + \left(\frac{\varepsilon}{2} - \frac{m}{4} - \frac{|m|}{4} - \frac{1}{4}\right) w(z) = 0. \tag{3.47}$$

Replacing the variable $\overline{z} = \frac{z}{2}$, that is, $z = 2\overline{z}$, we have

$$\begin{aligned}
w(z) &= w(2\overline{z}) \equiv v(\overline{z}), \\
\frac{\partial w(z)}{\partial z} &= \frac{\partial v(\overline{z})}{\partial \overline{z}}\frac{\partial \overline{z}}{\partial z} = \frac{1}{2}\frac{\partial v(\overline{z})}{\partial \overline{z}}, \\
\frac{\partial^2 w(z)}{\partial z^2} &= \frac{1}{2}\frac{\partial}{\partial z}\frac{\partial v(\overline{z})}{\partial \overline{z}} = \frac{1}{4}\frac{\partial^2 v(\overline{z})}{\partial \overline{z}^2}.
\end{aligned} \tag{3.48}$$

Thus, plugging these expressions into Eq. (3.47), we finally obtain the equation for generalized Laguerre polynomials

$$\overline{z}\frac{\partial^2 v(\overline{z})}{\partial \overline{z}^2} + (|m| + 1 - \overline{z})\frac{\partial v(\overline{z})}{\partial \overline{z}} + \left(\varepsilon - \frac{|m| + m + 1}{2}\right) v(\overline{z}) = 0. \tag{3.49}$$

The solutions of the associated Laguerre equations which are bounded exist for

$$\begin{aligned}
\varepsilon - \frac{|m| + m + 1}{2} &= n, \ n = 0, 1, 2, \cdots, \\
v(\overline{z}) &= L_n^{|m|}(\overline{z}),
\end{aligned} \tag{3.50}$$

where the associated Laguerre polynomials $L_n^k(x)$ are related to the Laguerre polynomials $L_n(x)$ by $L_n^k(x) = (-1)^k \frac{d}{dx^k} L_{n+k}(x)$ with $k \geq 0$. We here sum-

marize variable notations,

$$\begin{aligned} z = \bar{\rho}^2 \text{ and } R(\bar{\rho}) &= \widetilde{R}(z) \\ \Downarrow & \\ \widetilde{R}(z) &= \mathrm{e}^{-\frac{z}{4}} \widetilde{w}(z) \\ \Downarrow & \\ \widetilde{w}(z) &= z^{\frac{|m|}{2}} w(z) \\ \Downarrow & \\ \overline{z} = \frac{z}{2} \text{ and } v(\overline{z}) &= w(z). \end{aligned} \tag{3.51}$$

Thus we obtain the the radial part of the wavefunction in the original notation ρ as

$$R(\bar{\rho}) = N\bar{\rho}^{|m|}\mathrm{e}^{-\frac{\bar{\rho}^2}{4}} L_n^{|m|}\left(\frac{\bar{\rho}^2}{2}\right), \tag{3.52}$$

that is,

$$R(\rho) = N \exp\left(-\frac{\rho^2}{4l_B^2}\right)\left(\frac{\rho}{l_B}\right)^{|m|} L_n^{|m|}\left(\frac{\rho^2}{2l_B^2}\right). \tag{3.53}$$

To determine the normalization constant, we use the orthonormality of $L_n^{(\alpha)}(x)$:

$$\int_0^\infty dx \mathrm{e}^{-x} x^\alpha L_n^{(\alpha)}(x) L_m^{(\alpha)}(x) = \frac{\Gamma(\alpha+n+1)}{n!}\delta_{nm} \tag{3.54}$$

and

$$\int_0^\infty d\rho\rho R(\rho)^2 = 1. \tag{3.55}$$

By calculating the normalization condition as the following,

$$\begin{aligned} 1 &= N^2 \int_0^\infty d\rho\rho \exp\left(-\frac{\rho^2}{2l_B^2}\right)\left(\frac{\rho}{l_B}\right)^{2|m|}\left[L_n^{|m|}\left(\frac{\rho^2}{2l_B^2}\right)\right]^2 \\ &= N^2 l_B^2 2^{|m|}\frac{\Gamma(n+|m|+1)}{n!}, \end{aligned} \tag{3.56}$$

we thus obtain the normalization constant

$$N = \left[\frac{n!}{(n+|m|)!}\right]^{\frac{1}{2}} \frac{1}{2^{\frac{|m|}{2}} l_B}. \tag{3.57}$$

We here summarize the normalized wave function for 2DEG,

$$E_{nm} = \hbar\omega_c \left(n + \frac{|m| + m}{2} + \frac{1}{2} \right), \tag{3.58}$$

$$n = 0, 1, 2, \cdots, \text{ and } m = 0, \pm 1, \pm 2, \cdots,$$

$$\Psi_{nm}(\rho, \phi) = \frac{1}{\sqrt{2\pi}} \mathrm{e}^{im\phi} R_{nm}(\rho), \tag{3.59}$$

$$R_{nm}(\rho) = N_{nm} \exp\left(-\frac{\rho^2}{4l_B^2} \right) \left(\frac{\rho}{l_B} \right)^{|m|} L_n^{|m|} \left(\frac{\rho^2}{2l_B^2} \right), \tag{3.60}$$

$$N_{nm} = \left[\frac{n!}{(n + |m|)!} \right]^{\frac{1}{2}} \frac{1}{2^{\frac{|m|}{2}} l_B}. \tag{3.61}$$

In two dimension, when we denote that m represents a magnetic quantum number, $|m|$ represents an azimuthal quantum number.

On the other hands, we consider the plane wave part H_0^{plane} or z-direction-dependent part. This describes the Hamiltonian that the electron travels along z direction as a plane wave. We assume the electron is in a cylinder with thickness d. By solving the Schrödinger equation with the Hamiltonian,

$$H_0^{\text{plane}} = \frac{\hbar^2}{2m_e} \frac{\partial^2}{\partial z^2}, \tag{3.62}$$

we obtain the plane wave solution as

$$\Psi_l(z) = \frac{1}{\sqrt{d}} \mathrm{e}^{ik_l z}, \tag{3.63}$$

$$E_l = \frac{\hbar^2 k_l^2}{2m_e} = \frac{\hbar^2}{2m_e} \left(\frac{l\pi}{d} \right)^2 \quad l = 0, \pm 1, \pm 2, \cdots. \tag{3.64}$$

By combining the solutions of H_0^{2D} and H_0^{plane}, we can obtain the three dimensional solution of a free electron in the magnetic field. Consequently, we arrive at the eigenvalue and eigenfunction of three dimensional electron gas in the external magnetic field,

$$\begin{aligned} E_{nml} &= E_{nm} + E_l \\ &= \hbar\omega_c \left(n + \frac{|m| + m}{2} + \frac{1}{2} \right) + \frac{\hbar^2}{2m_e} \left(\frac{l\pi}{d} \right)^2, \end{aligned} \tag{3.65}$$

$$\text{with } n = 0, 1, 2, \cdots, \ m = 0, \pm 1, \pm 2, \cdots, \text{ and } l = 0, \pm 1, \pm 2, \cdots,$$

$$\begin{aligned} \Psi_{nml}(\mathbf{r}) &= \Psi_{nm}(\rho, \phi) \Psi_l(z) \\ &= \frac{1}{\sqrt{d}} \Psi_{nm}(\rho, \phi) \mathrm{e}^{ik_l z}. \end{aligned} \tag{3.66}$$

When we consider the 2D system ($d \sim 0$), the excitation energy (energy difference) with respect to the state l reaches an infinite value. Therefore, as far as the low energy states are concerned, it is only necessary to consider $l = 0$.

3.3 Filling Factor and Degeneracy

Energy spectrum (3.65) shows that each LL has infinite degeneracy. It indicates that all electrons in the ground state belong to only the lowest energy level of (3.65). However, such a thing is not realistic. In the real-world, some electrons in the ground state should also belong to higher levels. This indicates that the infinite degeneracy is cut off by some kinds of parameter. We will resultingly show that the cutoff parameter is related to the number of area of one-electron states in the area of system, which gives the limitation of electron angular momentum in each LL. Accordingly, this cutoff parameter will well define a filling factor and a degeneracy of 2DEG. In this section, we precisely discuss a filling factor and a degeneracy of Landau levels.

To see the structure of degeneracy, it is good to see the relation of the energy spectrum (3.65) to the ordinary Landau levels

$$E_N = \hbar\omega_c \left(N + \frac{1}{2} \right), \quad N = 0, 1, 2, ... \tag{3.67}$$

Then the relation between of the ordinary Landau levels (3.67) and (3.58) is given by

$$N = n + \frac{|m| + m}{2}. \tag{3.68}$$

When we focus on the lowest Landau level ($N = 0$) (LLL), the relation (3.68) leads to

$$0 = n + \frac{|m| + m}{2}. \tag{3.69}$$

For $m \geq 0$, we have $n = m = 0$ because of $n \geq 0$. But, for $m < 0$, m can be taken an arbitrary negative integer in addition to $n = 0$. That is to say, there exists an infinite degeneracy. The LLL $N = 0$ is thus constructed by $n = 0$ and $m = -m' \leq 0$ (m' is a positive integer). Since the wave function in the LLL is given by

$$\psi_{0,-m'}(\rho, \phi) = \left(\frac{1}{2^{m'} m'!} \right)^{\frac{1}{2}} \frac{1}{l_B} \exp\left(-\frac{\rho^2}{4l_B^2} \right) \left(\frac{\rho}{l_B} \right)^{m'} \frac{\mathrm{e}^{-im'\phi}}{\sqrt{2\pi}}, \tag{3.70}$$

we obtain the existence probability, $P(\rho,\phi) = \rho|\psi_{0,-m'}(\rho,\phi)|^2$, as

$$P(\rho,\phi) = \frac{1}{2\pi 2^{m'} m'! l_B^{2m'+2}} \rho^{2m'+1} \exp\left(-\frac{\rho^2}{2l_B^2}\right). \tag{3.71}$$

Since differentiation of $P(\rho,\phi)$ with respect to ρ gives

$$\frac{\partial P(\rho,\phi)}{\partial \rho} = \frac{1}{2\pi 2^{m'} m'! l_B^{2m'+2}} \rho^{2m'} \exp\left(-\frac{\rho^2}{2l_B^2}\right)\left(2m'+1-\frac{\rho^2}{l_B^2}\right), \tag{3.72}$$

we find that the existence probability $P(\rho,\phi)$ has the maximal value at $\rho = \sqrt{2m'+1}l_B$. That is to say, electrons exist on the circle with radius $\sqrt{2m'+1}l_B$. Furthermore, we can evaluate the expectation value of ρ^2,

$$\begin{aligned}
\langle 0,-m'|\rho^2|0,-m'\rangle &= \int_0^{2\pi}\frac{d\varphi}{2\pi}\int_0^\infty \rho^3 d\rho \frac{1}{2^{m'}m'!l_B^2}\exp\left(-\frac{\rho^2}{2l_B^2}\right)\left(\frac{\rho}{l_B}\right)^{2m'} \\
&= \frac{1}{2^{m'}m'!l_B^{2+2m'}}\int_0^\infty \rho^{3+2m'}\exp\left(-\frac{\rho^2}{2l_B^2}\right)d\rho \\
&= 2(m'+1)l_B^2,
\end{aligned} \tag{3.73}$$

where we used a Gauss integral formula,

$$\int_0^\infty x^n \exp(-ax^2)dx = \frac{1}{2}\left(\frac{n-1}{2}\right)! a^{-\frac{n+1}{2}}. \tag{3.74}$$

Hence, when we consider a circular disk geometry with the area $S = \pi R^2$ with the radius R, the number of one-electron state in the LLL $N = 0$ is determined by $S/2\pi l_B^2$. Thus, the maximum of $|m|$ is limited by

$$|m| < m_{\max} = \text{floor}\left[\frac{1}{2}\left(\frac{R^2}{l_B^2}-1\right)\right] = \text{floor}\left[\frac{1}{2}\left(\frac{S}{\pi l_B^2}-1\right)\right], \tag{3.75}$$

where floor$[x]$ is a floor function. This indicates the maximum of $|m|$ is proportional to the size of system and the magnitude of the magnetic field. In general, the degeneracy is given by $m_{\max}+N$ for arbitrary N. Then, we can define a filling factor as

$$\nu \equiv \frac{N_e}{m_{\max}+N}, \tag{3.76}$$

where N_e is total number of electrons.

In condensed matter system, because $S \gg \pi l_B^2$, $m_{\max}$ would be satisfied, reduces to

$$m_{\max} \sim \text{floor}\left[\frac{R^2}{2l_B^2}\right] = \text{floor}\left[\frac{S}{2\pi l_B^2}\right]. \tag{3.77}$$

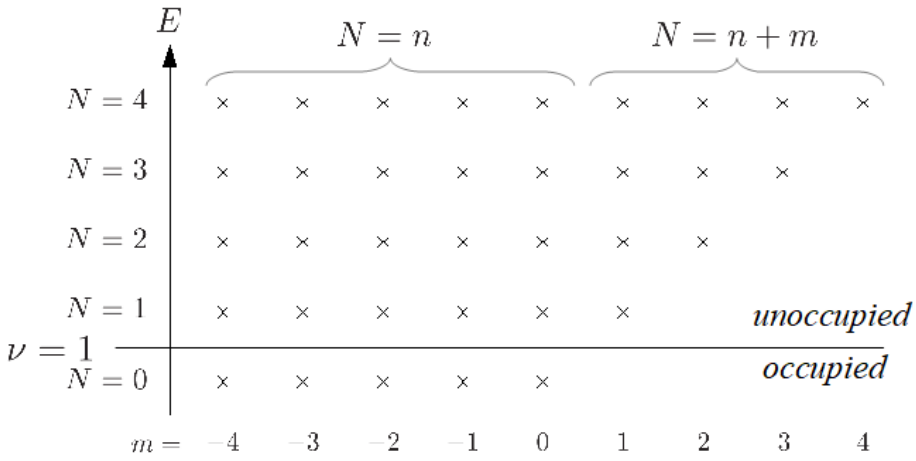

Figure 3.3: The illustration of the Landau levels in angular momentum picture. Crosses lined up along the horizontal line N describe the degenerated state in each Landau level N. The states under the line $\nu = 1$ are occupied and those above the line $\nu = 1$ are unoccupied.

And when we assume the low $N(\ll m_{\max})$, the filling factor is described by

$$\nu \sim \frac{N_e}{m_{\max}} \sim 2\pi l_B^2 \frac{N_e}{\pi R^2}. \tag{3.78}$$

For example, in the case of $\nu = 1$, the state $N = 0$ is occupied and its degeneracy is $R^2/2l_B^2$ in Fig. 3.3.

3.4 Density of States

In condensed matter physics, a density of states of a system plays important role to investigate the various physical properties of matter and is defined by the number of states per interval of energy at each energy level that are available to be occupied. Therefore, the density of states is closely related to the degeneracy of system. In the previous section, we discussed the degeneracy of 2DEG. In this section, we derive the density of state of the electron in magnetic field.

First, we consider the density of state in 3D system. The definition of the density of states in 3D system is given by

$$D(E) = \frac{1}{V} \sum_{\mathbf{k}} \delta(E - E(\mathbf{k})) \tag{3.79}$$

We here neglected the spin degree of freedom. Because our considering 3D-system is confined in a cylinder, the energy spectrum is discretized as Eq. (3.65). The density of states is then written by

$$D_{\mathrm{3D}}(E) = \frac{1}{V}\sum_{n=0}^{\infty}\sum_{m=-m_{\max}}^{\infty}\sum_{l=-\infty}^{\infty}\delta\left(E-\hbar\omega_c\left[n+\frac{|m|+m}{2}+\frac{1}{2}\right]+\frac{\hbar^2}{2m_e}\left[\frac{l\pi}{d}\right]^2\right). \tag{3.80}$$

We now transform indexes n, m into N, M as

$$N = n + \frac{|m|+m}{2}, \tag{3.81}$$

$$M = n + \frac{|m|-m}{2}. \tag{3.82}$$

Since the upper limit of M is then determined by the degeneracy in the state N, we see $N + m_{\max}$. Therefore, the density of states is described by

$$\begin{aligned} D_{\mathrm{3D}}(E) &= \frac{1}{V}\sum_{N=0}^{\infty}\sum_{l=-\infty}^{\infty}\sum_{M=0}^{N+m_{\max}}\delta\left(E-\hbar\omega_c\left[N+\frac{1}{2}\right]+\frac{\hbar^2}{2m_e}\left[\frac{l\pi}{d}\right]^2\right) \\ &= \frac{1}{V}\sum_{N=0}^{\infty}\sum_{l=-\infty}^{\infty}(N+m_{\max})\,\delta\left(E-\hbar\omega_c\left[N+\frac{1}{2}\right]+\frac{\hbar^2}{2m_e}\left[\frac{l\pi}{d}\right]^2\right) \\ &= \frac{1}{\nu}\frac{N_e}{V}\sum_{N=0}^{\infty}\sum_{l=-\infty}^{\infty}\delta\left(E-\hbar\omega_c\left[N+\frac{1}{2}\right]+\frac{\hbar^2}{2m_e}\left[\frac{l\pi}{d}\right]^2\right), \end{aligned} \tag{3.83}$$

where we used the filling factor ν given by (3.76) in the last step.

Next, when we consider 2D system ($d \ll R$), the density of states is then given by

$$D_{\mathrm{2D}}(E) = \frac{1}{\nu}\frac{N_e}{V}\sum_{N=0}^{\infty}\sum_{l=-\infty}^{\infty}\delta\left(E-\hbar\omega_c\left[N+\frac{1}{2}\right]\right). \tag{3.84}$$

In particular, assuming the LLL $N = 0$, we obtain

$$\begin{aligned} D_{\mathrm{2D}}(E) &= \frac{m_{\max}}{S}\delta\left(E-\frac{\hbar\omega_c}{2}\right) \\ &= \frac{1}{2\pi l_B^2}\delta\left(E-\frac{\hbar\omega_c}{2}\right). \end{aligned} \tag{3.85}$$

Thus the density of one-electron state is reproduced. At any rate, the density of states of 2DEG is described by δ-function. This is one of the remarkable features of 2DEG.

3.5 Effective Mass (Cyclotron Mass) of Electron

In condensed matter physics, an effective mass of particle is the mass that it seems to have when interacting with the particle's environment. For example, the motion of particles in a periodic potential is very different from their motion in a vacuum. The effective mass is a quantity that is introduced to simplify band structures by regarding the behavior of a particle in periodic potential as that of a free particle[48]. Thus, the effective mass can be seen as an important basic parameter that influences various properties of a solid. In general, the value of effective mass depends on the purpose for which it is used. Therefore, there are some definitions of the effective mass for some purposes and some materials. One of them is a cyclotron mass. As we consider the cyclotron motion of the electron which moves under the magnetic field, we will here discuss the cyclotron effective mass.

Classically, the electron in the magnetic field $\mathbf{B}$ is governed by the equation of motion,

$$\frac{\partial \mathbf{k}_e}{\partial t} = -\frac{e}{\hbar}\mathbf{v} \times \mathbf{B}, \tag{3.86}$$

where $\mathbf{v}$ is a velocity of electron. $\mathbf{k}_e$ changes on a Fermi surface perpendicular to the magnetic field. When the Fermi surface is closed, this equation represents the rotational motion of the electron. The integral of this equation then gives the period T

$$T = \frac{\hbar}{eB}\oint \frac{d\mathbf{k}_e}{|\mathbf{v}_\perp|}, \tag{3.87}$$

where $\mathbf{v}_\perp$ is the electron velocity perpendicular to the magnetic field. Since the velocity is given by

$$|\mathbf{v}_\perp| = \frac{1}{\hbar}\left|\left(\frac{\partial E}{\partial \mathbf{k}_e}\right)_\perp\right|, \tag{3.88}$$

the period is represented by

$$\begin{aligned} T &= \frac{\hbar^2}{eB}\oint \frac{d\mathbf{k}_e}{\left|\left(\frac{\partial E}{\partial \mathbf{k}_e}\right)_\perp\right|} \\ &= \frac{\hbar^2}{eB}\left(\frac{\partial}{\partial E}\oint |\mathbf{k}_e|\, d\mathbf{k}_e\right)_\perp . \end{aligned} \tag{3.89}$$

$\oint |\mathbf{k}_e|\, d\mathbf{k}_e$ is an area of the intersection of the energy surface in k-space, that is,

$$A(E) = \oint |\mathbf{k}_e|\, d\mathbf{k}_e. \tag{3.90}$$

It can be shown that the angular (cyclotron) frequency depends on the derivative of this area in energy. The angular frequency is then given by

$$\omega_c = \frac{2\pi eB}{\hbar^2} / \left| \left(\frac{\partial A}{\partial E} \right)_\perp \right|, \tag{3.91}$$

where the area A perpendicular to the magnetic field is given by

$$A_\perp = \pi k^{\perp 2}. \tag{3.92}$$

When we introduce the cyclotron effective electron mass m_e^*, the wavenumber in perpendicular plane to the magnetic field is related to dispersion relation as $E^\perp = \hbar^2 k^{\perp 2}/2m_e^*$. Consequently, we obtain

$$\left| \left(\frac{\partial A}{\partial E} \right)_\perp \right| = \frac{2\pi m_e^*}{\hbar^2}. \tag{3.93}$$

This leads to the definition of the cyclotron mass:

$$m_e^* = \frac{\hbar^2}{2\pi} \left| \left(\frac{\partial A}{\partial E} \right)_\perp \right|. \tag{3.94}$$

Consequently, by using (3.91), the angular cyclotron frequency is obtained as

$$\omega_c = \frac{eB}{m_e^*}, \tag{3.95}$$

which is the same form with the cyclotron frequency for a free electron mass in a vacuum m_e. By measuring the cyclotron frequency, we can know the cyclotron effective mass and the information of the Fermi surface. For example, the cyclotron electron mass of GaAs is known to be $m_e^* = 0.067 m_e$. As such experiments to measure the cyclotrons frequency, the cyclotron resonance, de Haas–van Alphen effect, etc. are known.

On the other hand, in quantum mechanics, when we compare the dispersion of free electron, $E = \hbar^2 k_e^2/2m_e^*$, to the energy spectrum (3.65), the Landau orbit in k-space in xy-plane (perpendicular to z axis) is described by a circle with a radius

$$k_{nm}^\perp = \sqrt{\frac{2eB}{\hbar} \left(n + \frac{|m| + m}{2} + \frac{1}{2} \right)}, \tag{3.96}$$

and the wavenumber in z-direction is given by

$$k_l^z = \frac{l\pi}{d}. \tag{3.97}$$

Now we assume that we distribute the electrons on 2D plane, which corresponds to very thin thickness d. Then the difference between arbitrary k_l^z becomes large and almost the Landau orbits belongs to the lowest wavenumber (energy) in z-direction, $k_0^z = 0$ (or $E_0^z = 0$) due to $l = 0$. Therefore, we can concentrate on the wavenumber in xy-plane. The area of orbital in k-space is then obtained as

$$\begin{aligned} A(E_{nm}) &= \pi k_{nm}^{\perp 2} \\ &= \frac{2\pi eB}{\hbar}\left(n + \frac{|m| + m}{2} + \frac{1}{2}\right). \end{aligned} \tag{3.98}$$

Since this area is discretized by n and m, it is known that $A(E_{nm})$ forms a Landau tube, which causes de Haas–van Alphen effect.

3.6 Coherent State of 2DEG in Cylindrical System

In quantum mechanics, since the electron's position and momentum are simultaneously undetermined because of the uncertainty principle, the electron's trajectory becomes uncertain. Therefore, to retrieve the electron's classical trajectory, we consider the semi-classical state, so-called coherent state, which is constructed by the eigenstate of the annihilation operator and minimizes the uncertainty relation, $\Delta x \Delta p = \hbar/2$.

In this section, we discuss how the classical motion of the electron in a circular disk geometry under the magnetic field is described by using the coherent state. The electron under the magnetic field exhibits the cyclotron motion, which produces a circular electric current. Considering how such circular electric currents are spread all over the circular disk geometry by superposition of the coherent states, we know the behavior of the total electric current. We will then show that the bulk currents are canceled out and only the edge current survives.

3.6.1 Second Quantization

Non-commutative Geometry

In this subsection, to construct the coherent states of electron under the magnetic field, we rebuild the theory by the second quantization approach. The reason is that the coherent states can be constructed by the eigenstate of the annihilation operator. After that, we review the construction of the wavefunction and their property.

We first introduce the commutation relation:

$$\begin{aligned}[x, p_x] = [y, p_y] = i\hbar, \\ [x, y] = [p_x, p_y] = [x, p_y] = [y, p_x] = 0,\end{aligned} \tag{3.99}$$

where $\hbar$ is a reduced Planck constant. By these commutation relations, we obtain the relation between the guiding center $\mathbf{r}_0$ and Larmor radius $\boldsymbol{\eta}$

$$\begin{aligned}0 &= [x, y] \\ &= [x_0, y_0] + \left[\eta_x, \eta_y\right],\end{aligned} \tag{3.100}$$

that is,

$$\left[\eta_x, \eta_y\right] = -\left[x_0, y_0\right]. \tag{3.101}$$

By help of the Larmor radius in phase space (3.19), the symmetric gauge (3.12), and the formula

$$\left[A, f\left(B\right)\right] = \frac{\partial f}{\partial B}\left[A, B\right], \tag{3.102}$$

which is valid for

$$[A, [A, B]] = [B, [A, B]] = 0, \tag{3.103}$$

we obtain the commutation relation of $\boldsymbol{\eta}$:

$$\begin{aligned}\left[\eta_x, \eta_y\right] &= -\frac{e}{m^2\omega_c^2}\left\{\left[p_y, A_x\left(y\right)\right] - \left[p_x, A_y\left(x\right)\right]\right\} \\ &= -\frac{e}{m^2\omega_c^2}\left\{\frac{\partial A_x\left(y\right)}{\partial y}\left[p_y, y\right] - \frac{\partial A_y\left(x\right)}{\partial x}\left[p_x, x\right]\right\} \\ &= -\frac{i\hbar}{eB} \\ &= -il_B,\end{aligned} \tag{3.104}$$

where we used the magnetic length $l_B = \sqrt{\hbar/eB}$. From the commutator (3.101), we also obtain the commutation relation of $\mathbf{r}_0$,

$$[x_0, y_0] = il_B. \tag{3.105}$$

We note that these results are gauge invariant.

Degeneracy and Filling Factor

From (3.104) and (3.105), we notice that the each component of variables $\boldsymbol{\eta}$ and $\mathbf{r}_0$ do not commute. Since we can easily check that the commutator of between the Hamiltonian (3.18) and $\mathbf{r}_0$ commutes:

$$[x_0, H] = [y_0, H] = 0, \tag{3.106}$$

we find that the guiding center $\mathbf{r}_0$ is degenerate and is a constant of motion. Therefore, at any level, each one-electron state occupies a minimal area by the uncertainty principle:

$$\Delta S = \Delta x_0 \Delta y_0 = 2\pi l_B^2. \tag{3.107}$$

The energetic degeneracy may thus be written in terms of this minimal area ΔS. That is to say, the number of states per a given energy level and per an unit area being

$$n_B = \frac{1}{\Delta S} = \frac{eB}{2\pi\hbar} = \frac{B}{\Phi_0}, \tag{3.108}$$

which is the flux density per the flux quantum, $\Phi_0 = h/e$. This result is another interpretation of degeneracy (3.75) and the filling factor (3.76).

Ladder Operators and Hamiltonian

As the commutation relations (3.104) and (3.105) have suggested, we can construct the ladder operators $\left(a, a^\dagger\right)$ for $\boldsymbol{\eta}$ and $\left(b, b^\dagger\right)$ for $\mathbf{r}_0$. First, we introduce the ladder operators $\left(a, a^\dagger\right)$,

$$\begin{aligned} a &= \frac{1}{\sqrt{2}l_B}\left(\eta_x - i\eta_y\right), \\ a^\dagger &= \frac{1}{\sqrt{2}l_B}\left(\eta_x + i\eta_y\right). \end{aligned} \tag{3.109}$$

Then, we can express the Larmor radius vector by (3.109) as

$$\begin{aligned} \eta_x &= \frac{l_B}{\sqrt{2}}\left(a^\dagger + a\right), \\ \eta_y &= \frac{l_B}{\sqrt{2}i}\left(a^\dagger - a\right). \end{aligned} \tag{3.110}$$

Similarly, we can introduce the ladder operators $\left(b, b^\dagger\right)$,

$$\begin{aligned} b &= \frac{1}{\sqrt{2}l_B}\left(x_0 + iy_0\right), \\ b^\dagger &= \frac{1}{\sqrt{2}l_B}\left(x_0 - iy_0\right), \end{aligned} \tag{3.111}$$

and express the guiding center vector $\mathbf{r}_0$ by (3.111)

$$\begin{aligned} x_0 &= \frac{l_B}{\sqrt{2}}\left(b^\dagger + b\right), \\ y_0 &= -\frac{l_B}{\sqrt{2}i}\left(b^\dagger - b\right). \end{aligned} \tag{3.112}$$

We here note that $\left[a, a^\dagger\right] = \left[b, b^\dagger\right] = 1$, and $\left[a, b^{(\dagger)}\right] = 0$. In terms of the ladder operators (3.110), the Hamiltonian is rewritten by

$$\begin{aligned} H &= \frac{1}{2} m\omega_c^2 \left(\eta_x^2 + \eta_y^2\right) \\ &= \hbar\omega_c \left(a^\dagger a + \frac{1}{2}\right). \end{aligned} \tag{3.113}$$

The energy spectrum is thus given by $E_n = \hbar\omega_c \left(N + \frac{1}{2}\right)$, where N is the eigenvalue of operator $a^\dagger a$.

In fact the system may formally be viewed as a system of two harmonic oscillators,

$$\begin{aligned} H &= \hbar\omega_c \left(a^\dagger a + \frac{1}{2}\right) + \hbar\omega' \left(b^\dagger b + \frac{1}{2}\right) \\ &= \hbar\omega_c \left(N + \frac{1}{2}\right) + \hbar\omega' \left(M + \frac{1}{2}\right), \end{aligned} \tag{3.114}$$

where we introduced the second quantum number M which is the eigenvalue $b^\dagger b$. However, we note that the frequency of the second oscillator must vanishes, $\omega' = 0$, because the guiding center $\mathbf{r}_0$ is degenerate (a constant of motion).

The creation operator $a^\dagger(b^\dagger)$ works to increase the quantum number $N(M)$ by one. On the other hand, the annihilation operator $a(b)$ works to decrease the quantum number $N(M)$ by one. Thus, the eigenstates are assigned by the two quantum numbers, N and M. By the requirements of the normalization condition $\langle N, M|N, M\rangle = 1$, the eigenstates associated with the two species of ladder operators are determined by

$$\begin{aligned} &a^\dagger|N, M\rangle = \sqrt{N+1}|N+1, M\rangle, \qquad a|N, M\rangle = \sqrt{N}|N-1, M\rangle \quad \text{for } N > 0; \\ &b^\dagger|N, M\rangle = \sqrt{M+1}|N, M+1\rangle, \qquad b|N, M\rangle = \sqrt{M}|N, M-1\rangle \quad \text{for } M > 0. \end{aligned} \tag{3.115}$$

In particular, when the annihilation operator $a(b)$ works on the state $N = 0(M = 0)$, it breaks the state vector,

$$a|0, M\rangle = 0 \qquad (b|N, 0\rangle = 0)\,. \tag{3.116}$$

Then, the negative numbers $N, M < 0$ are prohibited.

By applying the creation operators to the ground state $|0, 0\rangle$, we can construct an arbitrary state $|N, M\rangle$,

$$|N, M\rangle = \frac{\left(a^\dagger\right)^N}{\sqrt{N!}} \frac{\left(b^\dagger\right)^M}{\sqrt{M!}} |0, 0\rangle. \tag{3.117}$$

We note that the wave functions in real space depend on the gauge choice of the vector potential.

Wave Functions in Symmetric Gauge

Although we have already derived the 2DEG wave function in symmetric gauge, we briefly review the construction of the real space representation of eigenstates, $\phi_{N,M}(x,y) = \langle x, y|N, M\rangle$, via the ladder operators (3.109) and (3.111)[49]. When we choose the symmetric gauge, $\mathbf{A}^{\text{ext}} = (B/2)(-y, x, 0)$, With the help of (3.15), and (3.110), the ladder operators (3.109) can be represented as

$$\begin{aligned} a &= \sqrt{2}\left\{\frac{1}{4l_B}(x - iy) + \frac{l_B}{2}(\partial_x - i\partial_y)\right\} \\ &= \sqrt{2}\left(\frac{z}{4l_B} + l_B\partial_{z^*}\right), \end{aligned} \tag{3.118}$$

and

$$\begin{aligned} a^\dagger &= \sqrt{2}\left\{\frac{1}{4l_B}(x + iy) - \frac{l_B}{2}(\partial_x + i\partial_y)\right\} \\ &= \sqrt{2}\left(\frac{z^*}{4l_B} - l_B\partial_z\right). \end{aligned} \tag{3.119}$$

Similarly, the ladder operators (3.111) can also be represented as

$$\begin{aligned} b &= \sqrt{2}\left\{\frac{l_B}{2}(\partial_x + i\partial_y) + \frac{1}{4l_B}(x + iy)\right\} \\ &= \sqrt{2}\left(\frac{z^*}{4l_B} + l_B\partial_z\right), \end{aligned} \tag{3.120}$$

and

$$\begin{aligned} b^\dagger &= \sqrt{2}\left\{\frac{1}{4l_B}(x - iy) - \frac{l_B}{2}(\partial_x - i\partial_y)\right\} \\ &= \sqrt{2}\left(\frac{z}{4l_B} - l_B\partial_{z^*}\right), \end{aligned} \tag{3.121}$$

where we introduced the electron position in the complex plane as $z = x - iy$ and the differential operator with respect to z as $\partial_z = (\partial_x + i\partial_y)/2$, and $z^* = x + iy$ and $\partial_{z^*} = (\partial_x - i\partial_y)/2$ are their complex conjugate.

We here note on the choice of sign of the imaginary part. At a glance, this choice seems to be unnatural. However, it is convenient for negatively

charged particle, for example, electrons. Because the negatively charged particle under the magnetic field along z axis rotates "clockwise" about z axis. In contrast, the positively charged particle then rotates "counterclockwise" about z axis. It is thus natural to describe the position of positively charged particle as $z^* = x + iy$. In other words, the difference of the sign of particle charge reflects the handedness of the rotation and corresponds to the sign of the imaginary part.

Since applying the annihilation operator a to the LLL state ($N = 0$) breaks the state vector as the expression of (3.116), the wave function in the LLL is thus determined by the differential equation,

$$\left(z + 4l_B^2 \partial_{z^*}\right) \phi_{N=0}(z, z^*) = 0. \tag{3.122}$$

Although the solution of this equation is a Gauss function, there is an arbitrary factor being an analytic function $f(z)$ with $\partial_{z^*} f(z) = 0$,

$$\phi_{N=0}(z, z^*) = f(z) \mathrm{e}^{-|z|^2/4l_B^2}. \tag{3.123}$$

On the other hand, we can find the differential equation for the state with $M = 0$,

$$\left(z^* + 4l_B^2 \partial_z\right) \phi_{M=0}(z, z^*) = 0. \tag{3.124}$$

This equation has the solution such as

$$\phi_{M=0}(z, z^*) = g(z^*) \mathrm{e}^{-|z|^2/4l_B^2}, \tag{3.125}$$

where $g(z^*)$ is the anti-analytic function with $\partial_z g(z^*) = 0$. Therefore, the state with $N = 0$ and $M = 0$ must thus have a factor satisfying both analytic and anti-analytic condition. Such a factor is only a constant. Thus the wave function with $N = 0$ and $M = 0$ is written by $\phi_{N=0,M=0}(z, z^*) = C\mathrm{e}^{-|z|^2/4l_B^2}$, where C is a normalization constant. Since the normalization constant is given by $C = 1/l_B\sqrt{2\pi}$, we obtain the normalized solution,

$$\phi_{N=0,M=0}(z, z^*) = \frac{1}{l_B\sqrt{2\pi}} \mathrm{e}^{-|z|^2/4l_B^2}. \tag{3.126}$$

By multiplying M pieces of the creation operator $b^\dagger$ to (3.126), we can construct a wave function corresponding to the quantum number M in the LLL. By using (3.121) and $\partial_{z^*} \mathrm{e}^{-|z|^2/4l_B^2} = -z\mathrm{e}^{-|z|^2/4l_B^2}/4l_B^2$, we obtain the

wave function with $N = 0$ and M,

$$\begin{aligned}\phi_{N=0,M}(z,z^*) &= \frac{\left(b^\dagger\right)^M}{\sqrt{M!}}\phi_{N=0,M=0}(z,z^*) \\ &= \sqrt{\frac{2^M}{M!}}\left(\frac{z}{4l_B} - l_B\partial_{z^*}\right)^M \frac{1}{\sqrt{2\pi}l_B}\mathrm{e}^{-|z|^2/4l_B^2} \\ &= \frac{1}{l_B\sqrt{2\pi M!}}\left(\frac{z}{\sqrt{2}l_B}\right)^M \mathrm{e}^{-|z|^2/4l_B^2}. \end{aligned} \tag{3.127}$$

Similarly, by multiplying N pieces of the creation operator $b^\dagger$ to (3.126), we can construct a wave function corresponding to the quantum number N in the state $M = 0$ as

$$\begin{aligned}\phi_{N,M=0}(z,z^*) &= \frac{\left(a^\dagger\right)^N}{\sqrt{N!}}\phi_{N=0,M=0}(z,z^*) \\ &= \sqrt{\frac{2^N}{N!}}\left(\frac{z^*}{4l_B} - l_B\partial_z\right)^N \frac{1}{\sqrt{2\pi}l_B}\mathrm{e}^{-|z|^2/4l_B^2} \\ &= \frac{1}{l_B\sqrt{2\pi N!}}\left(\frac{z^*}{\sqrt{2}l_B}\right)^N \mathrm{e}^{-|z|^2/4l_B^2}, \end{aligned} \tag{3.128}$$

where we used (3.119) and $\partial_z \mathrm{e}^{-|z|^2/4l_B^2} = -z^*\mathrm{e}^{-|z|^2/4l_B^2}/4l_B^2$. An arbitrary state is thus written by

$$\begin{aligned}\phi_{N,M}(z,z^*) &= \frac{1}{l_B}\sqrt{\frac{2^M}{2\pi N!M!}}\left(\frac{z}{4l_B} - l_B\partial_{z^*}\right)^M \left(\frac{z^*}{\sqrt{2}l_B}\right)^N \mathrm{e}^{-|z|^2/4l_B^2} \\ &= \frac{1}{l_B}\sqrt{\frac{2^M}{2\pi N!M!}}\mathrm{e}^{i(N-M)\arg z^*}\mathrm{e}^{-|z|^2/4l_B^2}\left(\frac{|z|^2}{l_B^2}\right)^{|M-N|/2} \\ &\quad \times L^{|M-N|}_{(N+M-|M-N|)/2}\left(\frac{|z|^2}{2l_B^2}\right), \end{aligned} \tag{3.129}$$

where $L_n^m(x)$ is the associated Laguerre polynomials. Since $|z| = \rho$ and $\arg z^* = \phi$, we can again obtain the wave function in cylindrical coordinates (3.59) except for indexes.

Angular Momentum Operator

The z-component of the angular momentum operator is defined by

$$\hat{L}_z = x\hat{p}_y - \hat{p}_x y. \tag{3.130}$$

We describe this eigenvalue via the ladder operators. We first note that the mechanical momentum relates to the Larmor radius $\boldsymbol{\eta}$,

$$\begin{aligned} m\dot{x} &= p_x + eA_x = -m\omega_c \eta_y, \\ m\dot{y} &= p_y + eA_y = m\omega_c \eta_x. \end{aligned} \tag{3.131}$$

We then rewrite the angular momentum operator as

$$\hat{L}_z = x\left(m\omega_c \eta_x - eA_y\right) - \left(-m\omega_c \eta_y - eA_x\right) y. \tag{3.132}$$

By using the symmetric gauge (3.12) and the guiding center $\mathbf{r}_0 = \mathbf{r} - \boldsymbol{\eta}$, we can write the angular momentum operator as

$$\hat{L}_z = \frac{1}{2} m\omega_c \left[\left(\eta_x^2 + \eta_y^2\right) - \left(x_0^2 + y_0^2\right)\right].$$

Now, we further use the ladder operators (3.110) and (3.112). Since they give

$$\eta_x^2 + \eta_y^2 = 2l_B^2 \left(a^\dagger a + \frac{1}{2}\right), \tag{3.133}$$

$$x_0^2 + y_0^2 = 2l_B^2 \left(b^\dagger b + \frac{1}{2}\right), \tag{3.134}$$

we obtain the angular momentum operator by the ladder operators,

$$\hat{L}_z = \hbar \left[a^\dagger a - b^\dagger b\right]. \tag{3.135}$$

Because $a^\dagger a$ and $b^\dagger b$ are number operators corresponding to N and M, the eigenvalue of the angular momentum can be described by N and M,

$$L_z = (N - M)\hbar. \tag{3.136}$$

In contrast, the analytically derived wavefunction (3.59) leads to the angular momentum by its operator $L_z = i\frac{\partial}{\partial \phi}$,

$$L_z = m\hbar. \tag{3.137}$$

On the other hand, we see the correspondence of energy eigenvalue. LL derived by the ladder operators is

$$E = \hbar\omega_c \left(N + \frac{1}{2}\right), \tag{3.138}$$

and that analytically derived is

$$E = \hbar\omega_c \left(n + \frac{|m| + m}{2} + \frac{1}{2} \right). \tag{3.139}$$

We thus find that the relation of indexes (n, m) and (N, M) is given by

$$N = n + \frac{|m| + m}{2}, \tag{3.140}$$

$$M = n + \frac{|m| - m}{2}. \tag{3.141}$$

Guiding Center and Larmor Radius

To see the orbital structure of the electron under the magnetic field, it is worth to see the average value of the guiding center and Larmor radius and the absolute value of them. We first compute the average value of the guiding center operator as

$$\begin{aligned} \langle N, M|\mathbf{r}_0|N, M\rangle &= \langle N, M|x_0|N, M\rangle \hat{\mathbf{e}}_x + \langle N, M|y_0|N, M\rangle \hat{\mathbf{e}}_y \\ &= \frac{l_B}{\sqrt{2}} \langle N, M| \left(b^\dagger + b\right) |N, M\rangle \hat{\mathbf{e}}_x \\ &- \frac{l_B}{\sqrt{2}i} \langle N, M| \left(b^\dagger - b\right) |N, M\rangle \hat{\mathbf{e}}_y \\ &= 0, \end{aligned} \tag{3.142}$$

but the absolute value of it is given by

$$\begin{aligned} \langle |\mathbf{r}_0| \rangle_{N,M} &\equiv \sqrt{\langle N, M \left| x_0^2 + y_0^2 \right| N, M\rangle} \\ &= l_B \sqrt{\langle N, M \left| 2b^\dagger b + 1 \right| N, M\rangle} \\ &= l_B \sqrt{2M + 1}. \end{aligned} \tag{3.143}$$

This means that the particle's guiding center is located on the circle of radius $l_B\sqrt{2M+1}$, but the phase is undetermined.

On the other hand, the average value of Larmor radius operator gives

$$\langle N, M \left| \boldsymbol{\eta} \right| N, M\rangle = 0, \tag{3.144}$$

but its absolute value is given by

$$\langle |\boldsymbol{\eta}| \rangle_{N,M} \equiv \sqrt{\langle N, M \left| \boldsymbol{\eta}^2 \right| N, M\rangle} = l_B \sqrt{2N + 1}. \tag{3.145}$$

Therefore, we find that the arbitrary state $|N, M\rangle$ distributes at the center of the Larmor motion with radius $\langle|\boldsymbol{\eta}|\rangle_{N,M}$ located at the position of guiding center $\langle|\mathbf{r}_0|\rangle_{N,M}$. The geometric meaning of this is illustrated in Fig. 3.4[50]. In particular, when we focus on the LLL, that is, $n = 0$ and $m \leq 0$, we see $N = 0$ and $M = |m|$. The guiding center in the LLL is then $\langle|\mathbf{r}_0|\rangle_{0,|m|} = l_B\sqrt{2\,|m|+1}$, and the Larmor radius is $\langle|\boldsymbol{\eta}|\rangle_{0,|m|} = l_B$.

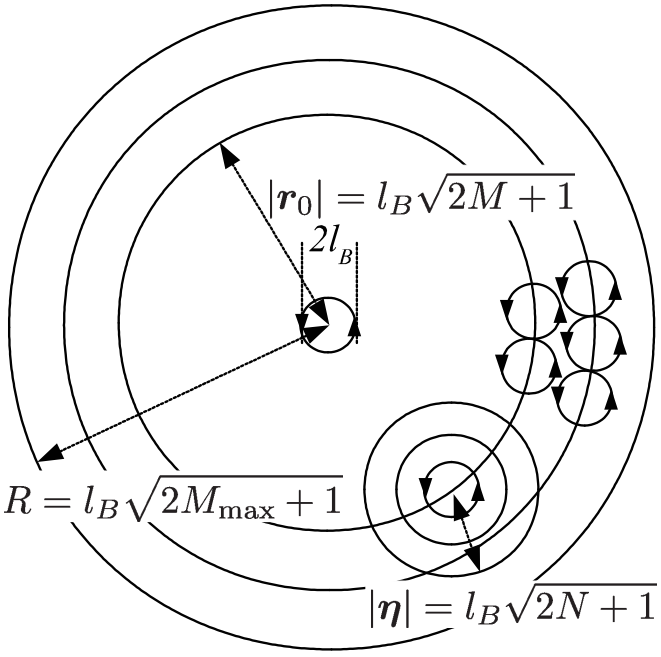

Figure 3.4: Schematics of the classical orbits of Landau levels. The quantum number M assigns the radius of the guiding center $|\mathbf{r}_0|$, whereas N is the radius of Larmor orbit $|\boldsymbol{\eta}|$.

3.6.2 Coherent States and Semi-Classical Motion

To reproduce the classical trajectory (3.5) as shown in previous section, we must construct semi-classical states, so-called coherent states. The coherent states are the specific quantum states of the quantum harmonic oscillator. And it is known that the coherent states often describes the oscillatory behavior of a classical harmonic oscillator, which is the motion of a particle confined in a quadratic potential well. The coherent states are concerned with a displacement of the ground-state wavepacket from the origin of the system. This displacement is equivalent to an amplitude of a particle oscillating. The

coherent states are expressed as eigenvectors of the annihilation operator and forming an overcompleteness and minimum uncertainty states[51].

In general, a displacement operator can be constructed from a pair of non-commutative operator. In case of Landau-quantized 2DEG, as we have seen, two pairs of non-commutative conjugate operators are introduced,

$$[\hat{x}_0, \hat{y}_0] = il_B^2, \tag{3.146}$$
$$\left[\hat{\eta}_x, \hat{\eta}_y\right] = -il_B^2, \tag{3.147}$$

where the symbol with hats intends operator in this section. We can introduce two types of the displacement operator which act in real space,

$$D\left(x_0, y_0\right) = \mathrm{e}^{-i(x_0\hat{y}_0 - y_0\hat{x}_0)/l_B^2}, \tag{3.148}$$
$$\tilde{D}\left(\eta_0^x, \eta_0^y\right) = \mathrm{e}^{i\left(\eta_0^x\hat{\eta}_y - \eta_0^y\hat{\eta}_x\right)/l_B^2}. \tag{3.149}$$

The first operator (3.148) displaces the position of the guiding center to $\mathbf{r}_0 = (x_0, y_0)$ as

$$\begin{aligned} D^\dagger\left(x_0, y_0\right)\hat{x}_0 D\left(x_0, y_0\right) &= \mathrm{e}^{i(x_0\hat{y}_0 - y_0\hat{x}_0)/l_B^2}\hat{x}_0\mathrm{e}^{-i(x_0\hat{y}_0 - y_0\hat{x}_0)/l_B^2} \\ &= \mathrm{e}^{ix_0\hat{y}_0/l_B^2}\hat{x}_0\mathrm{e}^{-ix_0\hat{y}_0/l_B^2} \\ &= \mathrm{e}^{ix_0\hat{y}_0/l_B^2}\left\{\mathrm{e}^{-ix_0\hat{y}_0/l_B^2}\hat{x}_0 + \frac{\partial \mathrm{e}^{-ix_0\hat{y}_0/l_B^2}}{\partial\hat{y}_0}\left[\hat{x}_0, \hat{y}_0\right]\right\} \\ &= \hat{x}_0 + x_0, \end{aligned} \tag{3.150}$$

and

$$D^\dagger\left(x_0, y_0\right)\hat{y}_0 D\left(x_0, y_0\right) = \hat{y}_0 + y_0, \tag{3.151}$$

where we used the formula

$$\left[A, f\left(B\right)\right] = \frac{\partial f}{\partial B}\left[A, B\right]. \tag{3.152}$$

Similarly, the second operator (3.149) displaces the Larmor radius vector to position $\boldsymbol{\eta}_0 = (\eta_0^x, \eta_0^y)$ as

$$\begin{aligned} \tilde{D}^\dagger\left(\eta_0^x, \eta_0^y\right)\hat{\eta}_x\tilde{D}\left(\eta_0^x, \eta_0^y\right) &= \hat{\eta}_x + \eta_0^x, \\ \tilde{D}^\dagger\left(\eta_0^x, \eta_0^y\right)\hat{\eta}_y\tilde{D}\left(\eta_0^x, \eta_0^y\right) &= \hat{\eta}_y + \eta_0^y. \end{aligned} \tag{3.153}$$

Since the guiding center is a constant of motion, the displacement operator $D\left(x_0, y_0\right)$ commutes with the Hamiltonian and does not change the quantum number N. Thus the coherent state in the LLL is represented by

$$\left|x_0, y_0; N = 0\right\rangle = D\left(x_0, y_0\right)\left|0, 0\right\rangle, \tag{3.154}$$

where $|0,0\rangle = |N=0, M=0\rangle$. The state $|x_0, y_0; N=0\rangle$ remains an eigenstate of the Hamiltonian. The dynamics enters with this displacement operator (3.149).

Therefore, the general semi-classical state can be written by these two displacement operators (3.148) and (3.149),

$$|x_0, y_0; \eta_0^x, \eta_0^y\rangle = \tilde{D}\left(\eta_0^x, \eta_0^y\right) D\left(x_0, y_0\right) |0,0\rangle. \tag{3.155}$$

The physical meaning of this operation is that the guiding center is centered at $\mathbf{r}_0 = (x_0, y_0)$, and the electron turns around on a circle with radius $|\boldsymbol{\eta}_0|$. We can describe thus the motion illustrated on Fig. 3.2 by a displacement of a Gaussian wave packet.

We check the average values of the guiding center operator for the coherent states:

$$\begin{aligned}
&\langle x_0, y_0; \eta_0^x, \eta_0^y \left|\hat{x}_0\right| x_0, y_0; \eta_0^x, \eta_0^y\rangle \\
&= \left\langle 0,0 \left| D^\dagger\left(x_0, y_0\right) \tilde{D}^\dagger\left(\eta_0^x, \eta_0^y\right) \hat{x}_0 \tilde{D}\left(\eta_0^x, \eta_0^y\right) D\left(x_0, y_0\right) \right| 0,0 \right\rangle \\
&= \left\langle 0,0 \left| D^\dagger\left(x_0, y_0\right) \hat{x}_0 D\left(x_0, y_0\right) \right| 0,0 \right\rangle \\
&= \langle 0,0 \left|\left(\hat{x}_0 + x_0\right)\right| 0,0\rangle \\
&= x_0,
\end{aligned} \tag{3.156}$$

$$\langle x_0, y_0; \eta_0^x, \eta_0^y \left|\hat{y}_0\right| x_0, y_0; \eta_0^x, \eta_0^y\rangle = y_0. \tag{3.157}$$

This means that the guiding center is positioned at $\mathbf{r}_0 = (x_0, y_0)$,

$$\langle x_0, y_0; \eta_0^x, \eta_0^y \left|\hat{\mathbf{r}}_0\right| x_0, y_0; \eta_0^x, \eta_0^y\rangle = \mathbf{r}_0. \tag{3.158}$$

On the other hand, the average value of the Larmor radius for the coherent states is similarly given by

$$\langle x_0, y_0; \eta_0^x, \eta_0^y \left|\hat{\boldsymbol{\eta}}\right| x_0, y_0; \eta_0^x, \eta_0^y\rangle = \boldsymbol{\eta}_0. \tag{3.159}$$

A coherent state is an eigenstate of the ladder operators a and b in our case. To find the eigenvalues, we first show that the displacement operators $D\left(x_0, y_0\right)$ and $\tilde{D}\left(\eta_0^x, \eta_0^y\right)$ are represented by these ladder operators $\left(a, a^\dagger\right)$ and $\left(b, b^\dagger\right)$,

$$\begin{aligned}
D\left(x_0, y_0\right) &= \exp\left(\frac{1}{\sqrt{2} l_B}\left\{\left(x_0 + i y_0\right) b^\dagger - \left(x_0 - i y_0\right) b\right\}\right) \\
&= \exp\left(\beta b^\dagger - \beta^* b\right) \\
&= \mathrm{e}^{\beta b^\dagger} \mathrm{e}^{-\beta^* b} \mathrm{e}^{\left[\beta b^\dagger, \beta^* b\right]/2} \\
&= \mathrm{e}^{-|\beta|^2/2} \mathrm{e}^{\beta b^\dagger} \mathrm{e}^{-\beta^* b},
\end{aligned} \tag{3.160}$$

and

$$\begin{aligned}\tilde{D}\left(\eta_0^x, \eta_0^y\right) &= \exp\left(\frac{1}{\sqrt{2}l_B}\left\{\left(\eta_0^x - i\eta_0^y\right)a^\dagger - \left(\eta_0^x + i\eta_0^y\right)a\right\}\right) \\ &= \exp\left(\alpha a^\dagger - \alpha^* a\right) \\ &= \mathrm{e}^{-|\alpha|^2/2}\mathrm{e}^{\alpha a^\dagger}\mathrm{e}^{-\alpha^* a}, \end{aligned} \tag{3.161}$$

where we defined

$$\alpha = \frac{1}{\sqrt{2}l_B}\left(\eta_0^x - i\eta_0^y\right), \tag{3.162}$$

$$\beta = \frac{1}{\sqrt{2}l_B}\left(x_0 + iy_0\right). \tag{3.163}$$

(We here comment the usage of a character α. We require attention to the difference from the definition of α in Chapter 2 with (3.162). Only in this Chapter, we will use (3.162) as the definition of α.) and used the Baker-Hausdorff formula

$$\mathrm{e}^{A+B} = \mathrm{e}^A\mathrm{e}^B\mathrm{e}^{-[A,B]/2}, \tag{3.164}$$

which valid when $[A,[A,B]] = [B,[A,B]] = 0$. Therefore, we can rewrite the coherent state as

$$\begin{aligned}|x_0, y_0; \eta_0^x, \eta_0^y\rangle &= \tilde{D}\left(\eta_0^x, \eta_0^y\right) D\left(x_0, y_0\right)|0,0\rangle \\ &= \mathrm{e}^{-\left(|\alpha|^2+|\beta|^2\right)/2}\mathrm{e}^{\alpha a^\dagger}\mathrm{e}^{\beta b^\dagger}|0,0\rangle. \end{aligned} \tag{3.165}$$

By applying the annihilation operator to this expression, we can find the eigenvalue of it. First, when we apply the operator a, we find

$$\begin{aligned}a|x_0, y_0; \eta_0^x, \eta_0^y\rangle &= \mathrm{e}^{-\left(|\alpha|^2+|\beta|^2\right)/2}\left[a, \mathrm{e}^{\alpha a^\dagger}\right]\mathrm{e}^{\beta b^\dagger}|0,0\rangle \\ &= \mathrm{e}^{-\left(|\alpha|^2+|\beta|^2\right)/2}\frac{\partial \mathrm{e}^{\alpha a^\dagger}}{\partial a^\dagger}\left[a, a^\dagger\right]\mathrm{e}^{\beta b^\dagger}|0,0\rangle \\ &= \alpha\mathrm{e}^{-\left(|\alpha|^2+|\beta|^2\right)/2}\mathrm{e}^{\alpha a^\dagger}\mathrm{e}^{\beta b^\dagger}|0,0\rangle \\ &= \alpha|x_0, y_0; \eta_0^x, \eta_0^y\rangle, \end{aligned} \tag{3.166}$$

and for the operator b, we similarly find

$$\begin{aligned}b|x_0, y_0; \eta_0^x, \eta_0^y\rangle &= \mathrm{e}^{-\left(|\alpha|^2+|\beta|^2\right)/2}\mathrm{e}^{\alpha a^\dagger}\left[b, \mathrm{e}^{\beta b^\dagger}\right]|0,0\rangle \\ &= \beta|x_0, y_0; \eta_0^x, \eta_0^y\rangle. \end{aligned} \tag{3.167}$$

Here in these derivations, we used the formula

$$\left[A, f\left(B\right)\right] = \frac{\partial f}{\partial B}\left[A, B\right]. \tag{3.168}$$

Probability Distribution

We here comment the property of the coherent state, the probability distribution. To see this, we find that the coherent states $|x_0, y_0; \eta_0^x, \eta_0^y\rangle$ can be expanded by the arbitrary state $|N, M\rangle$ as

$$\begin{aligned} |x_0, y_0; \eta_0^x, \eta_0^y\rangle &= \mathrm{e}^{-\left(|\alpha|^2+|\beta|^2\right)/2} \sum_{N=0}^{\infty}\sum_{M=0}^{\infty} \frac{\alpha^N}{\sqrt{N!}} \frac{\beta^M}{\sqrt{M!}} |N, M\rangle \\ &\equiv \sum_{N=0}^{\infty}\sum_{M=0}^{\infty} C_{\alpha,\beta}\left(N, M\right) |N, M\rangle, \end{aligned} \tag{3.169}$$

We can check it as below: First, the arbitrary state $|N, M\rangle$ can be expressed by the creation operators,

$$|N, M\rangle = \frac{\left(a^\dagger\right)^N}{\sqrt{N!}} \frac{\left(b^\dagger\right)^M}{\sqrt{M!}} |0, 0\rangle. \tag{3.170}$$

Next, we multiply $\mathrm{e}^{-\left(|\alpha|^2+|\beta|^2\right)/2}\alpha^N\beta^M/\sqrt{N!M!}$ by both side and sum with respect to N and M,

$$\begin{aligned} &\mathrm{e}^{-\left(|\alpha|^2+|\beta|^2\right)/2} \sum_{N=0}^{\infty}\sum_{M=0}^{\infty} \frac{\alpha^N}{\sqrt{N!}} \frac{\beta^M}{\sqrt{M!}} |N, M\rangle \\ &\quad = \mathrm{e}^{-\left(|\alpha|^2+|\beta|^2\right)/2} \sum_{N=0}^{\infty}\sum_{M=0}^{\infty} \frac{\left(\alpha a^\dagger\right)^N}{N!} \frac{\left(\beta b^\dagger\right)^M}{M!} |0, 0\rangle \\ &\quad = \mathrm{e}^{-\left(|\alpha|^2+|\beta|^2\right)/2}\, \mathrm{e}^{\alpha a^\dagger} \mathrm{e}^{\beta b^\dagger} |0, 0\rangle. \end{aligned} \tag{3.171}$$

The last expression is nothing but the coherent state (3.165), that is,

$$|x_0, y_0; \eta_0^x, \eta_0^y\rangle = \mathrm{e}^{-\left(|\alpha|^2+|\beta|^2\right)/2} \sum_{N=0}^{\infty}\sum_{M=0}^{\infty} \frac{\alpha^N}{\sqrt{N!}} \frac{\beta^M}{\sqrt{M!}} |N, M\rangle. \tag{3.172}$$

The projection of the coherent states $|x_0, y_0; \eta_0^x, \eta_0^y\rangle$ to the arbitrary Landau state $|N, M\rangle$ is written by

$$\begin{aligned} \langle N, M|x_0, y_0; \eta_0^x, \eta_0^y\rangle &= \mathrm{e}^{-\left(|\alpha|^2+|\beta|^2\right)/2} \frac{\alpha^N}{\sqrt{N!}} \frac{\beta^M}{\sqrt{M!}} \\ &= C_{\alpha,\beta}\left(N, M\right). \end{aligned} \tag{3.173}$$

This projection can lead to the probability distribution in the state $|N, M\rangle$ at the position $\mathbf{r} = \mathbf{r}_0 + \boldsymbol{\eta}_0$. That is to say, by squaring $C_{\alpha,\beta}\left(N, M\right)$, we

obtain

$$W_{\alpha,\beta}(N,M) = |C_{\alpha,\beta}(N,M)|^2 = \mathrm{e}^{-|\alpha|^2-|\beta|^2}\frac{|\alpha|^{2N}}{N!}\frac{|\beta|^{2M}}{M!}. \tag{3.174}$$

Taking into account that $|\alpha|^2 = \langle x_0, y_0; \eta_0^x, \eta_0^y | a^\dagger a | x_0, y_0; \eta_0^x, \eta_0^y \rangle = \bar{N}$ and $|\beta|^2 = \langle x_0, y_0; \eta_0^x, \eta_0^y | b^\dagger b | x_0, y_0; \eta_0^x, \eta_0^y \rangle = \bar{M}$ which stands for the average of the quantities N, M in the $|N, M\rangle$-state, we thus see this probability distribution is nothing but the Poisson probability distribution

$$W_{\alpha,\beta}(N,M) = \mathrm{e}^{-\bar{N}-\bar{M}}\frac{\bar{N}^N}{N!}\frac{\bar{M}^M}{M!}. \tag{3.175}$$

On the other hand, when we take into account that $|\alpha|^2 = |\boldsymbol{\eta}_0|^2/2l_B^2$ and $|\beta|^2 = |\mathbf{r}_0|^2/2l_B^2$, the probability distribution can be represented by the guiding center and the Larmor radius as

$$W_{\alpha,\beta}(N,M) = \mathrm{e}^{-\left(|\boldsymbol{\eta}_0|^2+|\mathbf{r}_0|^2\right)/2l_B^2}\frac{1}{N!}\left(\frac{|\boldsymbol{\eta}_0|^2}{2l_B^2}\right)^N\frac{1}{M!}\left(\frac{|\mathbf{r}_0|^2}{2l_B^2}\right)^M. \tag{3.176}$$

Time Evolution of Coherent State

To obtain the time evolution of the coherent state $|\alpha,\beta\rangle = |x_0, y_0; \eta_0^x, \eta_0^y\rangle$, we use the time evolution operator $\mathrm{e}^{-\frac{i}{\hbar}Ht}$. We can proceed to calculate as below: We first extract the displacement operator (3.149) from the coherent state at $t = 0$,

$$\begin{aligned}|\alpha,\beta\rangle(t) &= \mathrm{e}^{-\frac{i}{\hbar}Ht}|\alpha,\beta\rangle(t=0)\\ &= \mathrm{e}^{-\frac{i}{\hbar}Ht}\tilde{D}(\eta_0^x,\eta_0^y)|0,\beta\rangle(t=0)\\ &= \mathrm{e}^{-|\alpha|^2/2}\mathrm{e}^{-\frac{i}{\hbar}Ht}\left\{\sum_{N=0}^{\infty}\frac{\left(\alpha a^\dagger\right)^N}{N!}\right\}|0,\beta\rangle(t=0).\end{aligned} \tag{3.177}$$

To change the Hamilton operator to c-number, we use (3.170) for the operator $a^\dagger$,

$$\begin{aligned}|\alpha,\beta\rangle(t) &= \mathrm{e}^{-|\alpha|^2/2}\mathrm{e}^{-\frac{i}{\hbar}Ht}\left\{\sum_{N=0}^{\infty}\frac{\alpha^N}{\sqrt{N!}}|N,\beta\rangle(t=0)\right\}\\ &= \mathrm{e}^{-|\alpha|^2/2}\left\{\sum_{N=0}^{\infty}\frac{\alpha^N}{\sqrt{N!}}\mathrm{e}^{-i\omega_c\left(N+\frac{1}{2}\right)t}|N,\beta\rangle(t=0)\right\}\\ &= \mathrm{e}^{-i\omega_c t/2}\left\{\sum_{N=0}^{\infty}\mathrm{e}^{-|\alpha|^2/2}\frac{\left(\alpha\mathrm{e}^{-i\omega_c t}\right)^N}{\sqrt{N!}}|N,\beta\rangle(t=0)\right\}.\end{aligned} \tag{3.178}$$

Assuming $\alpha e^{-i\omega_c t}$ as an eigenvalue of a at t, we obtain the time-evolved coherent state by using (3.172),

$$|\alpha, \beta\rangle (t) = e^{-i\omega_c t/2} |\alpha (t=0) e^{-i\omega_c t}, \beta (t=0)\rangle. \tag{3.179}$$

This yields the time evolution of the eigenvalue,

$$\begin{aligned} \alpha (t) &= \alpha (t=0) e^{-i\omega_c t}, \\ \beta (t) &= \beta (t=0). \end{aligned} \tag{3.180}$$

Since $x_0 = \sqrt{2} l_B \, \mathrm{Re}[\beta]$ and $y_0 = \sqrt{2} l_B \, \mathrm{Im}[\beta]$, we see that the guiding center $\mathbf{r}_0$ is a constant of motion. On the other hand, since $\eta_0^x (t) = \sqrt{2} l_B \, \mathrm{Re}[\alpha (t)]$ and $\eta_0^y (t) = -\sqrt{2} l_B \, \mathrm{Im}[\alpha (t)]$, we can reproduce the classical trajectory (3.5),

$$\begin{aligned} \eta_0^x (t) &= \eta_0^x (t=0) \cos \omega_c t - \eta_0^y (t=0) \sin \omega_c t \\ &= |\boldsymbol{\eta}_0 (t=0)| \left\{ \frac{\eta_0^x (t=0)}{|\boldsymbol{\eta}_0 (t=0)|} \cos \omega_c t - \frac{\eta_0^y (t=0)}{|\boldsymbol{\eta}_0 (t=0)|} \sin \omega_c t \right\} \\ &= \eta \cos (\omega_c t + \gamma), \end{aligned} \tag{3.181}$$

and

$$\begin{aligned} \eta_0^y (t) &= \eta_0^x (t=0) \sin \omega_c t + \eta_0^y (t=0) \cos \omega_c t \\ &= |\boldsymbol{\eta}_0 (t=0)| \left\{ \frac{\eta_0^x (t=0)}{|\boldsymbol{\eta}_0 (t=0)|} \sin \omega_c t + \frac{\eta_0^y (t=0)}{|\boldsymbol{\eta}_0 (t=0)|} \cos \omega_c t \right\} \\ &= \eta \sin (\omega_c t + \gamma), \end{aligned} \tag{3.182}$$

where we denoted $\eta = |\boldsymbol{\eta}_0 (t=0)|$, and $\gamma = \arctan \left(\frac{\eta_0^y (t=0)}{\eta_0^x (t=0)} \right)$ [52].

3.6.3 Physical Meaning of Cancellation of Bulk Currents

In this section, we discuss that only the current on the edge of system carries all of the total amount of current in system. To see this, we pay our attention to one coherent state at the guiding center $\mathbf{r}_0$, which produces the circular current by the Larmor motion with radius $|\boldsymbol{\eta}|$ from (3.181) and (3.182). Because of the uncertainty (3.107), it seems that the circular current flows the edge of the area ΔS. When the LLs state can be constructed by the superposition of the coherent states, the superposition produces contact points of the circular current at the center $\mathbf{r}_0$ with the surrounding circular currents. Thus, the circular current at the center $\mathbf{r}_0$ is canceled out by the surrounding circular current. Such the cancellation occurs on whole system except to

the edge. Thus, when we decompose the total amount of circular current to the bulk current and edge current as $\mathbf{j}_{\text{bulk}} + \mathbf{j}_{\text{edge}}$, the bulk currents are all cancelled out, i.e.,

$$\mathbf{j}_{\text{bulk}} = 0, \tag{3.183}$$

and all of the total amount of circular current is carried by only the edge current. This result is considered to discuss the magnetization induced by the current in Sec. 4.3.

Chapter 4

Landau Level Spectroscopy by OV

As discussed above, we know that an optical OAM can be transferred only to the center-of-mass motion of the electron in a electric dipole transition, and that, to absorb a photon, the electron must be bounded. Also, we see that the Landau-quantized electron in an axial symmetric system can carries an orbital angular momentum. Therefore, it is naturally expected that the degenerated 2DEG in magnetic field can absorb the optical OAM in the electric dipole transition and that the selection rules by optical OAM can be modified.

In this Chapter, we thus investigate the optical conductivity and the selection rules in 2DEG under the magnetic field by irradiating with lights carrying OAM in addition to spin angular momentum (SAM). We will demonstrate that the bulk current induced by OV disappears, and only the edge current survives when the 2DEG is irradiated with a Bessel beam. After that, the result of the magnetic field dependence of the induced current will be given. It will also be demonstrated an orbital magnetization due to the existence of the edge currents.

4.1 Landau-quantized Electron

The quantized energy levels (Landau levels, LLs) of 2DEG in the magnetic field B are given by [47] $E_N = \hbar\omega_c\,(N + 1/2)$, which usually appear by solving the Schrödinger equation in the Landau's gauge, where $N = 0, 1, 2, \ldots$ is the Landau level index, and $\omega_c = eB/m_e$ is the cyclotron frequency with the elementary charge $e\,(> 0)$, and the rest electron mass m_e. However, when we consider 2DEG interacting with the Bessel OV light beam, the symmetric

gauge in the cylindrical coordinates becomes a natural choice. Hence, we consider 2DEG on a circularly shaped disk geometry and take the cylindrical coordinates as shown in Fig. 4.1.

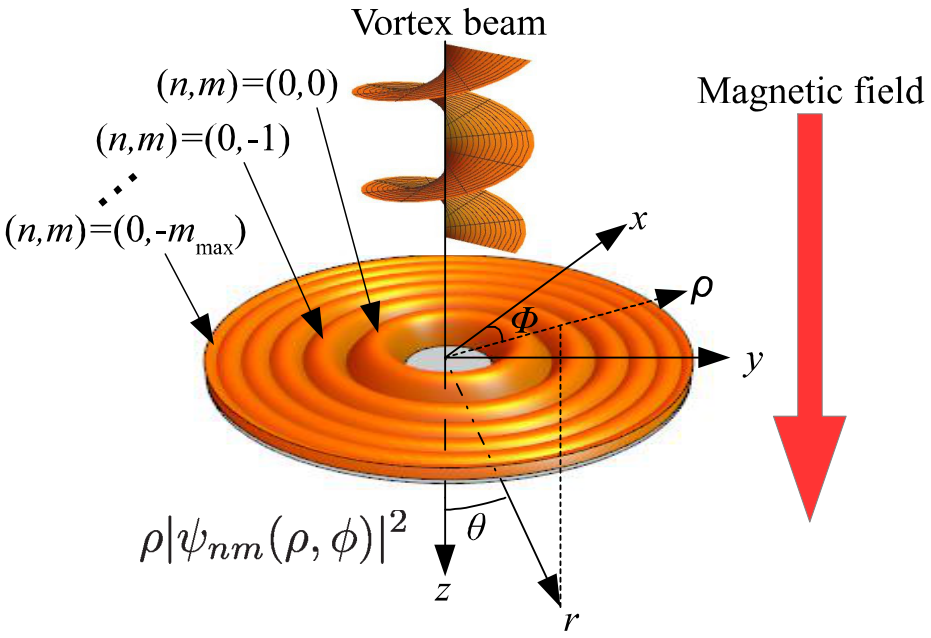

Figure 4.1: Schematic picture showing 2D electron distributions in the lowest LLs on the circular disc geometry. The OV beam is vertically irradiated to 2DEG. The direction of propagation of OV is taken the z-axis. The azimuthal angle ϕ is on the 2D electron system.

The non-perturbative Hamiltonian for 2DEG under the magnetic field is given by

$$H_0 = \frac{1}{2m_e}\left[-i\hbar\boldsymbol{\nabla} + e\mathbf{A}^{\rm ext}(\mathbf{r})\right]^2 \tag{4.1}$$

where we use the symmetric gauge, $\mathbf{A}^{\rm ext}(\mathbf{r}) = (-By/2, Bx/2, 0)$, which describes the magnetic field along the z-axis direction. The energy spectrum is obtained by solving the Schrödinger equation $H_0\Psi = E\Psi$ which gives[53]

$$E_{n,m} = \hbar\omega_c\left(n + \frac{|m|+m}{2} + \frac{1}{2}\right), \\ n = 0, 1, 2, ..., \text{and } m = 0, \pm1, \pm2, ..., \tag{4.2}$$

where m is the magnetic quantum number related to the orbital angular

momentum of the electron. The eigenfunction is also obtained as

$$\Psi_{nm}(\rho,\phi,z) = N_{nm}\mathrm{e}^{-\frac{\rho^2}{4l_B^2}}\left(\frac{\rho}{l_B}\right)^{|m|} L_n^{|m|}\left(\frac{\rho^2}{2l_B^2}\right)\frac{\mathrm{e}^{im\phi}}{\sqrt{2\pi}}$$
$$= R_{nm}(\rho)\frac{\mathrm{e}^{im\phi}}{\sqrt{2\pi}}, \tag{4.3}$$

where $l_B = \sqrt{\hbar/eB}$ is the magnetic length, $N_{nm} = (n!/(n+|m|)!)^{1/2}\, 2^{-|m|/2} l_B^{-1}$ is the normalization constant, and $L_n^{|m|}(x)$ is the associated Laguerre polynomials. As shown in previous section, each LL with given N is multiple degenerated with respect to n and m due to the finite system size with the degeneracy factor given by $S/2\pi l_B^2$, where S is the area of 2DEG.

For the lowest Landau level (LLL), $N = 0$, we find that the one-electron state covers the area $2\pi l_B^2$. Then, the degeneracy or the maximum m for the disk geometry is given by

$$m_{\max} \simeq \frac{S}{2\pi l_B^2} = \frac{R^2}{2l_B^2}, \tag{4.4}$$

which allows us to define the filling factor as

$$\nu \equiv \frac{N_e}{m_{\max}} \simeq 2\pi l_B^2 \frac{N_e}{\pi R^2}, \tag{4.5}$$

where N_e is the total number of electrons on the disk[54]. Throughout this dissertation, we concentrate on the system with the filling factor $\nu = 1$, where the Fermi energy lies in the gap between the LLL and the second Landau level (2LL). We display the energy diagram of the axial symmetric 2DEG system as shown in Fig. 4.2.

4.2 Photocurrent Induced by Optical Vortex

We here investigate the interaction of a Landau-quantized 2DEG with the Bessel OV by applying the linear response theory based on Refs. [39, 55]. We start with the following total Hamiltonian, which contains the non-perturbative Hamiltonian (4.1) interacting with the vector potential of the OV:

$$H{=}H_0 + \Delta H = \frac{1}{2m_e}\left[-i\hbar\boldsymbol{\nabla} + e\mathbf{A}^{\mathrm{ext}}(\mathbf{r})\right]^2 - \boldsymbol{A}^{\mathrm{OV}}_{\ell,\sigma}\cdot\mathbf{j}, \tag{4.6}$$

where $\boldsymbol{A}^{\mathrm{OV}}_{\ell,\sigma}$ is given by Eq. (2.37), and the electric current is determined by $\mathbf{j} = \frac{e}{m_e}(\mathbf{p} + e\mathbf{A}^{\mathrm{ext}})$. We here neglect the electron spin and assume the optical vortices are illuminated at the center of circular disk geometry.

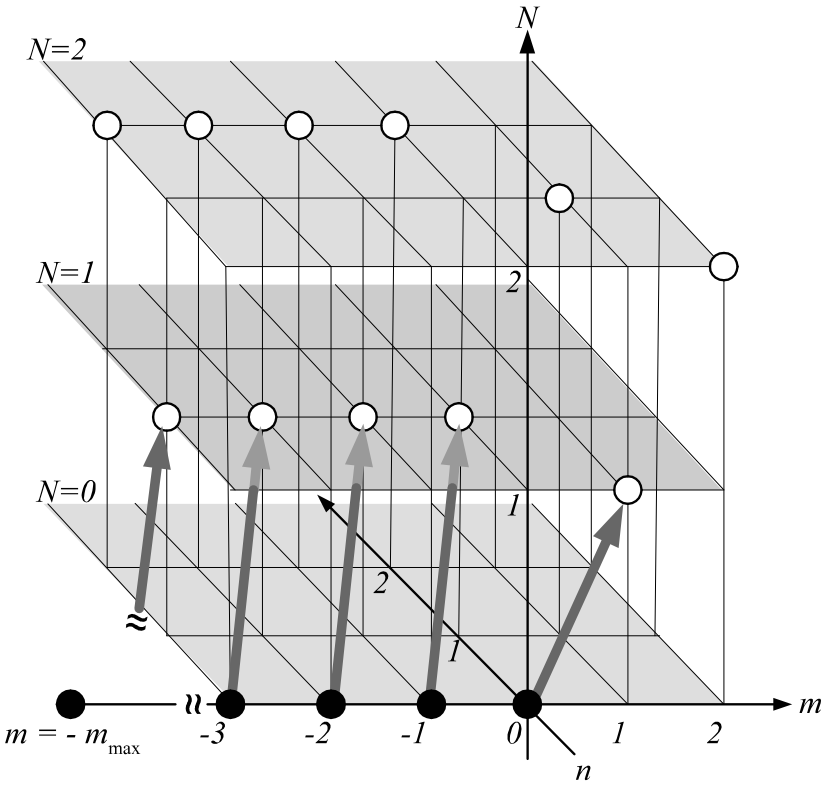

Figure 4.2: Allowed transitions from the lowest LL ($N = 0$) to the second LL ($N = 1$) are indicated by the gray thick allows. The opened circles denote unoccupied states, whereas closed ones are occupied.

As we derived in Appendix A, the Kubo formula for i-component of the induced current [56, 57] is written by

$$\delta j_i(\omega) = -\sum_{n,m}\sum_{n',m'} \left(f(E_{n,m}) - f(E_{n',m'})\right) \times \frac{\langle n,m|j_i|n',m'\rangle\langle n',m'|\boldsymbol{A}^{\rm OV}_{\ell,\sigma}\cdot\mathbf{j}|n,m\rangle}{E_{n,m}-E_{n',m'}+\hbar\omega+i\delta}. \tag{4.7}$$

where $f(E_{n,m})$ is the Fermi distribution $f(\epsilon) = \left[\exp\beta\left(\epsilon-\mu\right)+1\right]^{-1}$ with a chemical potential μ and an inverse temperature β, and $|n,m\rangle$ is the electron wavefunction in Eq.(4.3) and we abbreviated hats "$\hat{O}$" indicating being operators. From now on, we assume zero-temperature limit and keeping the chemical potential lie between the LLL ($N=0$) and the second LL ($N=1$).

To investigate the OV-induced photocurrent, we adopt the chiral basis, $j_\pm = \left(j_x \mp i j_y\right)/\sqrt{2}$. We will show the vector components in chiral basis in Appendix B. First, we consider the matrix element of photocurrent $j_\pm$. By using the commutation relation (3.23) or $j_\pm = i\left(e/\sqrt{2}\hbar\right)[H_0, x\mp iy]$, this can be written as

$$\begin{aligned}\langle n,m\left|j_\pm\right|n',m'\rangle &= i\frac{e}{\sqrt{2}\hbar}\langle n,m|[H_0,x\mp iy]|n',m'\rangle \\ &= i\frac{e}{\sqrt{2}\hbar}(E_{n,m}-E_{n',m'})\langle n,m|\rho e^{\mp i\phi}|n',m'\rangle \\ &= i\frac{e}{\sqrt{2}\hbar}(E_{n,m}-E_{n',m'})\int_0^{2\pi}\frac{d\phi}{2\pi}e^{i(m'-m\mp1)\phi} \\ &\times\int_0^\infty d\rho\rho^2 R_{nm}(\rho)R_{n'm'}(\rho)\int_0^d dz\frac{e^{i(k'-k)z}}{d},\end{aligned} \tag{4.8}$$

where $d(\ll R)$ is the thickness of 2DEG. Then when we assume $(k'-k)\,d \ll 1$, since the integral with respect to z reduces to

$$\begin{aligned}\int_0^d dz\frac{e^{i(k'-k)z}}{d} &= \frac{1}{i\left(k'-k\right)d}\left\{e^{i(k'-k)d}-1\right\} \\ &\simeq 1,\end{aligned} \tag{4.9}$$

we can obtain the matrix element as

$$\begin{aligned}\langle n,m\left|j_\pm\right|n',m'\rangle &\sim i\frac{e}{\sqrt{2}\hbar}(E_{n,m}-E_{n',m'})\delta_{m',m\pm1}\int_0^\infty d\rho\rho^2 R_{nm}(\rho)R_{n'm'}(\rho) \\ &= i\frac{e}{\sqrt{2}\hbar}(E_{n,m}-E_{n',m'})C^{n',m'}_{n,m}\delta_{m',m\pm1},\end{aligned} \tag{4.10}$$

where we denoted the radial integral as

$$C_{n,m}^{n',m'} = \int d\rho \rho^2 R_{n',m'}(\rho) R_{n,m}(\rho). \tag{4.11}$$

Here, we obtain the selection rule $m' = m \pm 1$ from the azimuthal integral $\int_0^{2\pi} \frac{d\phi}{2\pi} \mathrm{e}^{i(m'-m\mp 1)\phi}$. After calculating the radial integral $C_{n,m}^{n',m'}$ as we derive in Appendix C and the energy factor $E_{n,m} - E_{n',m'}$ as we derive in Appendix D by using Eq.(4.2), we can obtain the matrix elements of the photocurrent as

$$\langle n,m|j_+|n',m+1\rangle = \begin{cases} 0 & \text{for } n'=n,\ m<0, \\ -iel_B\omega_c\sqrt{2n+|m|+m+2} & \\ \qquad\qquad \text{for } n'=n,\ m\geq 0, & \\ 0 & \text{for } n'=n-1,\ m\geq 0, \\ iel_B\omega_c\sqrt{2n+|m|+m+2} & \\ \qquad\qquad \text{for } n'=n+1,\ m<0, & \\ 0 & \text{for otherwise,} \end{cases} , \tag{4.12}$$

$$\langle n,m|j_-|n',m-1\rangle = \begin{cases} 0 & \text{for } n'=n,\ m\leq 0, \\ iel_B\omega_c\sqrt{2n+|m|+m} & \\ \qquad\qquad \text{for } n'=n,\ m>0, & \\ -iel_B\omega_c\sqrt{2n+|m|+m} & \\ \qquad\qquad \text{for } n'=n-1,\ m\leq 0, & \\ 0 & \text{for } n'=n+1,\ m>0, \\ 0 & \text{for otherwise,} \end{cases} . \tag{4.13}$$

For the filling factor $\nu = 1$ ($n = 0, m \leq 0$), these matrix elements reduce to

$$\langle 0,m|j_+|n',m+1\rangle = \begin{cases} -iel_B\omega_c\sqrt{2} & \text{for } n'=0,\ m=0 \\ iel_B\omega_c\sqrt{2} & \text{for } n'=1,\ m<0 \\ 0 & \text{for otherwise} \end{cases} ,$$

$$\langle 0,m|j_-|n',m-1\rangle = 0 \quad \text{for all } n', m. \tag{4.14}$$

Therefore, we find that the transition is allowed only $N \to N+1$[57]. We summarize possible transitions from the LLL ($N = 0$) to the second LL ($N = 1$),

$$\begin{cases} (n,m,N) & & (n',m',N') & \\ (0,0,0) & \to & (0,1,1) & \text{for } m=0 \\ (0,m,0) & \to & (1,m+1,1) & \text{for } m<0 \end{cases} . \tag{4.15}$$

Next, we consider the matrix element of the minimal coupling of 2DEG with OV. As shown in Appendix E, the dipole approximation is justified in our model. Then the matrix element for the photon absorption in this approximation is obtained as

$$\begin{aligned}
&\langle n', m'|\boldsymbol{A}^{\mathrm{OV}}_{\ell,\sigma}\cdot\mathbf{j}|n,m\rangle \\
&\quad\sim i\frac{e}{\hbar}(E_{n',m'}-E_{n,m})\langle n',m'|\boldsymbol{A}^{\mathrm{OV}}_{\ell,\sigma}\cdot\mathbf{r}|n,m\rangle \qquad (4.16)\\
&\quad= i\frac{e}{\hbar}A_0\sqrt{\frac{k_\perp}{2\pi}}(-i)^\sigma(E_{n',m'}-E_{n,m}) \\
&\quad\times\langle n',m'|J_\ell(k_\perp\rho)\mathrm{e}^{i\ell\phi}\left(-\sigma\frac{\rho}{\sqrt{2}}\right)(\cos\phi+i\sigma\sin\phi)\mathrm{e}^{ik_z z}|n,m\rangle. \qquad (4.17)
\end{aligned}$$

Noting that $(-i)^\sigma=-\sigma i$ is valid for $\sigma=\pm1$, we can proceed to calculate as

$$\begin{aligned}
&\langle n', m'|\boldsymbol{A}^{\mathrm{OV}}_{\ell,\sigma}\cdot\mathbf{j}|n,m\rangle \\
&\quad=-\frac{e}{\hbar}A_0\sqrt{\frac{k_\perp}{4\pi}}(E_{n',m'}-E_{n,m})\langle n',m'|\rho J_\ell(k_\perp\rho)\mathrm{e}^{i(\ell+\sigma)\phi}\mathrm{e}^{ik_z z}|n,m\rangle \\
&\quad=-\frac{e}{\hbar}A_0\sqrt{\frac{k_\perp}{4\pi}}(E_{n',m'}-E_{n,m})\int_0^\infty d\rho\rho^2 R_{n',m'}(\rho)R_{n,m}(\rho)J_\ell(k_\perp\rho) \\
&\quad\times\int_0^{2\pi}\frac{d\phi}{2\pi}\mathrm{e}^{i(m-m'+\ell+\sigma)\phi}\int_0^d dz\frac{\mathrm{e}^{i(k_z+k-k')z}}{d}. \qquad (4.18)
\end{aligned}$$

Then when we assume $(k_z+k-k')\,d\ll1$, since the integral with respect to z reduces to

$$\begin{aligned}
\int_0^d dz\frac{\mathrm{e}^{i(k_z+k-k')z}}{d} &= \frac{1}{i\,(k_z+k-k')\,d}\left\{\mathrm{e}^{i(k_z+k-k')d}-1\right\} \\
&\simeq 1, \qquad (4.19)
\end{aligned}$$

we can obtain the matrix element as

$$\begin{aligned}
\langle n', m'|\boldsymbol{A}^{\mathrm{OV}}_{\ell,\sigma}\cdot\mathbf{j}|n,m\rangle &= -\frac{e}{\hbar}A_0\sqrt{\frac{k_\perp}{4\pi}}(E_{n',m'}-E_{n,m}) \\
&\quad\times\int_0^\infty d\rho\rho^2 R_{n',m'}(\rho)R_{n,m}(\rho)J_\ell(k_\perp\rho)\delta_{m',m+\ell+\sigma} \\
&= A_0\frac{e}{\hbar}\sqrt{\frac{k_\perp}{4\pi}}(E_{n,m}-E_{n',m'})D^{n',m'}_{n,m,\ell}\delta_{m',m+\ell+\sigma}, \qquad (4.20)
\end{aligned}$$

where we denoted the radial integral as

$$D^{n',m'}_{n,m,\ell}=\int d\rho\rho^2 R_{n',m'}(\rho)R_{n,m}(\rho)J_\ell(k_\perp\rho). \qquad (4.21)$$

We also obtain the selection rule $m' = m + \ell + \sigma$ from the azimuthal integral $\int_0^{2\pi} \frac{d\phi}{2\pi} \mathrm{e}^{i(m-m'+\ell+\sigma)\phi}$, where $\sigma = \pm 1$. This means that the OV can transfer its TAM to the electron via the dipole transition.

We note that, when we fix the filling factor $\nu = 1$ (the chemical potential lies between $N = 0$ and $N = 1$), the left-handed current is not induced. Therefore, only the right-handed current arises by transferring the optical TAM, $J = 1$. Because the OV carries the SAM $\sigma = \pm 1$, the OAM and SAM must be

$$\ell = 0, \sigma = 1, \text{or } \ell = 2, \sigma = -1, \tag{4.22}$$

respectively, with the other transitions being prohibited.

On the other hand, we can apply the external magnetic field anti-parallel to the light traveling. Since the magnetic field then breaks time-reversal symmetry, the direction of currents can be determined. When the magnetic field reverses into the anti-parallel direction to light's propagation, the optical angular momentum absorption must thus change into $J = -1$. As a result, the possible absorptions are reduced to $\ell = 0$, $\sigma = -1$, and $\ell = -2$, $\sigma = 1$.

Let us now return to the case of the magnetic field parallel to the light traveling. Next, we calculate the photocurrent using the Kubo formula. For the transition from $N = 0$ to $N = 1$ with $\nu = 1$, and at zero temperature, the OV-induced current (4.7) reduces to

$$\delta j_\ell^+ (\omega, B) = -i \frac{F^\ell (B)}{\hbar\omega - \hbar\omega_c + i\delta}, \tag{4.23}$$

where $\ell = 0$ or 2 and the factors F^ℓ are given by

$$F^\ell (B) = A_1 C_{0,0}^{0,1} D_{0,0,\ell}^{0,1} + A_1 \sum_{m<0}^{-m_{\max}} C_{0,m}^{1,m+1} D_{0,m,\ell}^{1,m+1}, \tag{4.24}$$

with $A_1 = A_0 e^2 \omega_c^2 \sqrt{k_\perp / 8\pi} / V$. In the summation with respect to m, by using the explicit form, $L_1^k (x) = 1 + k - x$, only one term corresponding to an edge current along the circle with the radius R survives. The other terms corresponding to the bulk currents cancel each other. After some algebra (as shown in appendix F), we obtain

$$\begin{aligned} F^\ell (B) \sim \frac{F_0}{\sqrt{\alpha^5}} \left(\frac{1+\alpha^2}{\alpha^2} \frac{\Phi_0^2}{\lambda_e^2 R^2 B^2} \left[1 + \frac{\Phi_0}{2\pi R^2 B} \right] \mathrm{e} \right)^{\frac{\pi R^2}{\Phi_0} B} \\ \times \int_0^{k_\perp R} dx x^{2m_{\max}(B)+3} \mathrm{e}^{-\frac{x^2}{2k_\perp^2 l_B^2}} J_\ell (x), \end{aligned} \tag{4.25}$$

where ℓ is 0 or 2, and we introduced $F_0 = A_0 e^2 c^2 / V\sqrt{4\pi\lambda_e \mathrm{e}}$ and $x = k_\perp \rho$, which has an order of magnitude of unity. $\Phi_0 = 2\pi\hbar/e$ is the flux quantum, and $\lambda_e = 2\pi\hbar/m_e c$ is the electron Compton wavelength.

The overall profile of these behaviors may be grasped through the qualitative nature of the integral in Eq. (4.25), we decompose the integrand into

$$g(x) = x^{2m_{\max}+3} \exp\left(-x^2/2k_\perp^2 l_B^2\right) \tag{4.26}$$

and the Bessel function $J_\ell(x)$. We first find that the upper limit of the integration can be written by

$$\begin{aligned} k_\perp R &= \frac{\alpha}{\sqrt{1+\alpha^2}} \frac{\lambda_e B R}{\Phi_0} \\ &\simeq \frac{\alpha \lambda_e B R}{\Phi_0} \\ &\simeq 587 \alpha R B, \end{aligned} \tag{4.27}$$

where $\alpha = k_\perp / k_z$ is the parameter which characterizes the degree of the paraxial approximation same as we introduced in Chapter 2. We next find the extremal value by $\frac{d}{dx} g(x) = 0$, which gives

$$2m_{\max} + 3 - \frac{1}{k_\perp(B)^2 l_B(B)^2} x^{*2} = 0.$$

Noting that $x \geq 0$ from definition $\rho \geq 0$, we obtain the important relation

$$\begin{aligned} x^{*2} &= k_\perp(B)^2 l_B(B)^2 \left(2m_{\max} + 3\right) \\ x^* &\simeq k_\perp R \\ &\simeq 587 \alpha R B \equiv B/B^*, \end{aligned} \tag{4.28}$$

where we used the relation $R \gg l_B$ and introduced,

$$B^* \simeq \frac{\Phi_0}{\alpha \lambda_e R} \simeq 1/587 \alpha R. \tag{4.29}$$

We note that the extrema x^* almost coincides with the upper limit of integration $k_\perp R$. Using the values $\alpha = 0.1$ and $R = 10^{-2}$ m as an example, we have $x^* \simeq 0.587B$ with B being measured in Tesla. On the other hand, the positive zeros of the Bessel functions $J_\ell(x)$ have also an order of magnitude of unity. Consequently, $g(x)$ and $J_\ell(x)$ significantly interfere with each other and demonstrate oscillating behavior. That is to say, when the dark rings of optical vortex determined by zeros of the profile, $J_\ell(k_\perp \rho) = 0$, coincides with this peak at x^*, the matrix element of the interaction vanishes and the

induced current doesn't appear. Furthermore, due to the factor in front of the integral in Eq. (4.25), $F^{\ell}(B)$ demonstrates evolving behavior.

Such a phenomenon can be controlled by the external magnetic field without modification to the optics system. By the energy conservation,

$$h\frac{c}{\lambda_{\mathrm{OV}}} = \hbar\omega_c, \tag{4.30}$$

the wavelength of optical vortex beam must be tuned to induce the cyclotron resonance. Therefore, the wavelength depends on the magnetic field as $\lambda_{\mathrm{OV}} \sim 1.07 \times 10^{-2} B^{-1}$ m. If the magnetic field B increases, the wavelength λ_{OV} is tuned to become small and the dark rings of optical vortex is converged. The dark rings will eventually coincide with the edge of system. The induced current can thus be disappeared at the specific magnetic field.

We here show the physical values of the magnetic length l_B, cyclotron frequency ω_c, excitation energy between the LLL and 2LL ΔE, wavelength of light to excite between the LLL and 2LL λ_{OV}, and the corresponding wavenumber k_{OV}, for the rest electron mass, $m_e = 9.11 \times 10^{-31}$ kg, in the Table 4.1. As we mentioned in Sec. 3.5, the electron mass m_e should be interpreted as an cyclotron effective mass $m_e^* = 0.067 m_e = 6.10 \times 10^{-33}$ kg for GaAs. For the purpose of reference, we also show these physical values for GaAs in the Table 4.2

Magnetic length $l_B = \sqrt{\frac{\hbar}{eB}}$	$2.56 \times 10^{-8}\sqrt{B}$ (m)
Cyclotron frequency $\omega_c = \frac{eB}{m_e}$	$1.76 \times 10^{11} B$ (rad·s^{-1})
Excitation energy $\Delta E = \hbar\omega_c$	$1.16 \times 10^{-4} B$ (eV)
Wave length of light $\lambda_{\mathrm{OV}} = \frac{2\pi c}{\omega_c}$	$1.07 \times 10^{-2} B^{-1}$ (m)
Wave number of light $k_{\mathrm{OV}} = \frac{2\pi}{\lambda_{\mathrm{OV}}}$	$5.87 \times 10^{2} B$ (m^{-1})

Table 4.1: Table of the physical values of the magnetic length l_B, cyclotron frequency ω_c, excitation energy between the LLL and 2LL ΔE, wavelength of light to excite between the LLL and 2LL λ_{OV}, and the corresponding wavenumber k_{OV}. These values are obtained by the rest electron mass $m_e = 9.11 \times 10^{-31}$ kg.

We more precisely see when the induced photocurrents are disappeared by varying the magnetic field B. Since the disappearing points are determined by the zeros of Bessel functions, $J_\ell(x_\ell^i) = 0$, whose i-th zeros were denoted by x_ℓ^i, the disappearing points in real space are related to the radii of the dark rings $r_\perp^{\ell,i}$ in Eq. (2.38). However, since x_ℓ^i can be viewed as fixed points, the size of the dark rings $r_\perp^{\ell,i}$ has correlation with the magnetic field B through the transverse wavenumber $k_\perp$ and the energy conservation (4.30). We thus see

Magnetic length $l_B = \sqrt{\frac{\hbar}{eB}}$	$2.56 \times 10^{-8}\sqrt{B}$ (m)
Cyclotron frequency $\omega_c = \frac{eB}{m_e}$	$2.63 \times 10^{12} B$ (rad·s^{-1})
Excitation energy $\Delta E = \hbar\omega_c$	$1.73 \times 10^{-3} B$ (eV)
Wave length of light $\lambda_{\rm OV} = \frac{2\pi c}{\omega_c}$	$7.17 \times 10^{-4} B^{-1}$ (m)
Wave number of light $k_{\rm OV} = \frac{2\pi}{\lambda_{\rm OV}}$	$8.76 \times 10^{3} B$ (m^{-1})

Table 4.2: Table of the physical values of the magnetic length l_B, cyclotron frequency ω_c, excitation energy between the LLL and 2LL ΔE, wavelength of light to excite between the LLL and 2LL $\lambda_{\rm OV}$, and the corresponding wavenumber $k_{\rm OV}$. These values are obtained by the effective electron mass for GaAs $m_e^* = 0.067 m_e = 6.10 \times 10^{-33}$ kg.

that the disappearing points depend on the magnetic field. We here denote the disappearing point by tuning the magnetic field as B_ℓ^i. In particular, we note that the electrons exist on the planar surface with the radius R and it is fixed. To find the disappearing points in varying magnetic field, we see the relation of i-th zeros of Bessel functions x_ℓ^i to the magnetic field,

$$\begin{aligned} x_\ell^i &\simeq \alpha \frac{\lambda_e R}{\Phi_0} B_\ell^i \\ &= \frac{B_\ell^i}{B^*}. \end{aligned} \tag{4.31}$$

We here give the examples of disappearing points B_ℓ^i in the Table 4.3. We used the parameters $\alpha = 0.1$ and $R = 10^{-2}$ m, and the physical values given in the Table 4.1 to estimate B_ℓ^i. The other values of B_ℓ^i are estimated by the

i-th zeros of $J_0\,(x_0^i)$	B_0^i
$x_0^1 = 2.40$	4.12 T
$x_0^2 = 5.52$	9.45 T
i-th zeros of $J_2\,(x_2^i)$	B_2^i
$x_2^1 = 5.14$	8.80 T
$x_2^2 = 8.42$	14.1 T

Table 4.3: Table of the examples of disappearing point B_ℓ^i via the zeros of Bessel functions, $J_\ell(x_\ell^i) = 0$. We here used the parameters $\alpha\,(= k_\perp/k_z) = 0.1$ and $R = 10^{-2}$ m, and the physical values given in the Table 4.1.

zeros of Bessel functions, $J_\ell(x_\ell^i) = 0$, via Eq. (4.31).

$F^\ell\,(B)$ (or $\delta j_i\,(\omega_c)$) demonstrates the oscillating behavior because of the Bessel function $J_\ell(k_\perp \rho)$. However, $F^\ell\,(B) < 0$ just shifts the phase in

$\langle \delta j_i(t) \rangle = \delta j_i(\omega_c) \, \mathrm{e}^{-i\omega_c t}$ by the phase π, but does not affect the direction of current. Then, to see the behavior of the amplitude of $\langle \delta j_i(t) \rangle$, we numerically demonstrate B-dependence of the absolute value of $F^\ell(B)$ for $\ell = 0, 2$ and for $R = 10^{-2}$m, 10^{-3}m, and 10^{-4}m in Fig. 4.3 for $\alpha = 0.1$, Fig. 4.4 for $\alpha = 0.01$, and Fig. 4.5 for $\alpha = 0.001$. Since the fixed points are given by $x_\ell^i \propto \alpha R B_\ell^i$, when α is fixed in addition to x_ℓ^i, B_ℓ^i and R is in an inverse relationship. On the other hand, when R is fixed in addition to x_ℓ^i, B_ℓ^i and α is in the inverse relationship.

By the asymptotic form of Bessel function at $B \gg 1$,

$$J_\ell\left(\frac{\lambda_e \alpha R}{\Phi_0} B\right) \approx \sqrt{\frac{2\Phi_0}{\pi \lambda_e \alpha R B}} \cos\left(\frac{\lambda_e \alpha R}{\Phi_0} B - \frac{2\ell+1}{4}\pi\right), \tag{4.32}$$

the distance of the disappearing points of $F^\ell(B)$ are determined by a half of a period of cosine function $\Phi_0/2\lambda_e \alpha R$. As shown in Figs. 4.3 - 4.5, because of this, we find that the period of the disappearing points of $F^\ell(B)$ and the parameter α or the system size R are in an inverse relationship via the half of the period of cosine function $\Phi_0/2\lambda_e \alpha R$.

Fig. 4.6 demonstrates the magnetic field dependencies of F^ℓ for $\ell = 0$ and 2 again. However, we take the horizontal axis as the dimensionless parameter B/B^*, which corresponds to $k_\perp R \sim 1$, and we chose $R = 10^{-2}$ m and $\alpha = 0.1$. That is to say, Fig. 4.6 can be viewed as the zoomed one of (a) in Fig. 4.3. Because the radial profile of OV has the oscillating behavior, the amplitudes of absorption F^ℓ oscillate and evolve with increasing the magnetic field strength, and have vanishing points.

4.3 Magnetization Induced by Edge Current

In electromagnetism, it is known that a circular current induces a magnetization via Biot-Savart law[58]. Then we naturally expect that the edge current induces an orbital magnetization, which can be observed experimentally. In this section, we see the magnetic vector potential separately contributed by bulk currents and an edge current, and because of absence of the bulk currents, only the edge current contributes to the orbital magnetization induced by OV-absorption.

In general, Maxwell's equations in matter in a microscopic (unobservable

atomic scale) region are written by

$$\boldsymbol{\nabla}\cdot\boldsymbol{\epsilon} = \frac{\rho}{\varepsilon_0}, \tag{4.33}$$

$$\boldsymbol{\nabla}\times\boldsymbol{\epsilon} = -\frac{\partial\boldsymbol{\beta}}{\partial t}, \tag{4.34}$$

$$\boldsymbol{\nabla}\cdot\boldsymbol{\beta} = 0, \tag{4.35}$$

$$\boldsymbol{\nabla}\times\boldsymbol{\beta} = \mu_0\mathbf{j}+\frac{1}{c^2}\frac{\partial\boldsymbol{\epsilon}}{\partial t}, \tag{4.36}$$

where $\boldsymbol{\epsilon}$ is a electric field in the microscopic region and $\boldsymbol{\beta}$ is the magnetic field in it. In actuality, physical quantities we observe are not microscopic ones but macroscopic ones (or that in an experimentally observable scale). Therefore, to connect microscopic Maxwell's equations to macroscopic ones, we introduce the macroscopic fields $\mathbf{E}$ and $\mathbf{B}$ by averaging the microscopic fields $\boldsymbol{\epsilon}$ and $\boldsymbol{\beta}$ over the experimentally observable macroscopic region $dV_0(\mathbf{r})$ near $\mathbf{r}$:

$$\mathbf{E}(\mathbf{r},t) = \frac{1}{dV_0(\mathbf{r})}\sum_i \boldsymbol{\epsilon}(\mathbf{r}_i,t) \equiv \langle\boldsymbol{\epsilon}(\mathbf{r},t)\rangle, \tag{4.37}$$

$$\mathbf{B}(\mathbf{r},t) = \frac{1}{dV_0(\mathbf{r})}\sum_i \boldsymbol{\beta}(\mathbf{r}_i,t) \equiv \langle\boldsymbol{\beta}(\mathbf{r},t)\rangle, \tag{4.38}$$

Such a spatial average was introduced by H. A. Lorentz[59]. Applying the spatial average, macroscopic Maxwell's equations are written as

$$\boldsymbol{\nabla}\cdot\mathbf{E} = \frac{\langle\rho\rangle}{\varepsilon_0}, \tag{4.39}$$

$$\boldsymbol{\nabla}\times\mathbf{E} = -\frac{\partial\mathbf{B}}{\partial t}, \tag{4.40}$$

$$\boldsymbol{\nabla}\cdot\mathbf{B} = 0, \tag{4.41}$$

$$\boldsymbol{\nabla}\times\mathbf{B} = \mu_0\langle\mathbf{j}\rangle+\frac{1}{c^2}\frac{\partial\mathbf{E}}{\partial t}, \tag{4.42}$$

where we introduced the spatial averaged charge density $\langle\rho\rangle$ and similar charge current density $\langle\mathbf{j}\rangle$. The spatial averaged charge density $\langle\rho\rangle$ may be written by a free charge part and a bound charge one as

$$\langle\rho\rangle = \langle\rho\rangle_{\text{free}}+\langle\rho\rangle_{\text{bound}}. \tag{4.43}$$

Similarly, the spatial averaged charge current density $\langle\mathbf{j}\rangle$ may also be written as

$$\langle\mathbf{j}\rangle = \langle\mathbf{j}\rangle_{\text{free}}+\langle\mathbf{j}\rangle_{\text{bound}}. \tag{4.44}$$

After this, since we now consider the magnetization induced by the circular current via the Larmor motion, we focus on the bound charge current density.

Since a magnetization induced by a circular current via a Larmor motion can be regarded a microscopic magnetic moment, before considering the macroscopic magnetic field generated by the orbital magnetization, we consider the vector potential by the microscopic bound current density, which is written by

$$\mathbf{a}(\mathbf{r}) = \frac{\mu_0}{4\pi}\int \frac{\mathbf{j}_{\text{bound}}(\mathbf{r}')}{|\mathbf{r}-\mathbf{r}'|}dV', \tag{4.45}$$

where this volume integral is done by the volume element with respect to $\mathbf{r}'$. This volume integral can be expanded by the multipole expansion under the region $r \gg r'$,

$$\frac{1}{|\mathbf{r}-\mathbf{r}'|} = \frac{1}{r}\sum_{k=0}^{\infty} P_k(\cos\theta)\left(\frac{r'}{r}\right)^k \tag{4.46}$$

$$= \frac{1}{r} + \frac{\mathbf{r}\cdot\mathbf{r}'}{r^3} + \cdots, \tag{4.47}$$

where $P_k(x)$ is a Legendre polynomials and θ is the angle between $\mathbf{r}$ and $\mathbf{r}'$. Because the first order of expansion gives zero by the volume integration, we consider the expansion up to the second order, which gives

$$\mathbf{a}(\mathbf{r}) = \frac{\mu_0}{4\pi}\int \frac{\mathbf{r}\cdot\mathbf{r}'}{r^3}\mathbf{j}_{\text{bound}}(\mathbf{r}')\,dV'. \tag{4.48}$$

When we introduce the microscopic magnetic moment by the microscopic bound current density,

$$\mathbf{m} = \frac{1}{2}\int \mathbf{r}'\times\mathbf{j}_{\text{bound}}(\mathbf{r}')\,dV', \tag{4.49}$$

the vector potential by the microscopic bound current density is rewritten as

$$\mathbf{a}(\mathbf{r}) = \frac{\mu_0}{4\pi}\frac{\mathbf{m}\times\mathbf{r}}{r^3}. \tag{4.50}$$

Thus, we can reinterpret (4.45) as the magnetic field in matter generated by the magnetic moment induced by the microscopic bound current density.

We next try to link the magnetic moment to a macroscopic orbital magnetization via spatial average by H. A. Lorentz. The vector potential at $\mathbf{r}$ by the sum of contribution of the magnetic moment at position $\mathbf{r}_i$ in the observable macroscopic region $dV_0(\mathbf{r}') \equiv dV'$ is written as

$$d\mathbf{a}(\mathbf{r}) = \frac{\mu_0}{4\pi}\sum_i \frac{\mathbf{m}(\mathbf{r}_i)\times(\mathbf{r}-\mathbf{r}_i)}{|\mathbf{r}-\mathbf{r}_i|^3}. \tag{4.51}$$

Then the spatial average of magnetic moments $\mathbf{m}(\mathbf{r}_i)$ in observable macroscopic region dV' near position $\mathbf{r}'$ gives the orbital magnetization at position $\mathbf{r}'$:

$$\sum_i \mathbf{m}(\mathbf{r}_i) = \mathbf{M}(\mathbf{r}')\, dV'. \tag{4.52}$$

Using this orbital magnetization, the spatial average of vector potential in the observable macroscopic region dV' is thus given by

$$d\langle \mathbf{a}(\mathbf{r})\rangle = \frac{\mu_0}{4\pi}\frac{\mathbf{M}(\mathbf{r}')\times(\mathbf{r}-\mathbf{r}')}{|\mathbf{r}-\mathbf{r}'|^3}dV', \tag{4.53}$$

where $\langle\cdots\rangle$ denotes the spatial average over observable macroscopic region dV'. Integrating the spatial average of vector potential over the whole region D, the macroscopic vector potential in region D is obtained

$$\mathbf{A}(\mathbf{r}) = \frac{\mu_0}{4\pi}\int_D \frac{\mathbf{M}(\mathbf{r}')\times(\mathbf{r}-\mathbf{r}')}{|\mathbf{r}-\mathbf{r}'|^3}dV'. \tag{4.54}$$

Noting that

$$\frac{\mathbf{r}-\mathbf{r}'}{|\mathbf{r}-\mathbf{r}'|^3} = \boldsymbol{\nabla}_{\mathbf{r}'}\left(\frac{1}{|\mathbf{r}-\mathbf{r}'|^3}\right), \tag{4.55}$$

where $\boldsymbol{\nabla}_{\mathbf{r}'}$ is denoted the gradient with respect to $\mathbf{r}'$, the integrand in (4.54) is written by

$$\mathbf{M}(\mathbf{r}')\times\boldsymbol{\nabla}_{\mathbf{r}'}\left(\frac{1}{|\mathbf{r}-\mathbf{r}'|^3}\right) = \frac{\boldsymbol{\nabla}_{\mathbf{r}'}\times\mathbf{M}(\mathbf{r}')}{|\mathbf{r}-\mathbf{r}'|^3} - \boldsymbol{\nabla}_{\mathbf{r}'}\times\left(\frac{\mathbf{M}(\mathbf{r}')}{|\mathbf{r}-\mathbf{r}'|^3}\right). \tag{4.56}$$

Then, applying the Stoke's theorem to the second term in integral (4.54) with (4.56) separates the integral to volume integral part and surface one:

$$\mathbf{A}(\mathbf{r}) = \frac{\mu_0}{4\pi}\int_D \frac{\boldsymbol{\nabla}_{\mathbf{r}'}\times\mathbf{M}(\mathbf{r}')}{|\mathbf{r}-\mathbf{r}'|}dV' + \frac{\mu_0}{4\pi}\int_{\partial D}\frac{\mathbf{M}(\mathbf{r}')\times\hat{\mathbf{n}}}{|\mathbf{r}-\mathbf{r}'|}dS', \tag{4.57}$$

where ∂D represents the surface of system volume D, $\hat{\mathbf{n}}$ is a normal vector with respect to the surface ∂D, dS' and dV' indicate that the integration is done with respect to a variable $\mathbf{r}'$. Because the first term can be regarded as the vector potential induced by the bulk current, $\mathbf{j}_{\text{bulk}} = \boldsymbol{\nabla}_{\mathbf{r}'}\times\mathbf{M}(\mathbf{r}')$, whereas the second term is due to the surface current, $\mathbf{j}_{\text{surface}} = \mathbf{M}(\mathbf{r}')\times\hat{\mathbf{n}}$, the macroscopic vector potential is written by

$$\mathbf{A}(\mathbf{r}) = \frac{\mu_0}{4\pi}\int_D \frac{\mathbf{j}_{\text{bulk}}(\mathbf{r}')}{|\mathbf{r}-\mathbf{r}'|}dV' + \frac{\mu_0}{4\pi}\int_{\partial D}\frac{\mathbf{j}_{\text{surface}}(\mathbf{r}')}{|\mathbf{r}-\mathbf{r}'|}dS'. \tag{4.58}$$

Thus far, we have discussed the macroscopic magnetic field (vector potential) induced by currents in system while keeping generality. We are now ready to consider the orbital magnetization induced by OV-induced 2DEG photocurrent. Regarding the position $\mathbf{r}'$ as the guiding center $\mathbf{r}_0$ in (4.58), the magnetic vector potential at the position $\mathbf{r}$ induced by the magnetization at the guiding center $\mathbf{r_0}$ is given by

$$\begin{aligned}\mathbf{A}^{\mathrm{2DEG}}(\mathbf{r}) &= \frac{\mu_0}{4\pi}\int_D \frac{\boldsymbol{\nabla}_{\mathbf{r}_0}\times\mathbf{M}(\mathbf{r}_0)}{|\mathbf{r}-\mathbf{r}_0|}dV_0 + \frac{\mu_0}{4\pi}\int_{\partial D}\frac{\mathbf{M}(\mathbf{r}_0)\times\hat{\mathbf{n}}}{|\mathbf{r}-\mathbf{r}_0|}dS_0 \\ &= \frac{\mu_0}{4\pi}\int_D \frac{\mathbf{j}_{\mathrm{bulk}}(\mathbf{r}_0)}{|\mathbf{r}-\mathbf{r}_0|}dV_0 + \frac{\mu_0}{4\pi}\int_{\partial D}\frac{\mathbf{j}_{\mathrm{edge}}(\mathbf{r}_0)}{|\mathbf{r}-\mathbf{r}_0|}dS_0, \qquad (4.59)\end{aligned}$$

where D and ∂D is replaced by the area of the 2D system and its edge, respectively. We note that dS_0 and dV_0 indicate that the integration is done with respect to a variable $\mathbf{r}_0$. In particular, the second term in (4.59) is due to the edge current at the system size R,

$$\mathbf{j}_{\mathrm{edge}} = \mathbf{M}(R)\times\hat{\mathbf{n}}. \qquad (4.60)$$

However, since the bulk currents cancel out by Eq. (3.183) as mentioned in the previous section and Sec. 3.6.3, that is, $\mathbf{j}_{\mathrm{bulk}} = 0$, only the edge current contributes to the magnetization in Eq. (4.59).

In Eq. (4.60), since the normal vector with respect to the edge of circular disk is given by $\hat{\mathbf{n}} = \hat{\mathbf{e}}_\rho$, and the edge current flows along the edge, $\mathbf{j}_{\mathrm{edge}} \sim \delta j_\ell^+(\omega, B)\,\hat{\mathbf{e}}_\phi$, the magnetization points along the z-direction, $\mathbf{M}(R)$ $\sim \mathcal{M}_\ell(\omega, B)\,\hat{\mathbf{e}}_z$, where

$$\mathcal{M}_\ell(\omega, B) = \delta j_\ell^+(\omega, B). \qquad (4.61)$$

The magnetization in Eq. (4.61) can be regarded as a manifestation of the magneto-electric effect, since it is induced by the electric field of OV[55].

Therefore, the magnetic field dependences of magnetization is the same as the behavior of the induced photocurrents. As discussed in the previous section, when the dark ring $r_\perp^{\ell,i}$ coincides with system edge R, that is, $r_\perp^{\ell,i} = R$, because of the roots of Bessel function, $J_\ell(k_\perp[B]\,R) = 0$, the vanishing points of absorption are caused. Physically it means that when the dark rings of OV coincide with the peak of electron distribution on the system edge, the orbital magnetization disappears. It is significant that this disappearance is induced despite non-zero total intensity, which is related to the fact that the photocurrent flows only along the edge[55]. We thus find that Figs. 4.3 - 4.6 can be viewed as the demonstrations of the magnetization. It is worth a mention that the similar result is obtained by using the cylindrical vector beams[60].

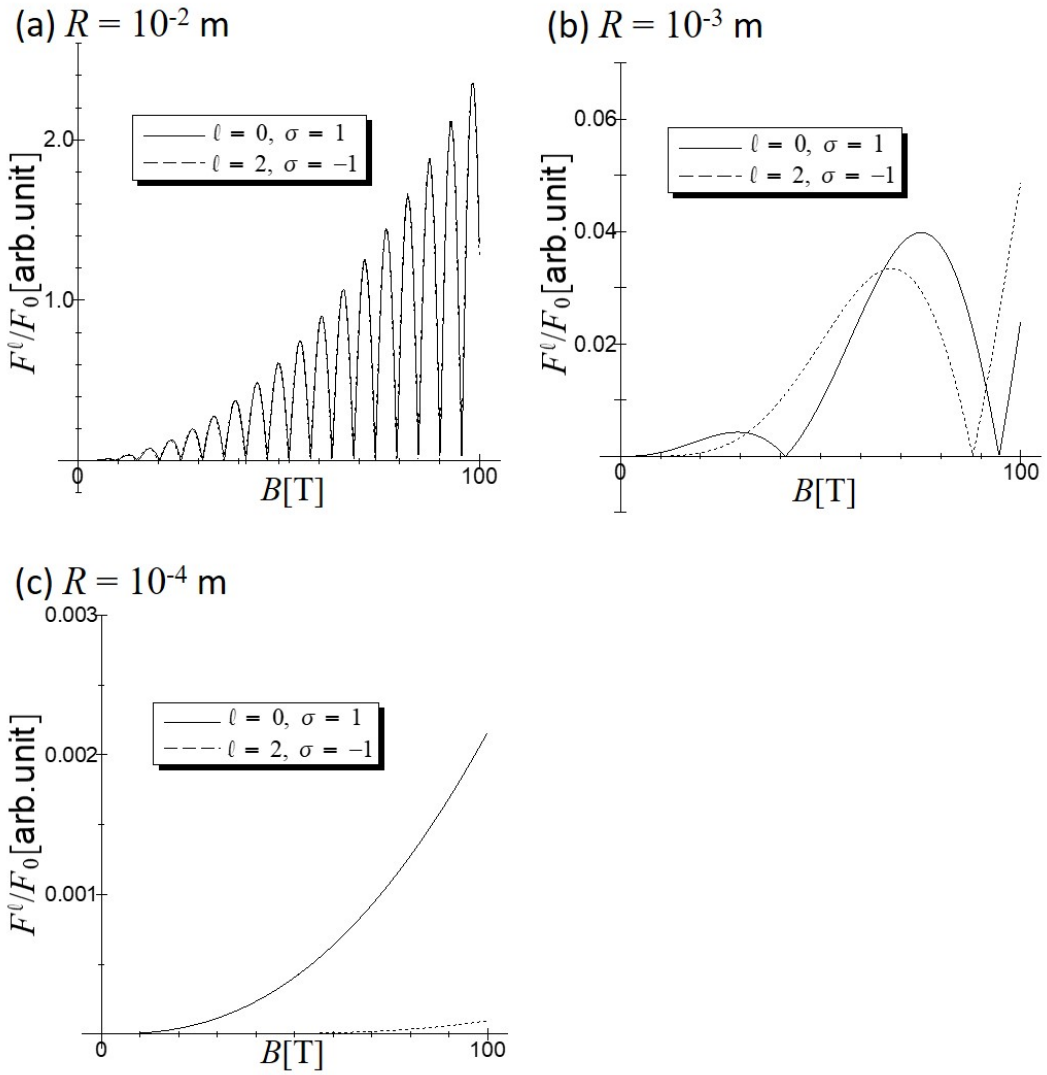

Figure 4.3: Magnetic field dependence of F^ℓ for $\alpha\,(=k_\perp/k_z) = 0.1$ when the chemical potential is kept between the LLL and the second LL. (a) $R = 10^{-2}$ m, (b) $R = 10^{-3}$ m, $R = 10^{-4}$ m. The solid line is for $\ell = 0$ and the dotted line $\ell = 2$. The wavenumber also has B dependence as $k_{\rm OV} = 5.87 \times 10^2 B$ m^{-1}.

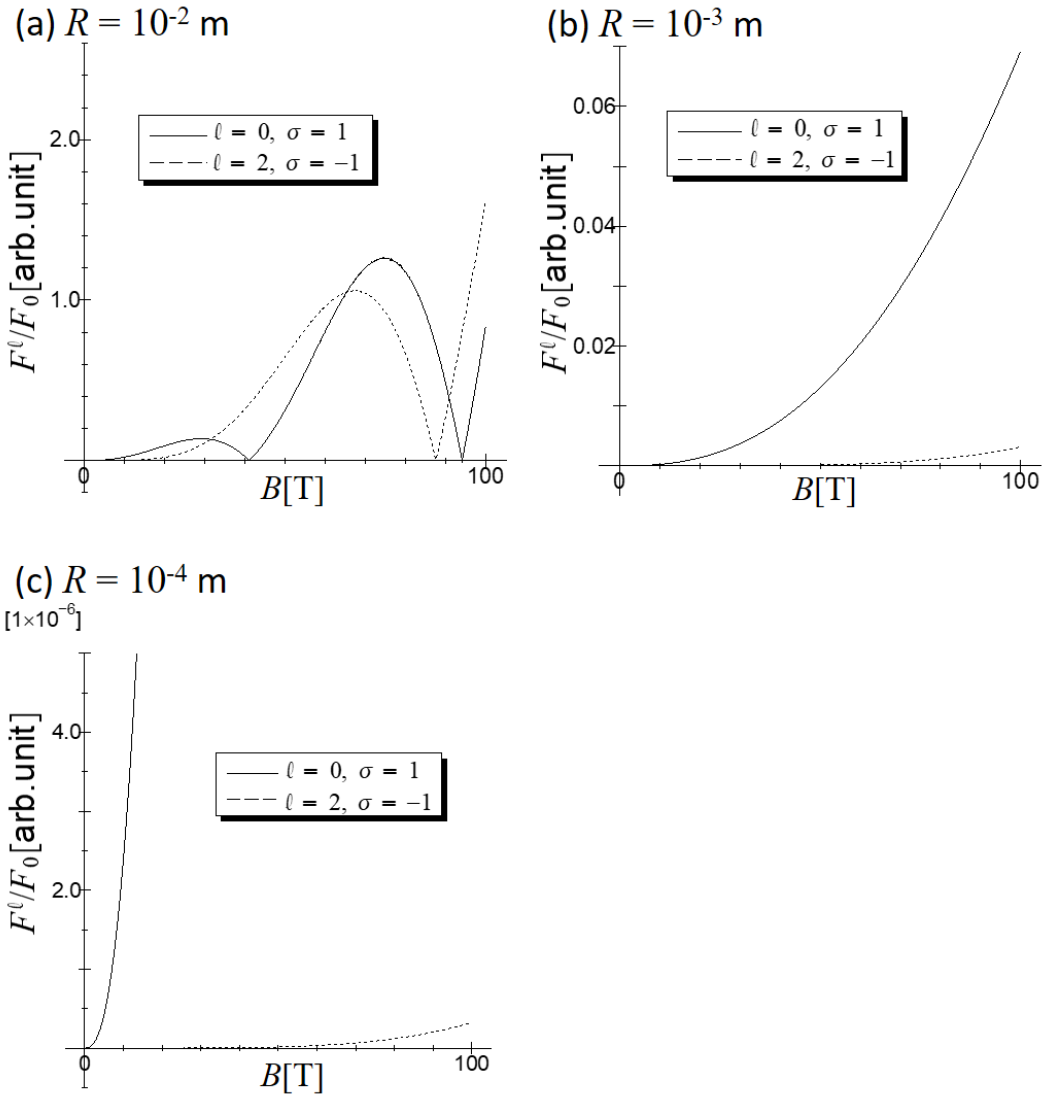

Figure 4.4: Magnetic field dependence of F^ℓ for $\alpha\,(=k_\perp/k_z) = 0.01$ when the chemical potential is kept between the LLL and the second LL. (a) $R = 10^{-2}$ m, (b) $R = 10^{-3}$ m, $R = 10^{-4}$ m. The solid line is for $\ell = 0$ and the dotted line $\ell = 2$. The wavenumber also has B dependence as $k_{\rm OV} = 5.87 \times 10^2 B$ m^{-1}.

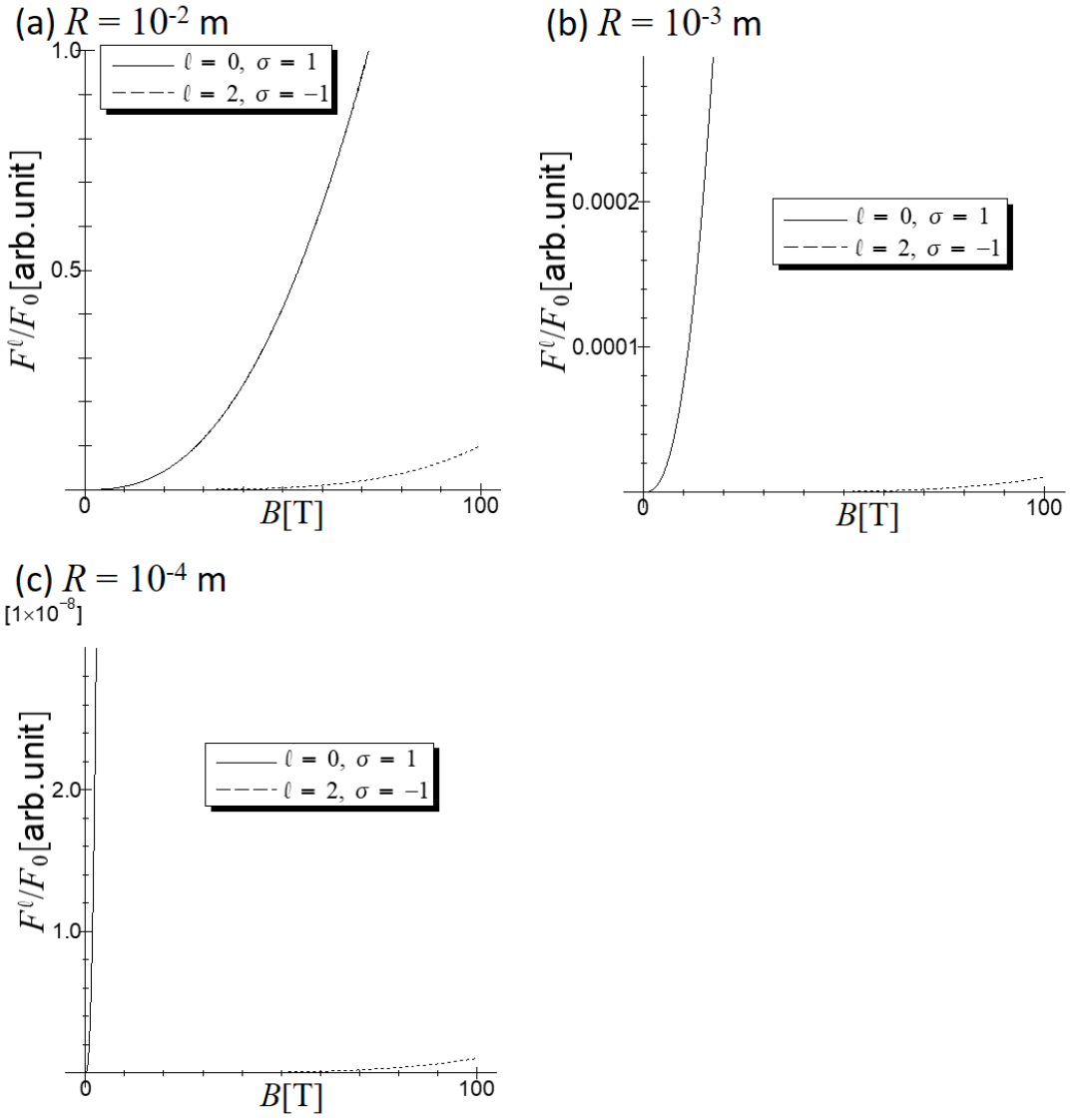

Figure 4.5: Magnetic field dependence of F^ℓ for $\alpha\,(= k_\perp/k_z) = 0.001$ when the chemical potential is kept between the LLL and the second LL. (a) $R = 10^{-2}$ m, (b) $R = 10^{-3}$ m, $R = 10^{-4}$ m. The solid line is for $\ell = 0$ and the dotted line $\ell = 2$. The wavenumber also has B dependence as $k_{\rm OV} = 5.87 \times 10^2 B$ m^{-1}.

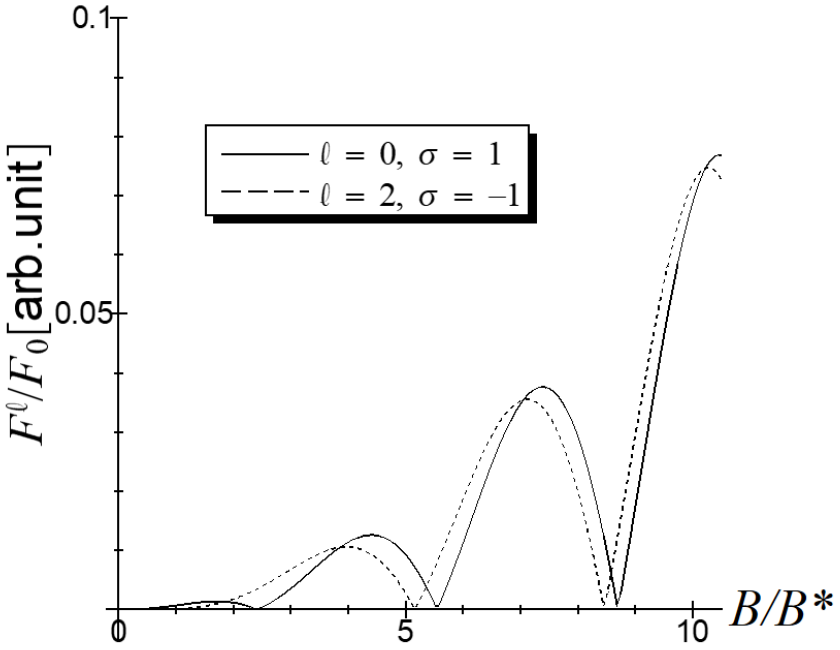

Figure 4.6: Magnetic field dependence of F^ℓ with $R = 10^{-2}$ m and $\alpha\,(= k_\perp/k_z) = 0.1$, when the chemical potential is kept between the LLL and the second LL. The solid line is for $\ell = 0$ and the dotted line $\ell = 2$. We scaled the horizontal axis by $B^* = \Phi_0/\alpha\lambda_e R = 1.70 \times 10^{-3}/\alpha R$ [T]. The wavenumber also has B dependence as $k_{\rm OV} = 5.87 \times 10^2 B$ m^{-1}.

Chapter 5

Proposal of Experimental Scheme

In this Chapter, we propose a possible experimental scheme to demonstrate theoretical results proposed in this dissertation.

5.1 Generation of Optical Vortex Beam

We describe the generation of the Bessel-mode optical vortex beams. A zeroth-order Bessel beam was first generated by Durnin *et al.* by illuminating an annular slit placed in the back focal plane of a lens with a plane wave[11]. However, because the illuminating beam is blocked by the aperture, this method loses most of the beam intensity. Although the method using holographic elements achieves more higher efficiency[61], using of an axicon lens which is conically shaped optical element is the most efficient technique to generate a zeroth-order Bessel beam [62]. The higher-order Bessel beams can also be produced by illuminating an axicon lens with a Laguerre–Gaussian mode[16]. Fig. 5.1 illustrates the method to generate the Bessel mode beam by use of the axicon lens. Since the Bessel-mode beam can be viewed as a superposition of plane waves propagating on the cone with the cone angle $\theta_k = \tan^{-1} k_\perp/k_z$, the Bessel beams are created within the yellow shaded region in Fig. 5.1. The propagation distance of the created Bessel beam can be estimated as $z_{\max} = w_0 k/k_\perp$, where w_0 is the beam waist of Gaussian (or LG) beam[16, 63]. In this region $z_{\max}$, the characteristic phenomenon that the intensity profile of the Bessel beam is reconstructed, that is, keeping the propagation invariant, is occurred. This effect is due to the conical wavefront of the beam.

As described above, a LG beam is needed to generate the higher-order

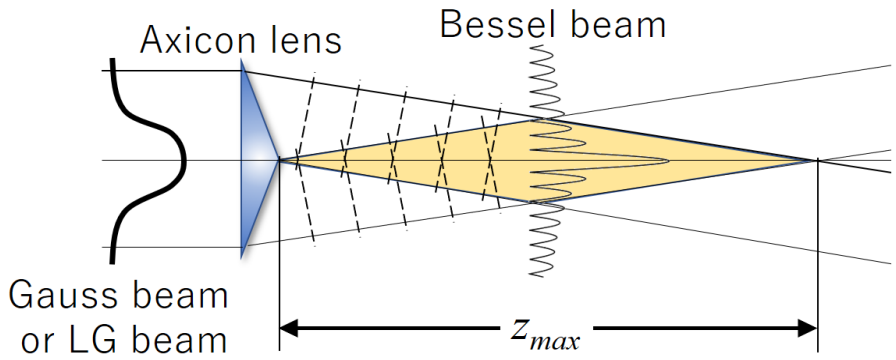

Figure 5.1: Generation of a Bessel beam by use of an axicon lens. Illuminating the axicon lens with a Laguerre-Gaussian (Gaussian) beam generates to a higher-order (zeroth-order) Bessel beam within the yellow shaded region. The propagation distance of Bessel beam is given by $z_{\max}$.

Bessel beam. The typical methods of generation of LG-mode beam are known: illuminating a spiral phase plate[64], a forked holographic filter[65, 66] with a Gaussian light beam, among other things.

First, we describe the generation of LG beam by use of a spiral phase plate. The spiral phase plate is a transparent plate whose thickness increases proportional to the azimuthal angle ϕ around the center of the plate as shown in Fig. 5.2. When the incident beam passes through the spiral phase plate, the amplitude of incident beam u changes to the amplitude after the plate u' as

$$u' = u \exp\left(-i\ \Delta\ell\ \phi\right), \tag{5.1}$$

with $\Delta\ell$ given by

$$\Delta\ell = \Delta n \frac{h}{\lambda}, \tag{5.2}$$

where Δn is the difference in refractive index between the plate and its surroundings and h is the step height of the plate[64]. The LG beam carrying the higher order OAM can be produced via satisfying the relation $\Delta\ell$.

Next, we describe the generation of LG beam by use of a numerically computed hologram. The holographic method can be available by use of a spatial light modulators (SLMs). A computer-generated folk-shaped hologram can produce a light wave with helical phasefronts and a desired orbital angular momentum in the direction of the first diffraction order by illuminating the hologram with a plane wave. If the ℓ-th folked hologram is illuminated with a plane wave, the first order diffracted beams have the OAM $L = \pm\ell\hbar$. For

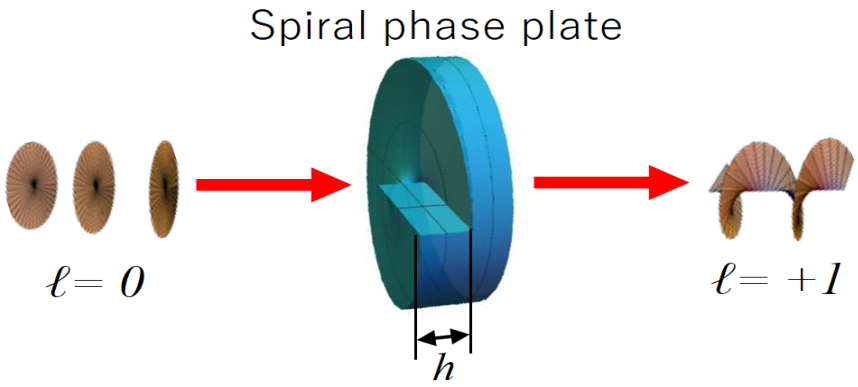

Figure 5.2: Schematic of the generation of the Laguerre-Gaussian beam by use of the spiral phase plate.

example, as shown in Fig. 5.3, two-folked hologram can produce the LG beam with $\ell = \pm 2$ in the direction of the first diffraction order[65].

5.2 Influence of Disorder and Spin in 2DEG

First, we discuss the influence of a disorder to our results. As reviewed in Chap. 3, 2DEG under the magnetic field has degenerate energy levels (3.58) and δ-function-shaped density of states (3.84). However, yet it is impossible to remove disorder, that is, impurities or defects, completely from real samples, the influence of disorder has been ignored there. The existence of the disorder changes both the spatial extent of the density of states and the electronic energy[67]. Thus, the degenerate Landau level (LL) is broadened into a Landau sub-band described by an approximate Lorentzian lineshape centered at the unperturbed LL. Recall our assumption that the chemical potential lies in a gap between the Landau levels, that is, in an insulating region. For this purpose, it is necessary that a width of the Landau sub-band Γ satisfies $\Gamma \ll \hbar\omega_c$. It was shown that, in the self-consistent Born approximation[68, 69], the width of the Landau sub-band is written in the form

$$\Gamma = \hbar\sqrt{\frac{2}{\pi\tau}\omega_c}, \tag{5.3}$$

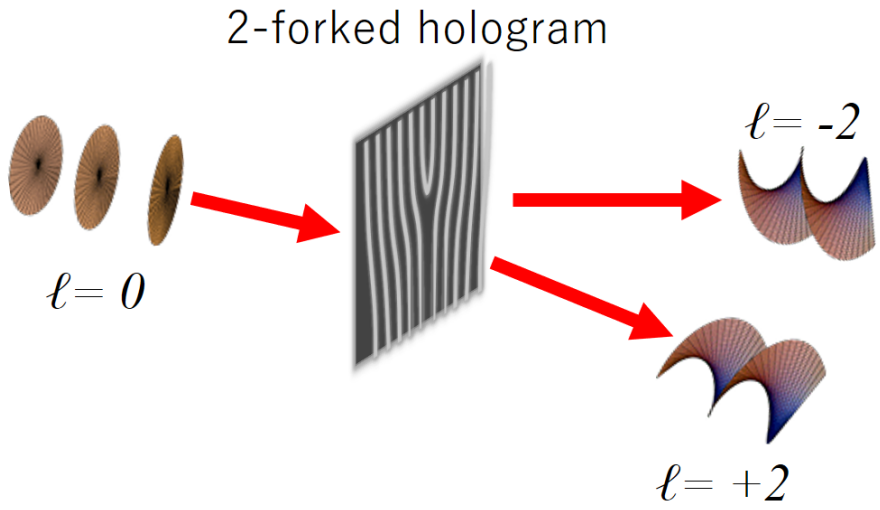

Figure 5.3: Schematic of the generation of the Laguerre-Gaussian beam by use of the holography. Twofold dislocation hologram can generate the LG beam with $\ell = \pm 2$ in the direction of the first diffraction order.

where τ is the relaxation time. Experimentally, the width of the Landau sub-band is estimated by

$$\Gamma = p\sqrt{\frac{B}{\mu_e}} \tag{5.4}$$

with the mobility of the sample μ_e and $p = 2.3 \pm 0.3 \times 10^{-2}$ meV/T[70] and that, for good quality samples, $\Gamma \ll \hbar\omega_c$ is satisfied. Therefore, as long as good quality samples are used, the existence of a disorder would be uninfluential in our discussion.

Next, although our results in Chap. 4 have been based on a spinless 2DEG model, we here discuss how our results are experimentally achieved in case of the existence of an electron spin. As well-known, when an atomic electron possesses a spin, the presence of a magnetic field splits an atomic energy level into several sub-levels due to Zeeman effect. Such the effect occurs also in 2DEG in a magnetic field. That is to say, in Landau-quantized electron with the spin degree of freedom, the presence of the strong magnetic field causes the splitting of the LL into the Zeeman sub-levels whose gap is proportional to the magnetic field strength, $\Delta E = g\mu_B B$ with Landé g-factor and the Bohr magneton μ_B. Nevertheless, even if the electron spin is considered, we can treat non–spin-flip electronic transitions between the Lowest Landau

level ($N = 0$) (LLL) and the second Landau level ($N = 1$) (2LL). If the chemical potential lies in the gap between the Zeeman sub-levels of the LLL in some way and other, the lower sub-level of the LLL is fully occupied by only the electrons with the spin parallel to the magnetic field and the upper sub-level of it becomes completely empty. When the photon possessing the same amount of the energy difference between the LLs, $E = \hbar\omega_c$, is incident to the system, the electron in the lower sub-level of the LLL transfers to the that of the 2LL. Such a transition does not involve a spin-flip process. In this way, non–spin-flip electronic transitions between the LLL and the 2LL would be achieved (see Fig. 5.4).

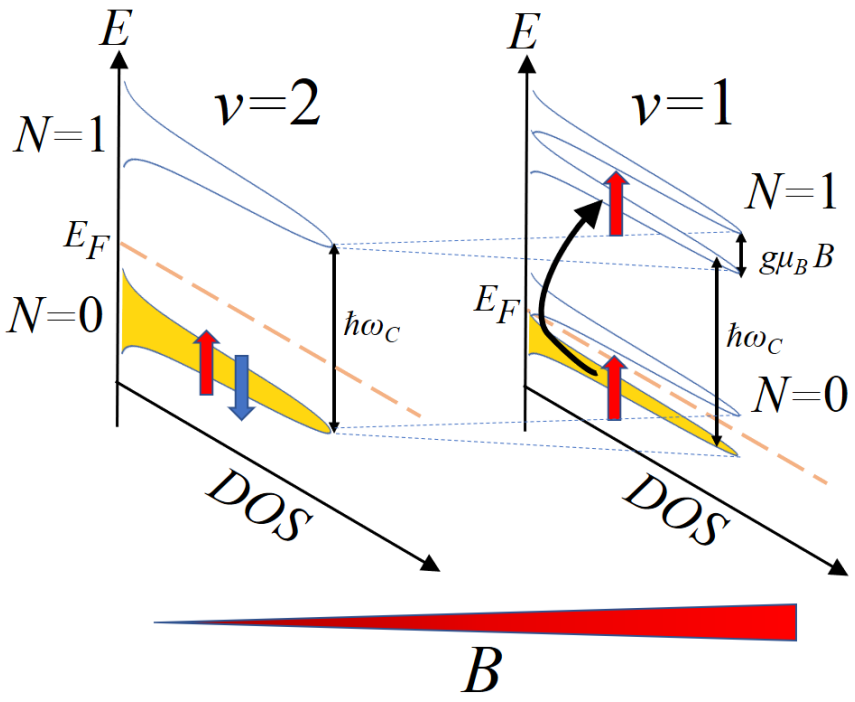

Figure 5.4: A non-spin-flip process in transition between the LLL to 2LL. The existence of impurity in a sample, each degenerate Landau level is broadened into a band. (left side) In case of presence of electron spin, each spin-degenerated Landau band splits into Zeeman sub-band. By tuning a chemical potential to lie in a gap between the Zeeman sub-band of the LLL, the non-spin-flip prosess in the transition between the LLL to 2LL would be achieved (right side).

5.3 Possible Experimental Setup

We illustrate the possible concept of experimental setup to confirm the consequence of our theory in Fig. 5.5. Throughout this section, we use the physical values for GaAs/AlGaAs heterostructures as the example.

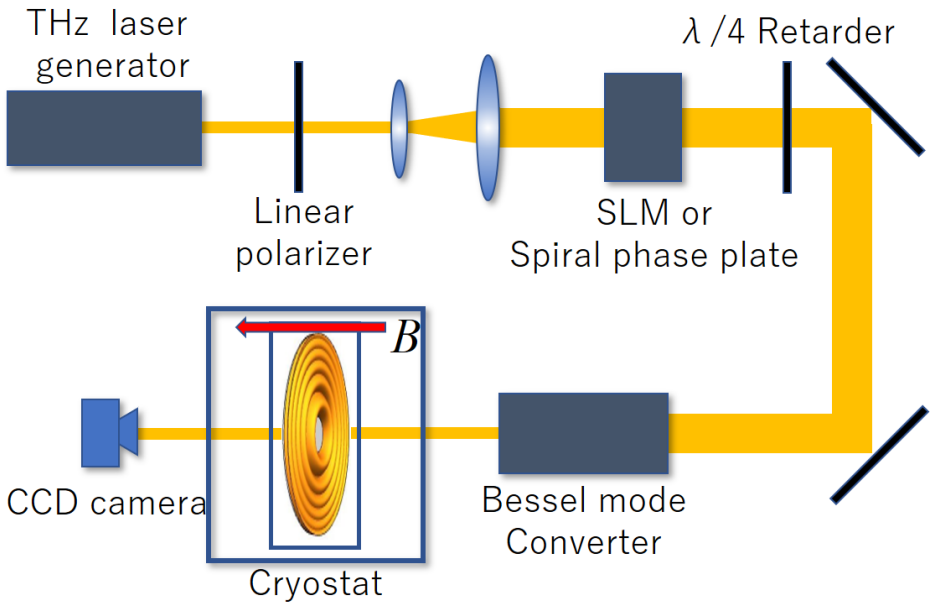

Figure 5.5: Conceptual illustration of the experimental setup. To cause the transion between the LLL and 2LL by a light beam, a THz laser generator would be used. A linear polarizer, SLM (or a spiral phase plate), and $\lambda/4$ retarder are used to generate LG-beam with the higher order OAM. The Bessel beam converter consists of an axicon lens. 2DEG sample is located in a cyostat to keep a low temperature. In case of observing a transmitted beam, CCD camera would be needed.

First, we consider the setup for the electron system as follows: To avoid a electronic thermal excitation, a 2DEG sample is located in a cryostat to keep a low temperature. We have considered the transition between the LLL and 2LL. It is known that electrons can occupy only the LLL when the magnetic field is applied typically over 8 T for GaAs/AlGaAs heterostructures with the electron density $n_e \sim 2.3 \times 10^{15}$ m^{-2}[71]. Furthermore, to realize the completely filled LLL even when $B > 8$ T or to keep the chemical potential between $N = 0$ and $N = 1$, we need to supply electrons externally via an electrode, etc. At this moment, the typical cyclotron frequency is given by

$f_c = \omega_c/2\pi = 4.19 \times 10^{12}$ Hz at $B = 10$ T (we used the effective electron mass for GaAs).

Next, we consider the generation of incident Bessel beams. To induce the cyclotron resonance by lights, a THz laser beam generator is required. The unpolarized beam generated by THz beam generator is converted into the linearly polarized beam by passing through a linear polarizer. The spatial light modulator (SLM) or the spiral phase plate produces the LG beam with an orbital angular momentum. A $\lambda/4$ retarder converts the linearly polarized beam into the circularly polarized beam. Thus, the light beam carrying an orbital angular momentum in addition to spin angular momentum is produced. We here note that the arrangement of the retarders and SLM is changed by the specification of SLM. After generation of the higher order LG beam, it is necessary to convert the LG beam into the higher order Bessel beam. How to convert is described in Sec. 5.1.

Thus, the higher order Bessel beam is input to 2DEG sample. The direction of light's propagation is tuned to be parallel to the magnetic field which is perpendicular to the 2DEG surface. We naturally arrive at two ideas how to confirm if the OV-photocurrent is induced. The first is the direct measurement of the induced current via an electric contact on the system edge. The second is to measure the intensity of transmitted light via CCD camera in back of the sample, because the camera would not observe the transmitted light when occurring OV-absorption (see Fig. 5.5).

Chapter 6

Summary and Future Perspective

An optical vortex has a helical wavefront in classical picture. Because the helical wavefront can apply an orbital angular momentum to matter, the optical vortex is characteristic light which can carry the orbital angular momentum, whereas the plane wave light carries only spin angular momentum via the helicity. The optical vortex has arose much attention to application by use of orbital angular momentum in the past decades. Additionally, the optical vortex has a cylindrical spatial distribution consisting of bright and dark rings which can trace back to transverse component of wavevector.

Babiker *et al.* has stated that the optical orbital angular momentum can be transferred only to the center of mass motion in the electric dipole transition[31]. Moreover, it is known that a free electron can not absorb a photon. Therefore, to avoid two difficulties and to consider an electric dipole transition in coupling with electrons, it is naturally expected that two dimensional electron gas is good candidate because the electron under the magnetic field can be quantized the energy and carry a quantized angular momentum.

In this dissertation, we demonstrated how the optical vortex beam carrying the orbital angular momentum modifies the selection rules for the absorption processes of the Landau-quantized two-dimensional electron gas. Concerning Kubo formula or the first order perturbation theory of photocurrent, the matrix elements of photocurrent $\langle n, m \left| j_{\pm} \right| n', m' \rangle$ are allowed when $\Delta m = m' - m = 1$. On the other hand, the matrix elements of interaction Hamiltonian $\langle n', m' | \boldsymbol{A}^{\mathrm{OV}}_{\ell,\sigma} \cdot \mathbf{r} | n, m \rangle$ gives the angular momentum conservation $\Delta m = J = \ell + \sigma$. We thus found that the vortex beam with the total angular momentum $J = 1$ can be absorbed to induce the photocurrents. Because the optical vortex carries the spin $\sigma = \pm 1$, we obtained two possible combina-

tions: $\ell = 2$ and $\sigma = -1$ or $\ell = 0$ and $\sigma = 1$, cause the transitions between the lowest ($N = 0$) and the second lowest ($N = 1$) Landau levels when the beam propagates along the direction of the external magnetic field and is illuminated at the center of circular disk geometry. While the case with $\ell = 0$ and $\sigma = 1$ corresponds to the well-known optical transitions under the circularly polarized light, the case with $\ell = 2$ and $\sigma = -1$ is a characteristic result, which shows that it is the total angular momentum of light that is absorbed by electrons[39].

We also demonstrated that, in the framework of Kubo's linear response theory, the optically induced current is localized near the edge of the sample, so that when excited with the Bessel beam, the photocurrent disappears when the dark rings of the Bessel beam coincide with the edge of the sample. To see this, we propose a measurement of induced photocurrent by varying magnetic field with keeping the chemical potential between $N = 0$ and $N = 1$ and without modification to the optics system. At this moment, we should notice that, since the electron excitation energy changes with varying the magnetic field, the energy of lights must be tuned to generate the excitation[39].

The cancellation (absence) of the bulk currents was also interpreted in terms of the coherent state representation. Consequently, we demonstrated how the orbital magnetization is induced by only the edge currents[55]. We may experimentally confirm the absence of bulk currents by measuring the disappearing of the orbital magnetization when the optical dark rings coincide with the system edge.

Concerning the quantitative values of parameters used in the present theory, we here give comments on the parameters experimentally to observe such phenomena. The first is on the external magnetic field. For example, for GaAs/AlGaAs heterostructures with the electron density $n_e \sim 2.3 \times 10^{15}$ m^{-2}, electrons can occupy only the lowest Landau level when the magnetic field is applied typically over 8 T[71]. To realize the completely filled lowest Landau level even when the external magnetic field is applied over 8 T or to keep the chemical potential between the lowest Landau level and the second Landau level, we need to supply electrons from the outside via an electrode, etc. The next is on the frequency of optical vortex. As shown in Table 4.2, the frequency of excitation energy between $N = 0$ and $N = 1$ gives 4.19 THz at $B = 10$ T for GaAs system. Therefore, to induce such excitation, the THz beams are needed.

For such electron systems, we proposed the possible experimental scheme to confirm our consequences. After generating the THz beam, it is necessary to convert the beam into the Bessel beam carrying the higher order orbital angular momentum. The methods of generations of the Bessel beam were overviewed in Sec. 5.1. Polarizers or retarders are available to produce the

Bessel beams carrying the spin angular momentum in addition to the orbital angular momentum. The higher order Bessel-mode optical vortex beams irradiate the 2DEG samples located in a cryostat to keep a low temperature. To observe the absorption of the optical vortex beam, the direct measurement of the induced photocurrent via electric contacts on the system edge or the observation of the transmitted light via CCD camera in back of the samples would be available.

To check the present theoretical scheme from more general viewpoints, we generalized the dipole coupling scheme to general multipolar couplings in Appendix H. Then we confirm the present results by regarding the dipole coupling as a special case with $l'' = 1$ in Eq. (H.8). We reconstructed the minimal-coupling Hamiltonian by expanding by the vector spherical Harmonics. When the dipole moment of current in rotation on a surface couples with the optical beam propagating normal to the surface, the photoabsorptions are allowed $\ell = 0$ and $\sigma = 1$, or $\ell = 2$ and $\sigma = -1$. This is completely consistent with calculation without multipolar expansion. When we know the symmetry of materials, we may assume the current distributions. Since we have obtained the general expressions of the multipolar Hamiltonian, we can know the spectroscopic selection rules beyond the dipole transition.

Throughout this dissertation, we assumed the propagation of optical vortex to be parallel to the magnetic field. However, it is possible to irradiate with the vortex light beam propagating anti-parallel to the magnetic field. Since the magnetic field then breaks time-reversal symmetry, the direction of currents is determined. When the magnetic field flips into the antiparallel direction to z axis, the optical angular momentum absorption must thus change into $J = -1$, that is, $\ell = 0$ and $\sigma = -1$, or $\ell = -2$ and $\sigma = 1$. This corresponds to change of the magnetic chirality via the electron orbital motion.

As future perspectives, the couplings of optical vortex with materials have various potentiality to give access to undiscovered phenomena. For examples, in heavy electrons in atoms, a spin-orbit interaction plays important role to unify spin and orbital degree of freedom. The optical vortex has multipolar degrees of freedom by nature due to the orbital angular momentum. Therefore, coupling of the multipoles in matter and in light will provide a huge variety of transitions.

The rotation of polarization of optical vortex itself is also considerable. The polarization of plane wave can be rotated when passing through an optical active material. That is to say, the material with inversion symmetry is essential to induce the optical rotation. On the other hand, optical vortex possessing the helical wavefront has finite angular momentum. Then, even when the optical vortex beam traverses a material with inversion symmetry,

the absorption strengths are expected to depend on the spin helicity of the light.

Finally, we comment a Rabi oscillation. The Rabi oscillation consists a periodic change between photoabsorption and stimulated photoemission in a two-level system with an illumination of a light beam. On the other hand, our present theory is based on only the one-photon absorption in the transition of a two-level system associated with the lowest Landau level ($N = 0$) and the second Landau level ($N = 1$). Thus, our theory is not exactly equivalent to the Rabi oscillation processes. However, as the further development of our present theory, the Rabi oscillation is also considerable. The Rabi frequency between each Landau level is given by[72]

$$\Omega = \sqrt{\frac{|\gamma|^2}{\hbar^2} + \frac{(\omega - \omega_c)^2}{4}}, \tag{6.1}$$

where $\gamma = \left\langle N = 1 \left| \boldsymbol{A}^{\mathrm{OV}}_{\ell,\sigma} \cdot \mathbf{j} \right| N = 0 \right\rangle$. Thus, it is expected that the absorption-emission cycle (the inverse of the Rabi frequency) depends on the radial profile of optical vortex beam.

Appendix A

Kubo Formula

We here review the derivation of Kubo formula[56]. The total Hamiltonian with weekly perturbed by external field given by a vector potential $\mathbf{A}$ is written by

$$\begin{aligned} H &= H_0 + \Delta H \\ &= H_0 - \mathbf{A} \cdot \mathbf{j}, \end{aligned} \tag{A.1}$$

where $\mathbf{j}$ is an electric current and H_0 is a non-perturbative Hamiltonian. We here assume time-dependence of the external field is given by $\mathbf{A}(t) = \mathbf{A}\mathrm{e}^{-i\omega t}$. The wave function in interaction picture in the first order perturbation is given by

$$|N\rangle_I = |n,m\rangle - \frac{i}{\hbar}\int_{-\infty}^{t} dt' \mathrm{e}^{\frac{i}{\hbar}\hat{H}_0 t'}(-\hat{\mathbf{A}}(t')\cdot\hat{\mathbf{j}})\mathrm{e}^{-\frac{i}{\hbar}\hat{H}_0 t'}|n,m\rangle, \tag{A.2}$$

where index I indicates that the wave functions or the operators are represented in the interaction picture. The operators in the interaction picture are transformed from the operators in the Schrödinger picture $\hat{O}$ by $\hat{O}_I(t) = \mathrm{e}^{\frac{i}{\hbar}\hat{H}_0 t}\hat{O}\mathrm{e}^{-\frac{i}{\hbar}\hat{H}_0 t}$. Then, we can calculate the expectation value of the response of i-th component of an observable operator $\hat{O}$ within the first order

in $\mathbf{A}$,

$$\begin{aligned}
\langle \delta O_i(t) \rangle &= \langle O_i(t) \rangle - \left\langle n,m \left| \hat{O}_{iI}(t) \right| n,m \right\rangle \\
&= \left\langle N \left| \hat{O}_{iI}(t) \right| N \right\rangle_I - \left\langle n,m \left| \hat{O}_{iI}(t) \right| n,m \right\rangle \\
&\simeq \frac{i}{\hbar} \int_{-\infty}^{t} dt' \langle n,m | \hat{O}_{iI}(t) (\hat{\mathbf{A}}(t') \cdot \hat{\mathbf{j}})_I | n,m \rangle \\
&- \frac{i}{\hbar} \int_{-\infty}^{t} dt' \langle n,m | (\hat{\mathbf{A}}(t') \cdot \hat{\mathbf{j}})_I \hat{O}_{iI}(t) | n,m \rangle \\
&= \frac{i}{\hbar} \int_{-\infty}^{t} dt' \langle n,m | [\hat{O}_{iI}(t), (\hat{\mathbf{A}}(t') \cdot \hat{\mathbf{j}})_I] | n,m \rangle \\
&= \frac{i}{\hbar} \int_{-\infty}^{t} dt' \langle n,m | [\hat{O}_{iI}(t), (\hat{\mathbf{A}} \cdot \hat{\mathbf{j}})_I(t')] | n,m \rangle \mathrm{e}^{-i\omega t'} \\
&= \frac{i}{\hbar} \int_{-\infty}^{\infty} dt' \theta(t-t') \langle n,m | [\hat{O}_{iI}(t), (\hat{\mathbf{A}} \cdot \hat{\mathbf{j}})_I(t')] | n,m \rangle \mathrm{e}^{-i\omega t'}. \qquad \text{(A.3)}
\end{aligned}$$

By replacing $\tau = t - t'$, we can write as

$$\begin{aligned}
\langle \delta O_i(t) \rangle &= \frac{i}{\hbar} \int_{-\infty}^{\infty} d\tau \theta(\tau) \langle n,m | [\hat{O}_{iI}(\tau), (\hat{\mathbf{A}} \cdot \hat{\mathbf{j}})_I(0)] | n,m \rangle \mathrm{e}^{-i\omega(t-\tau)} \\
&= \delta O_i(\omega) \mathrm{e}^{-i\omega t}, \qquad \text{(A.4)}
\end{aligned}$$

where the Fourier component is denoted by

$$\delta O_i(\omega) = \frac{i}{\hbar} \int_0^{\infty} dt \mathrm{e}^{i\omega t} \langle n,m | [\hat{O}_{iI}(t), (\hat{\mathbf{A}} \cdot \hat{\mathbf{j}})_I(0)] | n,m \rangle. \qquad \text{(A.5)}$$

Taking account of a finite temperature effect, we need to take the statistical average of (A.5),

$$\delta O_i(\omega) = \frac{i}{\hbar} \int_0^{\infty} dt \mathrm{e}^{i\omega t} \sum_{n,m} \frac{\mathrm{e}^{-\beta E_{n,m}}}{Z} \langle n,m | [\hat{O}_{iI}(t), (\hat{\mathbf{A}} \cdot \hat{\mathbf{j}})_I(0)] | n,m \rangle, \qquad \text{(A.6)}$$

where $\beta = 1/k_B T$ is an inverse temperature with a Boltzmann constant k_B, and Z is the canonical partition function. Furthermore, after integrating respect to t, when we take account of a impurity effect by replacement $\omega \to \omega + i\delta/\hbar$, we obtain

$$\delta O_i(\omega) = -\sum_{n,m} \sum_{n',m'} \frac{\mathrm{e}^{-\beta E_{n,m}} - \mathrm{e}^{-\beta E_{n',m'}}}{Z} \frac{\langle n,m | \hat{O}_i | n',m' \rangle \langle n',m' | \hat{\mathbf{A}} \cdot \hat{\mathbf{j}} | n,m \rangle}{E_{n,m} - E_{n',m'} + \hbar\omega + i\delta}. \qquad \text{(A.7)}$$

Or using a Fermi-Dirac distribution $f(E_{n,m}) = 1/\exp\left[\beta(E_{n,m} - \mu)\right] + 1$ with where the chemical potential μ, we have

$$\delta O_i(\omega) = -\sum_{n,m}\sum_{n',m'} \left(f(E_{n,m}) - f(E_{n',m'})\right) \frac{\langle n,m|\hat{O}_i|n',m'\rangle\langle n',m'|\hat{\mathbf{A}}\cdot\hat{\mathbf{j}}|n,m\rangle}{E_{n,m} - E_{n',m'} + \hbar\omega + i\delta}, \tag{A.8}$$

which gives Eq. (4.7) when we adopt $\hat{O}_i = j_i$.

Appendix B

Coordinate Transform

Cylindrical Basis

We here summarize the property of the cylindrical basis. The rotation matrix with respect to z axis is given by

$$R_z(\phi) = \begin{pmatrix} \cos\phi & \sin\phi \\ -\sin\phi & \cos\phi \end{pmatrix}, \tag{B.1}$$

which generates the transformation from Cartesian basis to the cylindrical one as the following

$$\begin{pmatrix} \hat{\mathbf{e}}_\rho \\ \hat{\mathbf{e}}_\phi \end{pmatrix} = R_z(\phi) \begin{pmatrix} \hat{\mathbf{e}}_x \\ \hat{\mathbf{e}}_y \end{pmatrix} = \begin{pmatrix} \cos\phi\hat{\mathbf{e}}_x + \sin\phi\hat{\mathbf{e}}_y \\ -\sin\phi\hat{\mathbf{e}}_x + \cos\phi\hat{\mathbf{e}}_y \end{pmatrix}. \tag{B.2}$$

Its inverse transformation is given by

$$\begin{pmatrix} \hat{\mathbf{e}}_x \\ \hat{\mathbf{e}}_y \end{pmatrix} = R_z^{-1}(\phi) \begin{pmatrix} \hat{\mathbf{e}}_\rho \\ \hat{\mathbf{e}}_\phi \end{pmatrix} = \begin{pmatrix} \cos\phi\hat{\mathbf{e}}_\rho - \sin\phi\hat{\mathbf{e}}_\phi \\ \sin\phi\hat{\mathbf{e}}_\rho + \cos\phi\hat{\mathbf{e}}_\phi \end{pmatrix}. \tag{B.3}$$

The vector components are given by the projection from an arbitrary vector $\mathbf{a}\,(= a_x\hat{\mathbf{e}}_x + a_y\hat{\mathbf{e}}_y)$ in the Cartesian coordinates,

$$\begin{aligned} a_\rho &= \mathbf{e}_\rho \cdot \mathbf{a} = a_x\cos\phi + a_y\sin\phi, \\ a_\phi &= \mathbf{e}_\phi \cdot \mathbf{a} = -a_x\sin\phi + a_y\cos\phi. \end{aligned} \tag{B.4}$$

Chiral (Helicity) Basis

The transformation matrix from the Cartesian basis to chiral one is defined by

$$R_{\rm ch} = \begin{pmatrix} \frac{1}{\sqrt{2}} & \frac{i}{\sqrt{2}} \\ \frac{1}{\sqrt{2}} & -\frac{i}{\sqrt{2}} \end{pmatrix}. \tag{B.5}$$

Then we see that its transformation is given by

$$\begin{pmatrix} \hat{\mathbf{e}}_+ \\ \hat{\mathbf{e}}_- \end{pmatrix} = R_{\rm ch} \begin{pmatrix} \hat{\mathbf{e}}_x \\ \hat{\mathbf{e}}_y \end{pmatrix} = \frac{1}{\sqrt{2}} \begin{pmatrix} \hat{\mathbf{e}}_x + i\hat{\mathbf{e}}_y \\ \hat{\mathbf{e}}_x - i\hat{\mathbf{e}}_y \end{pmatrix}. \tag{B.6}$$

Its inverse transformation is also given by

$$\begin{pmatrix} \hat{\mathbf{e}}_x \\ \hat{\mathbf{e}}_y \end{pmatrix} = R_{\rm ch}^{-1} \begin{pmatrix} \hat{\mathbf{e}}_+ \\ \hat{\mathbf{e}}_- \end{pmatrix} = \frac{1}{\sqrt{2}} \begin{pmatrix} \hat{\mathbf{e}}_+ + \hat{\mathbf{e}}_- \\ -i\left(\hat{\mathbf{e}}_+ - \hat{\mathbf{e}}_-\right) \end{pmatrix}. \tag{B.7}$$

The orthogonality satisfies the following relations,

$$\begin{aligned} \hat{\mathbf{e}}_i^* \cdot \hat{\mathbf{e}}_j &= \delta_{ij}, \\ \hat{\mathbf{e}}_\pm \times \hat{\mathbf{e}}_\pm &= 0, \\ \hat{\mathbf{e}}_+ \times \hat{\mathbf{e}}_- &= -i\hat{\mathbf{e}}_z, \\ \hat{\mathbf{e}}_\pm \times \hat{\mathbf{e}}_z &= \pm i\hat{\mathbf{e}}_\pm. \end{aligned} \tag{B.8}$$

The vector components in chiral basis is represented by those of the Cartesian basis are written by

$$\begin{aligned} a_+ &= \mathbf{e}_+^* \cdot \mathbf{a} = \frac{a_x - ia_y}{\sqrt{2}}, \\ a_- &= \mathbf{e}_-^* \cdot \mathbf{a} = \frac{a_x + ia_y}{\sqrt{2}}, \end{aligned} \tag{B.9}$$

where we used the arbitrary vector in the Cartesian coordinates as $\mathbf{a} = a_x\hat{\mathbf{e}}_x + a_y\hat{\mathbf{e}}_y$. The vector components in chiral basis can also be written in cylindrical basis by using (B.4) as

$$\begin{aligned} a_+ &= \frac{a_\rho - ia_\phi}{\sqrt{2}} \mathrm{e}^{-i\phi}, \\ a_- &= \frac{a_\rho + ia_\phi}{\sqrt{2}} \mathrm{e}^{i\phi}. \end{aligned} \tag{B.10}$$

Appendix C

Calculation of the Radial Integral $C_{n,m}^{n',m'}$

The radial integral $C_{n,m}^{n',m'}$ given by Eq. (4.11) is explicitly expressed as

$$\begin{aligned} C_{n,m}^{n',m'} &= \int_0^\infty d\rho\rho^2 \rho_{nm}(\rho) R_{n'm'}(\rho) \\ &= N_{nm}N_{n'm'} \int_0^\infty d\rho\rho^2 \exp\left(-\frac{\rho^2}{2l_B^2}\right)\left(\frac{\rho}{l_B}\right)^{|m|+|m'|} L_n^{|m|}\left(\frac{\rho^2}{2l_B^2}\right) L_{n'}^{|m'|}\left(\frac{\rho^2}{2l_B^2}\right), \end{aligned} \tag{C.1}$$

where the normalization constant is given by

$$N_{nm} = \left(\frac{n!}{(n+|m|)!}\right)^{1/2} \frac{1}{2^{|m|/2} l_B}. \tag{C.2}$$

Changing the variable ρ to $x = \rho^2/2l_B^2$, we can rewrite the radial integral as the following,

$$\begin{aligned} C_{n,m}^{n',m'} &= N_{nm}N_{n'm'} 2^{\frac{|m|+|m'|+1}{2}} l_B^3 \int_0^\infty dx \mathrm{e}^{-x} x^{\frac{|m|+|m'|+1}{2}} L_n^{|m|}(x) L_{n'}^{|m'|}(x) \\ &= \left(\frac{n!}{(n+|m|)!}\right)^{\frac{1}{2}} \left(\frac{n'!}{(n'+|m'|)!}\right)^{\frac{1}{2}} 2^{\frac{1}{2}} l_B \int_0^\infty dx \mathrm{e}^{-x} x^{\frac{|m|+|m'|+1}{2}} L_n^{|m|}(x) L_{n'}^{|m'|}(x)\,. \end{aligned} \tag{C.3}$$

Next, we calculate the integral $\int_0^\infty dx \mathrm{e}^{-x} x^{\frac{|m|+|m'|+1}{2}} L_n^{|m|}(x) L_{n'}^{|m'|}(x)$. We use the orthogonality of the associated Laguerre polynomials,

$$\int_0^\infty dx \mathrm{e}^{-x} x^\alpha L_n^\alpha(x) L_m^\alpha(x) = \begin{cases} 0 & \text{for } m \neq n \\ \frac{(\alpha+n)!}{n!} & \text{for } m = n \end{cases} \quad \text{for } \mathrm{Re}\alpha > -1, \tag{C.4}$$

and the formula

$$L_n^{\alpha-1}(x) = L_n^{\alpha}(x) - L_{n-1}^{\alpha}(x). \tag{C.5}$$

In case of $m' = m+1$ with $m \geq 0$, we have

$$\begin{aligned}
&\int_0^\infty dx \mathrm{e}^{-x} x^{\frac{|m|+|m+1|+1}{2}} L_n^{|m|}(x) L_{n'}^{|m+1|}(x) \\
&\qquad = \int_0^\infty dx \mathrm{e}^{-x} x^{m+1} L_n^{m}(x) L_{n'}^{m+1}(x) \\
&\qquad = \int_0^\infty dx \mathrm{e}^{-x} x^{m+1} L_n^{m+1}(x) L_{n'}^{m+1}(x) \\
&\qquad - \int_0^\infty dx \mathrm{e}^{-x} x^{m+1} L_{n-1}^{m+1}(x) L_{n'}^{m+1}(x) \\
&\qquad = \frac{(n+m+1)!}{n!}\delta_{n'n} - \frac{(n+m)!}{(n-1)!}\delta_{n'n-1}.
\end{aligned} \tag{C.6}$$

For $n' = n$, we obtain the radial integral $C_{n,m}^{n',m'}$ as

$$\begin{aligned}
C_{n,m}^{n,m+1} &= \left[\frac{n!}{(n+m)!}\right]^{\frac{1}{2}} \left[\frac{n!}{(n+m+1)!}\right]^{\frac{1}{2}} 2^{\frac{1}{2}} l_B \frac{(n+m+1)!}{n!} \\
&= \left[\frac{(n+m+1)!}{(n+m)!}\right]^{\frac{1}{2}} 2^{\frac{1}{2}} l_B \\
&= \sqrt{2(n+m+1)} l_B.
\end{aligned} \tag{C.7}$$

For $n' = n-1$, we obtain

$$\begin{aligned}
C_{n,m}^{n-1,m+1} &= \left[\frac{n!}{(n+m)!}\right]^{\frac{1}{2}} \left[\frac{(n-1)!}{(n+m)!}\right]^{\frac{1}{2}} 2^{\frac{1}{2}} l_B \left[-\frac{(n+m)!}{(n-1)!}\right] \\
&= -\left[\frac{n!}{(n-1)!}\right] 2^{\frac{1}{2}} l_B \\
&= -\sqrt{2n} l_B.
\end{aligned} \tag{C.8}$$

In case of $m' = m + 1$ with $m \leq -1$, we have

$$\begin{aligned}
&\int_0^\infty dx \mathrm{e}^{-x} x^{\frac{|m|+|m+1|+1}{2}} L_n^{|m|}(x) L_{n'}^{|m+1|}(x) \\
&\qquad = \int_0^\infty dx \mathrm{e}^{-x} x^{-m} L_n^{-m}(x) L_{n'}^{-m-1}(x) \\
&\qquad = \int_0^\infty dx \mathrm{e}^{-x} x^{-m} L_n^{-m}(x) L_{n'}^{-m}(x) \\
&\qquad - \int_0^\infty dx \mathrm{e}^{-x} x^{-m} L_n^{-m}(x) L_{n'-1}^{-m}(x) \\
&\qquad = \frac{(n-m)!}{n!} \delta_{n'n} - \frac{(n-m)!}{n!} \delta_{n'n+1}. \qquad \text{(C.9)}
\end{aligned}$$

For $n' = n$, we obtain the radial integral $C_{n,m}^{n',m'}$ as

$$\begin{aligned}
C_{n,m}^{n,m+1} &= \left[\frac{n!}{(n-m)!}\right]^{\frac{1}{2}} \left[\frac{n!}{(n-m-1)!}\right]^{\frac{1}{2}} 2^{\frac{1}{2}} l_B \frac{(n-m)!}{n!} \\
&= \left[\frac{(n-m)!}{(n-m-1)!}\right]^{\frac{1}{2}} 2^{\frac{1}{2}} l_B \\
&= \sqrt{2(n-m)} l_B. \qquad \text{(C.10)}
\end{aligned}$$

For $n' = n + 1$, we obtain

$$\begin{aligned}
C_{n,m}^{n+1,m+1} &= \left[\frac{n!}{(n-m)!}\right]^{\frac{1}{2}} \left[\frac{(n+1)!}{(n-m)!}\right]^{\frac{1}{2}} 2^{\frac{1}{2}} l_B \left[-\frac{(n-m)!}{n!}\right] \\
&= -\left[\frac{(n+1)!}{n!}\right] 2^{\frac{1}{2}} l_B \\
&= -\sqrt{2(n+1)} l_B. \qquad \text{(C.11)}
\end{aligned}$$

In case of $m' = m + 1$ with $-1 < m < 0$, by using a formula of integral[49],

$$\begin{aligned}
&\int_0^\infty dx \mathrm{e}^{-x} x^{\alpha+\beta} L_m^\alpha(x) L_n^\beta(x) \\
= \;& (-1)^{m+n} (\alpha+\beta)! \frac{(\alpha+m)!}{n!(\alpha+m-n)!} \frac{(\beta+n)!}{m!(\beta+n-m)!} \\
& \text{for} \;\; \mathrm{Re}(\alpha+\beta) > -1, \qquad \text{(C.12)}
\end{aligned}$$

it gives

$$\begin{aligned}\int_0^\infty dx\mathrm{e}^{-x}x^{\frac{|m|+|m+1|+1}{2}}L_n^{|m|}(x)\,L_{n'}^{|m+1|}(x)\\ &=\int_0^\infty dx\mathrm{e}^{-x}xL_n^{-m}(x)\,L_{n'}^{m+1}(x)\\ &=(-1)^{n+n'}\frac{(n-m)!}{n'!(n-m-n')!}\frac{(n'+m+1)!}{n!(n'+m+1-n)!}.\end{aligned}\tag{C.13}$$

We then obtain the radial integral $C_{n,m}^{n',m'}$ as

$$\begin{aligned}C_{n,m}^{n',m+1}&=\left[\frac{n!}{(n-m)!}\right]^{\frac{1}{2}}\left[\frac{n'!}{(n'+m+1)!}\right]^{\frac{1}{2}}2^{\frac{1}{2}}l_B\\ &\times(-1)^{n+n'}\frac{(n-m)!}{n'!(n-m-n')!}\frac{(n'+m+1)!}{n!(n'+m+1-n)!}\\ &=\sqrt{2\frac{(n-m)!(n'+m+1)!}{n!n'!}}\frac{(-1)^{n+n'}l_B}{(n-m-n')!(n'+m+1-n)!}.\end{aligned}\tag{C.14}$$

We mention that since m is not an integer in the region $-1<m<0$, this will not be used in our discussion.

In case of $m'=m-1$ with $m\geq 1$, we have

$$\begin{aligned}\int_0^\infty dx\mathrm{e}^{-x}x^{\frac{|m|+|m-1|+1}{2}}L_n^{|m|}(x)\,L_{n'}^{|m-1|}(x)\\ &=\int_0^\infty dx\mathrm{e}^{-x}x^mL_n^m(x)\,L_{n'}^{m-1}(x)\\ &=\int_0^\infty dx\mathrm{e}^{-x}x^mL_n^m(x)\,L_{n'}^{m}(x)\\ &-\int_0^\infty dx\mathrm{e}^{-x}x^mL_n^m(x)\,L_{n'-1}^{m}(x)\\ &=\frac{(n+m)!}{n!}\delta_{n'n}-\frac{(n+m)!}{n!}\delta_{n'n+1}.\end{aligned}\tag{C.15}$$

For $n'=n$, we obtain the radial integral $C_{n,m}^{n',m'}$ as

$$\begin{aligned}C_{n,m}^{n,m-1}&=\left[\frac{n!}{(n+m)!}\right]^{\frac{1}{2}}\left[\frac{n!}{(n+m-1)!}\right]^{\frac{1}{2}}2^{\frac{1}{2}}l_B\frac{(n+m)!}{n!}\\ &=\left[\frac{(n+m)!}{(n+m-1)!}\right]^{\frac{1}{2}}2^{\frac{1}{2}}l_B\\ &=\sqrt{2(n+m)}l_B.\end{aligned}\tag{C.16}$$

For $n' = n + 1$, we obtain

$$\begin{aligned} C_{n,m}^{n+1,m-1} &= \left[\frac{n!}{(n+m)!}\right]^{\frac{1}{2}} \left[\frac{(n+1)!}{(n+m)!}\right]^{\frac{1}{2}} 2^{\frac{1}{2}} l_B \left[-\frac{(n+m)!}{n!}\right] \\ &= -\left[\frac{(n+1)!}{n!}\right] 2^{\frac{1}{2}} l_B \\ &= -\sqrt{2(n+1)} l_B. \end{aligned} \tag{C.17}$$

In case of $m' = m - 1$ with $m \leq 0$, we have

$$\begin{aligned} &\int_0^\infty dx \mathrm{e}^{-x} x^{\frac{|m|+|m-1|+1}{2}} L_n^{|m|}(x) L_{n'}^{|m-1|}(x) \\ &\quad = \int_0^\infty dx \mathrm{e}^{-x} x^{-m+1} L_n^{-m}(x) L_{n'}^{-m+1}(x) \\ &\quad = \int_0^\infty dx \mathrm{e}^{-x} x^{-m+1} L_n^{-m+1}(x) L_{n'}^{-m+1}(x) \\ &\quad - \int_0^\infty dx \mathrm{e}^{-x} x^{-m+1} L_{n-1}^{-m+1}(x) L_{n'}^{-m+1}(x) \\ &\quad = \frac{(n-m+1)!}{n!} \delta_{n'n} - \frac{(n-m)!}{(n-1)!} \delta_{n'n-1}. \end{aligned} \tag{C.18}$$

For $n' = n$, we obtain the radial integral $C_{n,m}^{n',m'}$ as

$$\begin{aligned} C_{n,m}^{n,m-1} &= \left[\frac{n!}{(n-m)!}\right]^{\frac{1}{2}} \left[\frac{n!}{(n-m+1)!}\right]^{\frac{1}{2}} 2^{\frac{1}{2}} l_B \frac{(n-m+1)!}{n!} \\ &= \left[\frac{(n-m+1)!}{(n-m)!}\right]^{\frac{1}{2}} 2^{\frac{1}{2}} l_B \\ &= \sqrt{2(n-m+1)} l_B. \end{aligned} \tag{C.19}$$

For $n' = n - 1$, we obtain

$$\begin{aligned} C_{n,m}^{n-1,m-1} &= \left[\frac{n!}{(n-m)!}\right]^{\frac{1}{2}} \left[\frac{(n-1)!}{(n-m)!}\right]^{\frac{1}{2}} 2^{\frac{1}{2}} l_B \left[-\frac{(n-m)!}{(n-1)!}\right] \\ &= -\left[\frac{n!}{(n-1)!}\right] 2^{\frac{1}{2}} l_B \\ &= -\sqrt{2n} l_B. \end{aligned} \tag{C.20}$$

In case of $m' = m - 1$ with $0 < m < 1$, although m is not an integer in the region, we demonstrate the radial integral $C_{n,m}^{n',m'}$ for reference. Using an

integral formula (C.12), we obtain the integral as

$$\begin{aligned}
&\int_0^\infty dx \mathrm{e}^{-x} x^{\frac{|m|+|m-1|+1}{2}} L_n^{|m|}(x) L_{n'}^{|m-1|}(x) \\
&\qquad = \int_0^\infty dx \mathrm{e}^{-x} x L_n^m(x) L_{n'}^{-m+1}(x) \\
&\qquad = (-1)^{n+n'} \frac{(n+m)!}{n'!(n+m-n')!} \frac{(n'-m+1)!}{n!(n'-m+1-n)!}.
\end{aligned} \tag{C.21}$$

We then obtain the radial integral $C_{n,m}^{n',m'}$ as

$$\begin{aligned}
C_{n,m}^{n',m-1} &= \left[\frac{n!}{(n+m)!}\right]^{\frac{1}{2}} \left[\frac{n'!}{(n'-m+1)!}\right]^{\frac{1}{2}} 2^{\frac{1}{2}} l_B \\
&\quad \times (-1)^{n+n'} \frac{(n+m)!}{n'!(n+m-n')!} \frac{(n'-m+1)!}{n!(n'-m+1-n)!} \\
&= \sqrt{2\frac{(n+m)!(n'-m+1)!}{n!n'!}} \frac{(-1)^{n+n'} l_B}{(n+m-n')!(n'-m+1-n)!}.
\end{aligned} \tag{C.22}$$

This will not be used as mentioned before.

Appendix D

Energy Difference $E_{n,m} - E_{n',m'}$

In this appendix, we calculate the energy difference in case of transitions from $N = 0$ to $N = 1$. First, we consider $m' = m + 1$ case. Using the energy eigenvalue Eq. (3.58), we obtain

$$\begin{aligned} E_{nm} - E_{n,m+1} &= \hbar\omega_c \left[\frac{-m+m}{2} - \frac{-(m+1)+m+1}{2} \right] \\ &= 0 \end{aligned} \tag{D.1}$$

for $n' = n$ and $m \leq -1$,

$$\begin{aligned} E_{nm} - E_{n,m+1} &= \hbar\omega_c \left[\frac{m+m}{2} - \frac{(m+1)+m+1}{2} \right] \\ &= -\hbar\omega_c \end{aligned} \tag{D.2}$$

for $n' = n$ and $m \geq 0$,

$$\begin{aligned} E_{nm} - E_{n-1,m+1} &= \hbar\omega_c \left[1 + \frac{m+m}{2} - \frac{(m+1)+m+1}{2} \right] \\ &= 0 \end{aligned} \tag{D.3}$$

for $n' = n - 1$ and $m \geq 0$, and

$$\begin{aligned} E_{nm} - E_{n+1,m+1} &= \hbar\omega_c \left[-1 + \frac{-m+m}{2} - \frac{-(m+1)+m+1}{2} \right] \\ &= -\hbar\omega_c \end{aligned} \tag{D.4}$$

for $n' = n + 1$ and $m \leq -1$.

Next, we consider $m' = m - 1$ case. Similarly, we obtain

$$\begin{aligned} E_{nm} - E_{n,m-1} &= \hbar\omega_c \left[\frac{-m+m}{2} - \frac{-(m-1)+m-1}{2} \right] \\ &= 0. \end{aligned} \tag{D.5}$$

for $n' = n$ and $m \leq 0$,

$$\begin{aligned} E_{nm} - E_{n,m-1} &= \hbar\omega_c \left[\frac{m+m}{2} - \frac{(m-1)+m-1}{2} \right] \\ &= \hbar\omega_c \end{aligned} \tag{D.6}$$

for $n' = n$ and $m \geq 1$,

$$\begin{aligned} E_{nm} - E_{n-1,m-1} &= \hbar\omega_c \left[1 + \frac{-m+m}{2} - \frac{-(m-1)+m-1}{2} \right] \\ &= \hbar\omega_c \end{aligned} \tag{D.7}$$

for $n' = n - 1$ and $m \leq 0$, and

$$\begin{aligned} E_{nm} - E_{n+1,m-1} &= \hbar\omega_c \left[-1 + \frac{m+m}{2} - \frac{(m-1)+m-1}{2} \right] \\ &= 0 \end{aligned} \tag{D.8}$$

for $n' = n + 1$ and $m \geq 1$.

We summarize these results as below,

$$E_{n,m} - E_{n',m+1} = \begin{cases} 0 & \text{for } n' = n \text{ and } m \leq -1 \\ -\hbar\omega_c & \text{for } n' = n \text{ and } m \geq 0 \\ 0 & \text{for } n' = n-1 \text{ and } m \geq 0 \\ -\hbar\omega_c & \text{for } n' = n+1 \text{ and } m \leq -1 \end{cases}, \tag{D.9}$$

and

$$E_{n,m} - E_{n',m-1} = \begin{cases} 0 & \text{for } n' = n \text{ and } m \leq 0 \\ \hbar\omega_c & \text{for } n' = n \text{ and } m \geq 1 \\ \hbar\omega_c & \text{for } n' = n-1 \text{ and } m \leq 0 \\ 0 & \text{for } n' = n+1 \text{ and } m \geq 1 \end{cases}. \tag{D.10}$$

Appendix E

Dipole Transition from Minimal Coupling

We present the derivation of Eq. (4.16). We need to compute the commutator $\left[H_0, \mathbf{A}^{\mathrm{OV}}\right]$. After some calculations, we obtain

$$[H_0, \mathbf{A}^{\mathrm{OV}}] = \mathbf{A}^{\mathrm{OV}} \left\{ \frac{\hbar^2 k_{\mathrm{OV}}^2}{2m_e} - \left(\frac{\hbar \mathbf{k}_{\mathrm{OV}}}{m_e} \right) \cdot (-i\hbar \boldsymbol{\nabla}) + \frac{e}{m_e} \mathbf{A}^{\mathrm{ext}} \cdot \hbar \mathbf{k}_{\mathrm{OV}}) \right\}, \tag{E.1}$$

where $\mathbf{k}_{\mathrm{OV}}$ is the wavenumber vector of OV and k_{OV} is its magnitude.

Next, we evaluate the matrix element of the minimal coupling $\langle n', m' | \mathbf{A}^{\mathrm{OV}} \cdot \mathbf{j} | n, m \rangle$ with a current operator, $\mathbf{j} = (e/m_e)\,(\mathbf{p} + e\mathbf{A}^{\mathrm{ext}})$. Noting that this current operator satisfies $\mathbf{p} + e\mathbf{A}^{\mathrm{ext}} = (im_e/\hbar)\,[H_0, \mathbf{r}]$, by using the commutation relation (E.1), we obtain

$$\begin{aligned}
\langle n', m' | \mathbf{A}^{\mathrm{OV}} \cdot \mathbf{j} | n, m \rangle &= \frac{e}{m_e} \langle n', m' | \mathbf{A}^{\mathrm{OV}} \cdot \frac{im_e}{\hbar} [H_0, \mathbf{r}] | n, m \rangle \\
&= \frac{ie}{\hbar} (E_{n',m'} - E_{n,m}) \langle n', m' | \mathbf{A}^{\mathrm{OV}} \cdot \mathbf{r} | n, m \rangle \\
&- \frac{ie}{\hbar} \frac{\hbar^2 k_{\mathrm{OV}}^2}{2m_e} \langle n', m' | \mathbf{A}^{\mathrm{OV}} \cdot \mathbf{r} | n, m \rangle \\
&- \frac{ie}{\hbar} \frac{\hbar e}{m_e} \langle n', m' | (\mathbf{A}^{\mathrm{ext}} \cdot \mathbf{k}_{\mathrm{OV}}) (\mathbf{A}^{\mathrm{OV}} \cdot \mathbf{r}) | n, m \rangle \\
&- \frac{e}{\hbar} \frac{\hbar^2}{2m_e} \langle n', m' | \mathbf{A}^{\mathrm{OV}} \cdot \mathbf{k}_{\mathrm{OV}} | n, m \rangle \\
&- \frac{e}{\hbar} \frac{\hbar^2}{2m_e} \langle n', m' | (\mathbf{A}^{\mathrm{OV}} \cdot \mathbf{r}) \mathbf{k}_{\mathrm{OV}} \cdot \mathrm{grad} \, | n, m \rangle.
\end{aligned} \tag{E.2}$$

The second term is 10^{-11} times weaker than the first term for $B = 10$ T and can be dropped. Furthermore, the OV travels along z-axis and the

wavenumber vector of the OV is approximately described as, $\boldsymbol{k}_{\mathrm{OV}} \sim k_z \hat{\boldsymbol{e}}_z$, in the paraxial approximation as shown in Eq. (2.52). On the other hand, $\mathbf{A}^{\mathrm{ext}}$, $\mathbf{A}^{\mathrm{OV}}$, and, grad $\Psi_{nm}(\rho, \phi, z)$ have no z-component. The inner products with $\boldsymbol{k}_{\mathrm{OV}}$ in the third, fourth, and fifth terms in Eq. (E.2) thus vanishes. As a consequence, the first term only survives in the matrix element of the minimal coupling,

$$\langle n', m' | \mathbf{A}^{\mathrm{OV}} \cdot \mathbf{j} | n, m \rangle \sim \frac{ie}{\hbar} (E_{n',m'} - E_{n,m}) \langle n', m' | \mathbf{A}^{\mathrm{OV}} \cdot \mathbf{r} | n, m \rangle. \tag{E.3}$$

which is Eq. (4.16).

Appendix F

Calculation of $F^{\ell}(B)$

To obtain (4.25), we show the calculation $F^{\ell}(B)$ of Eq. (4.24). We have assumed the filling factor $\nu = 1$, that is, the initial state is in the ground state $n = 0$ and $m \leq 0$. When we use the results in Appendix C, Eq. (4.24) reduces to

$$\begin{aligned} F^{\ell}(B) &= \frac{A_0 e^2 \omega_c^2}{V} \sqrt{\frac{k_\perp}{8\pi}} \left[l_B \sqrt{2} D_{0,0,\ell}^{0,1} - \sum_{m<0}^{-m_{\max}} l_B \sqrt{2} D_{0,m,\ell}^{1,m+1} \right] \\ &= \frac{A_0 e^2 l_B \omega_c^2}{V} \sqrt{\frac{k_\perp}{4\pi}} \left[D_{0,0,\ell}^{0,1} - \sum_{m<0}^{-m_{\max}} D_{0,m,\ell}^{1,m+1} \right]. \end{aligned} \tag{F.1}$$

By using the explicit form of the associated Laguerre polynomials

$$\begin{aligned} L_0^k(x) &= 1, \\ L_1^k(x) &= 1 + k - x, \end{aligned} \tag{F.2}$$

and introducing a dimensionless variable $x = k_\perp \rho$, we can respectively rewrite $D_{0,0,\ell}^{0,1}$ and $D_{0,m,\ell}^{1,m+1}$ as

$$\begin{aligned} D_{0,0,\ell}^{0,1} &= \int_0^R d\rho \rho^2 R_{0,1}(\rho) R_{0,0}(\rho) J_\ell(k_\perp \rho) \\ &= \frac{1}{\sqrt{2} l_B^2} \int_0^R d\rho \rho^2 \mathrm{e}^{-\frac{\rho^2}{2l_B^2}} \left(\frac{\rho}{l_B} \right) L_0^1 \left(\frac{r^2}{2l_B^2} \right) L_0^0 \left(\frac{r^2}{2l_B^2} \right) J_\ell(k_\perp \rho) \\ &= \frac{l_B}{\sqrt{2}} \left(\frac{1}{k_\perp l_B} \right)^4 \int_0^{k_\perp R} dx x^3 \mathrm{e}^{-\frac{x^2}{2k_\perp^2 l_B^2}} J_\ell(x), \end{aligned} \tag{F.3}$$

and

$$\begin{aligned}
D^{1,m+1}_{0,m,\ell} &= \int_0^R d\rho\rho^2 R_{1,m+1}(\rho)R_{0,m}(\rho)J_\ell(k_\perp\rho) \\
&= \frac{1}{(-m)!}\frac{1}{2^{-m-\frac{1}{2}}l_B^2} \\
&\times \int_0^R d\rho\rho^2 \mathrm{e}^{-\frac{\rho^2}{2l_B^2}}\left(\frac{\rho}{l_B}\right)^{-2m-1} L_1^{-m-1}\left(\frac{\rho^2}{2l_B^2}\right) L_0^{-m}\left(\frac{\rho^2}{2l_B^2}\right) J_\ell(k_\perp\rho) \\
&= \frac{1}{(-m-1)!}\frac{l_B}{2^{-m-\frac{1}{2}}}\left(\frac{1}{k_\perp l_B}\right)^{-2m+2}\int_0^{k_\perp R} dx x^{-2m+1}\mathrm{e}^{-\frac{x^2}{2k_\perp^2 l_B^2}} J_\ell(x) \\
&- \frac{1}{(-m)!}\frac{l_B}{2^{-m+\frac{1}{2}}}\left(\frac{1}{k_\perp l_B}\right)^{-2m+4}\int_0^{k_\perp R} dx x^{-2m+3}\mathrm{e}^{-\frac{x^2}{2k_\perp^2 l_B^2}} J_\ell(x). \quad \text{(F.4)}
\end{aligned}$$

To viewability, we change m to $-m'$ ($m' > 0$),

$$\begin{aligned}
D^{1,-m'+1}_{0,-m',\ell} &= \frac{1}{(m'-1)!}\frac{l_B}{2^{m'-\frac{1}{2}}}\left(\frac{1}{k_\perp l_B}\right)^{2m'+2}\int_0^{k_\perp R} dx x^{2m'+1}\mathrm{e}^{-\frac{x^2}{2k_\perp^2 l_B^2}} J_\ell(x) \\
&- \frac{1}{m'!}\frac{l_B}{2^{m'+\frac{1}{2}}}\left(\frac{1}{k_\perp l_B}\right)^{2m'+4}\int_0^{k_\perp R} dx x^{2m'+3}\mathrm{e}^{-\frac{x^2}{2k_\perp^2 l_B^2}} J_\ell(x). \quad \text{(F.5)}
\end{aligned}$$

We proceed to sum with respect to m' up to $m_{\max}$. and show that only the last term survives because of cancellation,

$$\begin{aligned}
&D^{0,1}_{0,0,\ell} - \sum_{m'>0}^{m_{\max}} D^{1,-m'+1}_{0,-m',\ell} \\
&= \frac{l_B}{\sqrt{2}}\left(\frac{1}{k_\perp l_B}\right)^4\int_0^{k_\perp R} dx x^3\mathrm{e}^{-\frac{x^2}{2k_\perp^2 l_B^2}} J_\ell(x) \\
&- \sum_{m'>0}^{m_{\max}} \frac{1}{(m'-1)!}\frac{l_B}{2^{m'-\frac{1}{2}}}\left(\frac{1}{k_\perp l_B}\right)^{2m'+2}\int_0^{k_\perp R} dx x^{2m'+1}\mathrm{e}^{-\frac{x^2}{2k_\perp^2 l_B^2}} J_\ell(x) \\
&+ \sum_{m'>0}^{m_{\max}} \frac{1}{m'!}\frac{l_B}{2^{m'+\frac{1}{2}}}\left(\frac{1}{k_\perp l_B}\right)^{2m'+4}\int_0^{k_\perp R} dx x^{2m'+3}\mathrm{e}^{-\frac{x^2}{2k_\perp^2 l_B^2}} J_\ell(x) \\
&= \frac{1}{m_{\max}!}\frac{l_B}{2^{m_{\max}+\frac{1}{2}}}\left(\frac{1}{k_\perp l_B}\right)^{2m_{\max}+4}\int_0^{k_\perp R} dx x^{2m_{\max}+3}\mathrm{e}^{-\frac{x^2}{2k_\perp^2 l_B^2}} J_\ell(x).
\end{aligned} \quad \text{(F.6)}$$

We apply Stirling's approximation $n! \sim \sqrt{2\pi n}\,(n/\mathrm{e})^n$ since $m_{\max} \gg 1$,

$$D^{0,1}_{0,0,\ell} - \sum_{m'>0}^{m_{\max}} D^{1,-m'+1}_{0,-m',\ell} \sim \frac{1}{\sqrt{2\pi m_{\max}}} \left(\frac{\mathrm{e}}{2m_{\max}}\right)^{m_{\max}} \frac{l_B}{\sqrt{2}} \left(\frac{1}{k_\perp l_B}\right)^{2m_{\max}+4} \times \int_0^{k_\perp R} dx x^{2m_{\max}+3} \mathrm{e}^{-\frac{x^2}{2k_\perp^2 l_B^2}} J_\ell(x). \tag{F.7}$$

We thus obtain

$$F^{\ell}(B) = \frac{A_0 e^2 l_B^2 \omega_c^2}{2\sqrt{2}\pi V} \sqrt{\frac{k_\perp}{2m_{\max}}} \left(\frac{\mathrm{e}}{2m_{\max}}\right)^{m_{\max}} \left(\frac{1}{k_\perp l_B}\right)^{2m_{\max}+4} \times \int_0^{k_\perp R} dx x^{2m_{\max}+3} \mathrm{e}^{-\frac{x^2}{2k_\perp^2 l_B^2}} J_\ell(x). \tag{F.8}$$

We here denote the factor in front of the integral as (A). By using the notations $\omega_c = eB/m$, $l_B = \sqrt{\hbar/eB}$, and

$$m_{\max} = \frac{1}{2}\left(\frac{eR^2}{\hbar}B - 1\right), \tag{F.9}$$

we obtain

$$(\mathrm{A}) = \frac{A_0 e^2 \hbar^2}{2\sqrt{2}\pi V m_e^2} \frac{e^3 B^3}{\hbar^3 k_\perp^3} \sqrt{\frac{\hbar}{eB}\frac{k_\perp}{\mathrm{e}}} \left(\frac{\mathrm{e}}{k_\perp^2 R^2\left[1 - \frac{\hbar}{eBR^2}\right]}\right)^{\frac{eR^2}{2\hbar}B}.$$

Next, we use the approximate expressions

$$\frac{1}{1 - \frac{\hbar}{eBR^2}} \sim 1 + \frac{\hbar}{eBR^2} \tag{F.10}$$

for $\hbar/eBR^2 \ll 1$. We thus obtain

$$(\mathrm{A}) \sim \frac{A_0 e^2 \hbar^2}{2\sqrt{2}\pi V m_e^2} \frac{e^3 B^3}{\hbar^3 k_\perp^3} \sqrt{\frac{\hbar}{eB}\frac{k_\perp}{\mathrm{e}}} \left(\frac{1}{k_\perp^2 R^2}\left[1 + \frac{\hbar}{eBR^2}\right]\mathrm{e}\right)^{\frac{eR^2}{2\hbar}B}. \tag{F.11}$$

We here introduce the Compton wavelength, $\lambda_e = 2\pi\hbar/m_e c$, and the quantum flux, $\Phi_0 = 2\pi\hbar/e$. When we use the energy conservation, $eB/m_e = ck \sim ck_\perp/\alpha$, with $k = k_\perp\sqrt{(1+\alpha^2)/\alpha^2} \sim k_\perp/\alpha$, we can calculate (A) as

$$\begin{aligned}(\mathrm{A}) &\sim \frac{A_0 e^2 \hbar^2}{2\sqrt{2}\pi V m_e^2} \frac{eB}{\hbar} \frac{m_e^3 c^3}{\alpha^3 e^3 B^3} \left(\frac{eB}{\hbar}\right)^{3/2} \\ &\times \sqrt{\frac{\alpha e B}{m_e c \mathrm{e}}} \left(\frac{1+\alpha^2}{\alpha^2}\frac{m_e^2 c^2}{e^2 B^2 R^2}\left[1 + \frac{\hbar}{eBR^2}\right]\mathrm{e}\right)^{\frac{eR^2}{2\hbar}B} \\ &= \frac{A_0 e^2 c^2}{V\sqrt{4\pi\alpha^5 \lambda_e \mathrm{e}}} \left(\frac{1+\alpha^2}{\alpha^2}\frac{\Phi_0^2}{\lambda_e^2 B^2 R^2}\left[1 + \frac{\Phi_0}{2\pi B R^2}\right]\mathrm{e}\right)^{\pi R^2 B/\Phi_0},\end{aligned} \tag{F.12}$$

which is Eq. (4.25).

Appendix G

Coupling of LG-mode OV with 2DEG

G.1 LG-mode OV and Coupling with 2DEG

In a main body, we discussed the photocurrent induced by the optical angular momentum of the Bessel-mode optical vortex. In this appendix, we treat our problem by Laguerre Gaussian-mode (LG-mode) OV, again. As we reviewed in Sec. 2, since the Bessel-mode is the exact solution of the Helmholtz equation (2.8)

$$\Delta \mathbf{A}(\mathbf{r}) + k^2 \mathbf{A}(\mathbf{r}) = 0, \tag{G.1}$$

it naturally constitutes the OV solution for the non-paraxial region. However, it is thought that, the Bessel-mode solution is ideal one because the infinite energy is needed to generate a Bessel-mode photon experimentally. The one of more realistic solutions of (2.8) is a LG-mode.

When we write the form of the monochromatic vector potential of the LG-mode,

$$\mathbf{A}^{\mathrm{LG}}(\mathbf{r}, t) = \mathbf{A}^{\mathrm{LG}}(\mathbf{r})\, \mathrm{e}^{-i\omega t} = \boldsymbol{\varepsilon}_\sigma \frac{-i}{\omega} u(\mathbf{r})\, \mathrm{e}^{ikz - i\omega t}, \tag{G.2}$$

the Helmholtz equation (2.8) is written by

$$\Delta \left[u(\mathbf{r})\, \mathrm{e}^{ikz} \right] + k^2 u(\mathbf{r})\, \mathrm{e}^{ikz} = 0, \tag{G.3}$$

where we denote the Laplacian

$$\Delta = \frac{\partial^2}{\partial x^2} + \frac{\partial^2}{\partial y^2} + \frac{\partial^2}{\partial z^2}. \tag{G.4}$$

The key point to construct the LG-mode solution is that paraxial approximation

$$\frac{\partial^2 u(\mathbf{r})}{\partial z^2} \sim 0 \tag{G.5}$$

is applied to (G.3) before solving it. Then, (G.3) reduces to

$$\left[\frac{\partial^2}{\partial x^2}+\frac{\partial^2}{\partial y^2}\right] u(\mathbf{r}) + 2ik\frac{\partial F(\mathbf{r})}{\partial z} - k^2 u(\mathbf{r}) = 0, \tag{G.6}$$

and gives the solution at $z = 0$ (that is, the beam waist),

$$u_{p,\ell}(\mathbf{r}) = \frac{C_{p,|\ell|}}{w_0} \mathrm{e}^{-\frac{\rho^2}{w_0^2}} \left(\frac{\rho}{w_0}\right)^{|\ell|} L_p^{|\ell|}\left(\frac{2\rho^2}{w_0^2}\right) \mathrm{e}^{i\ell\phi}, \tag{G.7}$$

where $w_0 = \sqrt{2z_R/k}$ is the beam waist with the Rayleigh length z_R, ℓ is the z component of the optical orbital angular momentum, $C_{p,|\ell|}$ is a normalization constant, and $L_p^{|\ell|}(x)$ is the associated Laguerre polynomials[4]. Therefore, we write the vector potential of the circular-polarized LG-mode at beam waist as

$$\mathbf{A}^{\mathrm{LG}}_{p,\ell,\sigma}(\mathbf{r}) = \boldsymbol{\varepsilon}_\sigma \frac{-i}{\omega} u_{p,\ell}(\mathbf{r})\, \mathrm{e}^{ikz}, \tag{G.8}$$

with the circular polarization vector

$$\boldsymbol{\varepsilon}_\sigma = -\sigma\frac{1}{\sqrt{2}}\left(\hat{\mathbf{e}}_x + i\sigma\hat{\mathbf{e}}_y\right), \tag{G.9}$$

for the helicity $\sigma = \pm 1$.

To obtain the induced photocurrent via Kubo formula (4.7), we need to calculate the matrix element

$$\left\langle n', m' \left| \mathbf{A}^{\mathrm{LG}}_{p,\ell,\sigma}(\mathbf{r}) \cdot \mathbf{j} \right| n, m \right\rangle. \tag{G.10}$$

We now assume that the LG beam interacts with 2DEG at $z = 0$. In a similar way of Bessel-mode case, the matrix element reduces to

$$\left\langle n', m' \left| \mathbf{A}^{\mathrm{LG}}_{p,\ell,\sigma}(\mathbf{r}) \cdot \mathbf{j} \right| n, m \right\rangle \approx \frac{ie}{\hbar}\left(E_{n'm'} - E_{n,m}\right) \left\langle n', m' \left| \mathbf{A}^{\mathrm{LG}}_{p,\ell,\sigma}(\mathbf{r}) \cdot \mathbf{r} \right| n, m \right\rangle. \tag{G.11}$$

We next calculate the matrix element by using explicitly forms of LG-mode (G.8) and 2DEG wavefunction (3.59). Since the scalar product in the matrix element is written as

$$\begin{aligned} \mathbf{A}^{\mathrm{LG}}_{p,\ell,\sigma}(\mathbf{r}) \cdot \mathbf{r} &= \frac{-i}{\omega}\frac{C_{p,|\ell|}}{w_0} \mathrm{e}^{-\frac{\rho^2}{w_0^2}} \left(\frac{\rho}{w_0}\right)^{|\ell|} L_p^{|\ell|}\left(\frac{2\rho^2}{w_0^2}\right) \mathrm{e}^{i\ell\phi} \boldsymbol{\varepsilon}_\sigma \cdot \mathbf{r} \\ &= \sigma\frac{i}{\omega}\frac{C_{p,|\ell|}}{\sqrt{2}} \mathrm{e}^{-\frac{\rho^2}{w_0^2}} \left(\frac{\rho}{w_0}\right)^{|\ell|+1} L_p^{|\ell|}\left(\frac{2\rho^2}{w_0^2}\right) \mathrm{e}^{i(\ell+\sigma)\phi}, \end{aligned} \tag{G.12}$$

it leads to

$$\begin{aligned}
&\left\langle n', m' \left| \mathbf{A}^{\mathrm{LG}}_{p,\ell,\sigma}(\mathbf{r}) \cdot \mathbf{r} \right| n, m \right\rangle \\
&= \delta_{m',m+\ell+\sigma} \sigma \frac{i}{\omega} \frac{C_{p,|\ell|} N_{n'm'} N_{nm}}{\sqrt{2}} \left(\frac{1}{l_B}\right)^{|m'|+|m|} \left(\frac{1}{w_0}\right)^{|\ell|+1} \\
&\times \int d\rho \, \mathrm{e}^{-\left(\frac{1}{2l_B^2}+\frac{1}{w_0^2}\right)\rho^2} \rho^{|m'|+|m|+|\ell|+2} L_p^{|\ell|}\left(\frac{2\rho^2}{w_0^2}\right) L_{n'}^{|m'|}\left(\frac{\rho^2}{2l_B^2}\right) L_n^{|m|}\left(\frac{\rho^2}{2l_B^2}\right),
\end{aligned} \tag{G.13}$$

where l_B is the magnetic length. By changing the variable as $x = \rho^2/2l_B^2$, it gives

$$\begin{aligned}
&\left\langle n', m' \left| \mathbf{A}^{\mathrm{LG}}_{p,\ell,\sigma}(\mathbf{r}) \cdot \mathbf{r} \right| n, m \right\rangle \\
&= \delta_{m',m+\ell+\sigma} \sigma \frac{i}{\omega} \frac{C_{p,|\ell|} N_{n'm'} N_{nm} 2^{(|m'|+|m|+|\ell|)/2} l_B^{|\ell|+3}}{w_0^{|\ell|+1}} \\
&\times \int dx \mathrm{e}^{-\left(1+\frac{2l_B^2}{w_0^2}\right)x} x^{(|m'|+|m|+|\ell|+1)/2} L_p^{|\ell|}\left(\frac{4l_B^2}{w_0^2}x\right) L_{n'}^{|m'|}(x) L_n^{|m|}(x),
\end{aligned} \tag{G.14}$$

We need to calculate the integral consisting of three associated Laguerre polynomials

$$h^{(n',m')}_{(n,m)(p,\ell)}(x) = \int dx \mathrm{e}^{-\left(1+\frac{\xi}{2}\right)x} x^{(|m'|+|m|+|\ell|+1)/2} L_p^{|\ell|}(\xi x) L_{n'}^{|m'|}(x) L_n^{|m|}(x), \tag{G.15}$$

where we put $\xi = 4l_B^2/w_0^2$.

When we adopt the component of the helicity basis $j_\pm = (j_x \mp i j_y)/\sqrt{2}$, the matrix elements of photocurrent are given by

$$\langle 0, m | j_+ | n', m+1 \rangle = \begin{cases} -iedl_B\omega_c\sqrt{2} & \text{for } n'=0, m=0 \\ iedl_B\omega_c\sqrt{2} & \text{for } n'=1, m<0 \\ 0 & \text{for otherwise} \end{cases}, \tag{G.16}$$

$$\langle 0, m | j_- | n', m-1 \rangle = 0 \quad \text{for all } n', m. \tag{G.17}$$

By combining (G.11) (4.7), and (G.17), the induced photocurrent for LG-mode OV arrives at

$$\begin{aligned}
\delta j_+^{(p,\ell,\sigma)}(\omega) &= -\frac{1}{V} \frac{\sqrt{2} e^2 d \omega_c^2 l_B}{\hbar(\omega - \omega_c) + i\delta} \\
&\times \left[\left\langle 0, 1 \left| \mathbf{A}^{\mathrm{LG}}_{p,\ell,\sigma}(\mathbf{r}) \cdot \mathbf{r} \right| 0, 0 \right\rangle - \sum_{|m|=1}^{m_{\max}} \left\langle 1, m+1 \left| \mathbf{A}^{\mathrm{LG}}_{p,\ell,\sigma}(\mathbf{r}) \cdot \mathbf{r} \right| 0, m \right\rangle \right].
\end{aligned} \tag{G.18}$$

Therefore, we find that we need to calculate the sum like

$$\left\langle 0,1\left|\mathbf{A}_{p,\ell,\sigma}^{\mathrm{LG}}\left(\mathbf{r}\right)\cdot\mathbf{r}\right|0,0\right\rangle -\sum_{|m|=1}^{m_{\max}}\left\langle 1,m+1\left|\mathbf{A}_{p,\ell,\sigma}^{\mathrm{LG}}\left(\mathbf{r}\right)\cdot\mathbf{r}\right|0,m\right\rangle . \tag{G.19}$$

This summation factors are analogs of the factors F^{ℓ} (4.24).

G.2 Analytic Integration

In this section, we will do the integral (G.15). This integral has been done in G. F. Quinteiro *et al.*'s paper [73]. To achieve such a purpose, we need a formula of the associated Laguerre polynomials,

$$L_{p}^{|\ell|}\left(\xi x\right)=\sum_{r=0}^{\infty}\binom{p+|\ell|}{p-r}\xi^{r}\left(1-\xi\right)^{p-r}L_{r}^{|\ell|}\left(x\right). \tag{G.20}$$

When we assume $4l_B^2 \ll w_0^2$, that is $\xi \ll 1$, it is enough to consider the expansion of (G.20) up to the first order of ξ. Then we obtain

$$L_{p}^{|\ell|}\left(\xi x\right)\approx\binom{p+|\ell|}{p}\left(1-p\xi\right)L_{0}^{|\ell|}\left(x\right)+\binom{p+|\ell|}{p-1}\xi L_{1}^{|\ell|}\left(x\right). \tag{G.21}$$

Using $L_{1}^{|\ell|}\left(x\right)=\left(1+|\ell|\right)L_{0}^{|\ell|}\left(x\right)-x$ and $L_{0}^{|\ell|}\left(x\right)=1$ lead to

$$L_{p}^{|\ell|}\left(\xi x\right)=\binom{p+|\ell|}{p}-\binom{p+|\ell|}{p-1}\xi x. \tag{G.22}$$

Then we obtain

$$\begin{aligned} & h_{(n,m)(p,\ell)}^{(n',m')}\left(x\right)\\ = & \binom{p+|\ell|}{p}\int dx\mathsf{e}^{-\left(1+\frac{\xi}{2}\right)x}x^{(|m'|+|m|+|\ell|+1)/2}L_{n'}^{|m'|}\left(x\right)L_{n}^{|m|}\left(x\right)\\ & -\binom{p+|\ell|}{p-1}\xi\int dx\mathsf{e}^{-\left(1+\frac{\xi}{2}\right)x}x^{(|m'|+|m|+|\ell|+3)/2}L_{n'}^{|m'|}\left(x\right)L_{n}^{|m|}\left(x\right), \end{aligned} \tag{G.23}$$

In a similar way of Bessel-mode case, we confine our discussion to the transitions between the Lowest Landau level (LLL) to the second Landau Level (2LL). Such transitions are allowed when conditions (4.15) and (4.22) are satisfied.

First, we obtain $h_{(n,m)(p,\ell)}^{(n',m')}\left(x\right)$ for the transition $(0,0,0)\rightarrow(0,1,1)$ for $m=0$ with $\ell=0$ and $\sigma=1$,

$$h_{(0,0)(p,0)}^{(0,1)}\left(x\right)=\frac{4}{\left(\xi+2\right)^{2}}-p\xi\frac{16}{\left(\xi+2\right)^{3}}, \tag{G.24}$$

and with $\ell = 2$ and $\sigma = -1$,

$$\begin{aligned} & h^{(0,1)}_{(0,0)(p,2)}(x) \\ = \; & (p+2)(p+1)\frac{8}{(\xi+2)^3} - (p+2)(p+1)p\xi\frac{16}{(\xi+2)^4}, \end{aligned} \tag{G.25}$$

For the transition $(0,m,0) \to (1,m+1,1)$ for $m < 0$ with $\ell = 0$ and $\sigma = 1$, we obtain

$$\begin{aligned} h^{(1,m+1)}_{(0,m)(p,0)}(x) \; = \; & |m|\frac{|m|!2^{|m|+1}}{(\xi+2)^{|m|+1}} - (|m|p\xi+1)\frac{(|m|+1)!2^{|m|+2}}{(\xi+2)^{|m|+2}} \\ & + p\xi\frac{(|m|+2)!2^{|m|+3}}{(\xi+2)^{|m|+3}}, \end{aligned} \tag{G.26}$$

and for its transition with $\ell = 2$ and $\sigma = -1$,

$$\begin{aligned} h^{(1,m+1)}_{(0,m)(p,2)}(x) \; = \; & |m|\frac{(p+2)(p+1)}{2}\frac{(|m|+1)!2^{|m|+2}}{(\xi+2)^{|m|+2}} \\ & - \frac{(p+2)(p+1)}{2}\left(1+\frac{|m|p\xi}{3}\right)\frac{(|m|+2)!2^{|m|+3}}{(\xi+2)^{|m|+3}} \\ & + \frac{(p+2)(p+1)}{6}p\xi\frac{(|m|+3)!2^{|m|+4}}{(\xi+2)^{|m|+4}}. \end{aligned} \tag{G.27}$$

Next, after calculating the state sum (G.19), we obtain it for $\ell = 0$ and $\sigma = 1$ as

$$\begin{aligned} & \left\langle 0,1\left|\mathbf{A}^{\mathrm{LG}}_{p,0,1}(\mathbf{r})\cdot\mathbf{r}\right|0,0\right\rangle - \sum_{|m|=1}^{m_{\max}}\left\langle 1,m+1\left|\mathbf{A}^{\mathrm{LG}}_{p,0,1}(\mathbf{r})\cdot\mathbf{r}\right|0,m\right\rangle \\ = \; & -\frac{i}{\omega}\frac{C_{p,0}l_B}{w_0}\frac{(m_{\max}+1)2^{m_{\max}+3}}{(\xi+2)^{m_{\max}+3}}\left[-\left(1+\frac{\xi}{2}\right)+p\xi(m_{\max}+2)\right], \end{aligned} \tag{G.28}$$

and for $\ell = 2$ and $\sigma = -1$ as

$$\begin{aligned} & \left\langle 0,1\left|\mathbf{A}^{\mathrm{LG}}_{p,2,-1}(\mathbf{r})\cdot\mathbf{r}\right|0,0\right\rangle - \sum_{|m|=1}^{m_{\max}}\left\langle 1,m+1\left|\mathbf{A}^{\mathrm{LG}}_{p,2,-1}(\mathbf{r})\cdot\mathbf{r}\right|0,m\right\rangle \\ = \; & \frac{i}{\omega}\frac{C_{p,2}l_B^3}{w_0^3}\frac{(p+2)(p+1)(m_{\max}+2)(m_{\max}+1)2^{m_{\max}+4}}{(\xi+2)^{m_{\max}+4}} \\ & \times\left[-\left(1+\frac{\xi}{2}\right)+\frac{p\xi}{3}(m_{\max}+3)\right]. \end{aligned} \tag{G.29}$$

We thus find that the intermediate states are canceled out and only the edge state survives.

When $\xi \ll 1$ and $m_{\max} \gg 1$, the expressions (G.28) and (G.29) can reduce to

$$\begin{aligned} & \left\langle 0,1 \left| \mathbf{A}^{\mathrm{LG}}_{p,0,1}(\mathbf{r}) \cdot \mathbf{r} \right| 0,0 \right\rangle - \sum_{|m|=1}^{m_{\max}} \left\langle 1, m+1 \left| \mathbf{A}^{\mathrm{LG}}_{p,0,1}(\mathbf{r}) \cdot \mathbf{r} \right| 0, m \right\rangle \\ = & \frac{i}{\omega} \frac{C_{p,0} l_B}{w_0} m_{\max} \left[1 - m_{\max} \left(p + \frac{1}{2} \right) \xi \right], \end{aligned} \tag{G.30}$$

and

$$\begin{aligned} & \left\langle 0,1 \left| \mathbf{A}^{\mathrm{LG}}_{p,2,-1}(\mathbf{r}) \cdot \mathbf{r} \right| 0,0 \right\rangle - \sum_{|m|=1}^{m_{\max}} \left\langle 1, m+1 \left| \mathbf{A}^{\mathrm{LG}}_{p,2,-1}(\mathbf{r}) \cdot \mathbf{r} \right| 0, m \right\rangle \\ = & -\frac{i}{\omega} \frac{C_{p,2} l_B^3}{w_0^3} (p+2)(p+1) m_{\max}^2 \left[1 - m_{\max} \left(\frac{p}{3} + \frac{1}{2} \right) \xi \right], \end{aligned} \tag{G.31}$$

respectively. We thus obtain the induced photocurrent

$$\delta j_+^{(p,0,1)}(\omega) = \frac{-i}{\hbar(\omega - \omega_c) + i\delta} \frac{\sqrt{2} C_{p,0} e^2 d \omega_c^2 l_B^2}{V \omega w_0} m_{\max} \left[1 - m_{\max} \left(p + \frac{1}{2} \right) \xi \right], \tag{G.32}$$

and

$$\begin{aligned} \delta j_+^{(p,2,-1)}(\omega) = & \frac{-i}{\hbar(\omega - \omega_c) + i\delta} \frac{-\sqrt{2} C_{p,2} e^2 d \omega_c^2 l_B^4}{V \omega w_0^3} \\ & \times (p+2)(p+1) m_{\max}^2 \left[1 - m_{\max} \left(\frac{p}{3} + \frac{1}{2} \right) \xi \right]. \end{aligned} \tag{G.33}$$

We factorize (G.32) and (G.33) as done in (4.23):

$$\delta j_+^{(p,\ell,\sigma)}(\omega) = \frac{-i}{\hbar(\omega - \omega_c) + i\delta} F_{\mathrm{LG}}^{(p,\ell,\sigma)}(B). \tag{G.34}$$

For examples, when $p = 0$, we obtain

$$F_{\mathrm{LG}}^{(0,0,1)}(B) = \frac{\sqrt{2} C_{0,0} e^4 R^2 d}{2 V \omega w_0 m_e^2} B^2 \left(1 - \frac{R^2}{w_0^2} \right), \tag{G.35}$$

and

$$F_{\mathrm{LG}}^{(0,2,-1)}(B) = \frac{-C_{0,2} e^4 R^4 d}{\sqrt{2} V \omega w_0^3 m_e^2} B^2 \left(1 - \frac{R^2}{w_0^2} \right). \tag{G.36}$$

where we used that the maximum of electron angular momentum is given by

$$m_{\max} \simeq \frac{R^2}{2l_B^2}. \tag{G.37}$$

When $p = 1$, we obtain

$$F_{\mathrm{LG}}^{(1,0,1)}(B) = \frac{\sqrt{2}C_{1,0}e^4R^2d}{2V\omega w_0 m_e^2}B^2\left(1 - \frac{3R^2}{w_0^2}\right), \tag{G.38}$$

and

$$F_{\mathrm{LG}}^{(1,2,-1)}(B) = \frac{-C_{1,2}e^4R^4d}{\sqrt{2}V\omega w_0^3 m_e^2}B^2\left(3 - \frac{5R^2}{w_0^2}\right). \tag{G.39}$$

When $p = 2$, we obtain

$$F_{\mathrm{LG}}^{(2,0,1)}(B) = \frac{\sqrt{2}C_{2,0}e^4B^2R^2d}{2V\omega w_0 m_e^2}\left(1 - \frac{5R^2}{w_0^2}\right), \tag{G.40}$$

and

$$F_{\mathrm{LG}}^{(2,2,-1)}(B) = \frac{-\sqrt{2}C_{2,2}e^4R^4d}{V\omega w_0^3 m_e^2}B^2\left(3 - \frac{7R^2}{w_0^2}\right). \tag{G.41}$$

Thus, we are ready to discuss the magnetic field dependence of the induced currents.

G.3 B-dependence of the Induced Photocurrent

In a similar way of Bessel-mode case discussed in main body, we investigate the magnetic field dependence of induced photocurrent by LG-mode OV. The beam waist is defined by

$$w_0 = \sqrt{\frac{2z_R}{k}}. \tag{G.42}$$

In fact, the Rayleigh length depends on the wavelength. Since the parameter independent of the wavelength is the numerical aperture NA, the beam waist is rewritten by using the numerical aperture NA as

$$w_0 = \frac{\lambda}{\pi NA} = \frac{2}{kNA}, \tag{G.43}$$

and the Rayleigh length is also

$$z_R = \frac{\pi w_0^2}{\lambda} = \frac{\lambda}{\pi NA^2} = \frac{2}{kNA^2}. \tag{G.44}$$

We thus see the beam waist varies by controlling the wavelength λ or wavenumber k.

Now we assume the cyclotron resonance (transition between the LLL and 2LL). Then the wavenumber to induce the cyclotron resonance is related to cyclotron frequency ω_c as

$$k_c = \frac{\omega_c}{c} = \frac{eB}{m_e c}. \tag{G.45}$$

The wavenumber thus depends on the external magnetic field B. Therefore, the beam waist also depends on B as

$$w_0(B) = \frac{2m_e c}{eB\ NA}. \tag{G.46}$$

The physical part of B dependence of the photocurrent $\delta j_+^{(p,\ell,\sigma)}(\omega, B)$ for LG-mode OV with $p = 0$, $\ell = 0$, $\sigma = 1$, and $\omega = \omega_c$, is written as

$$\begin{aligned} F_{\mathrm{LG}}^{(0,0,1)}(B) &= \frac{\sqrt{2}C_{0,0}e^4R^2d\ NA}{4Vm_e^2c\hbar}B^2\left(1 - R^2\ NA^2\frac{e^2}{4m_e^2c^2}B^2\right) \\ &= F_0^{(0,0,1)}B^2\left(1 - R^2\ NA^2\frac{e^2}{4m_e^2c^2}B^2\right), \end{aligned} \tag{G.47}$$

and for that with $p = 0$, $\ell = 2$, $\sigma = -1$, and $\omega = \omega_c$,

$$\begin{aligned} F_{\mathrm{LG}}^{(0,2,-1)}(B) &= -\frac{C_{0,2}e^6R^4d\ NA^3}{8\sqrt{2}Vm_e^4c^3\hbar}B^4\left(1 - R^2\ NA^2\frac{e^2}{4m_e^2c^2}B^2\right) \\ &= F_0^{(0,2,-1)}B^4\left(1 - R^2\ NA^2\frac{e^2}{4m_e^2c^2}B^2\right), \end{aligned} \tag{G.48}$$

where we introduced the factor $F_0^{(p,\ell,\sigma)}$. The zero point of (G.47) and (G.48) are given by $B \sim 0.559$ T.

We here need to pay attention to the derivation of the vanishing points except for $B = 0$ in the amplitudes (G.47) and (G.48). The profile of LG-mode for $\ell = 0$, $p = 0$ (which is equivalent to a normal Gaussian beam) and that for $\ell = 2$, $p = 0$ (which has just one bright ring) have no zero point except for the optical axis. This means that the amplitudes $F_{\mathrm{LG}}^{(0,0,1)}(B)$ and $F_{\mathrm{LG}}^{(0,2,-1)}(B)$ essentially have no vanishing point in $B > 0$. In fact, the vanishing points of (G.47) and (G.48) in $B > 0$ is derived from the factor $1/(\xi + 2)^{m_{\max}+3} \approx 0$, which is equivalent to the limit $\xi \to \infty$, that is, the infinite magnitude of B. Therefore, we should notice that, to see more accurate behavior of the amplitudes, the higher orders of the expansion of

$1/(\xi+2)^{m_{\max}+3}$ with respect to ξ are needed. However, the vanishing points of (G.47) and (G.48) approximately indicate where the profiles of LG-mode for $p=0$ are sufficiently weak far from the optical axis. Therefore, it must be noted that the physical meaningful region of the amplitudes, (G.47) and (G.48) is in $B < 5$ T. We then demonstrate the numerical results of the normalized photocurrent for $p=0$ in the region $B<5$ T in Fig. G.1. We here used the rest mass of electron $m_e = 9.11\times10^{-31}$ kg, elementary charge $e = 1.60\times10^{-19}$ C, light speed $c = 3.00\times10^{8}$ m/s, and numerical aperture $NA = 0.61$.

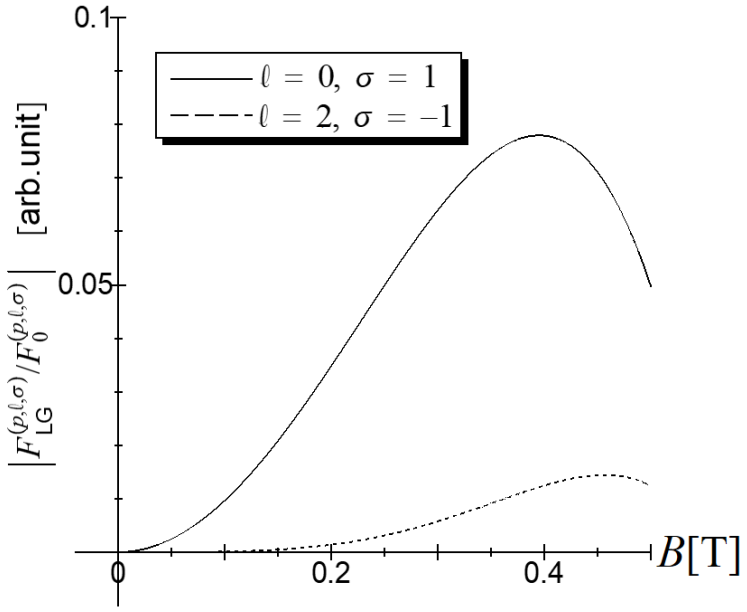

Figure G.1: B-dependence of the amplitude of $F_{\mathrm{LG}}^{(p,\ell,\sigma)}(B)$ for $p=0$. We used the rest mass of electron $m_e = 9.11\times10^{-31}$ kg, elementary charge $e = 1.60\times10^{-19}$ C, light speed $c = 3.00\times10^{8}$ m/s, and numerical aperture $NA = 0.61$. The wavenumber and beam waist also have B-dependence as $k_c \sim 5.85\times10^{2}B$ m^{-1} and $w_0 \sim 5.60\times10^{-3}B^{-1}$ m, respectively.

On the other hand, the expansion with respect to ξ for the amplitudes except for $p=0$ is worth to see that the first vanishing point resulted from the coincidence of the dark rings of LG-mode profile with the electron system edge, and that how much magnitude the amplitudes in the region between 0T and the first zero point is. As is the case with $p=0$, the physical part of B-dependence of the induced photocurrent $\delta j_{+}^{(p,\ell,\sigma)}(\omega,B)$ for LG-mode OV

with $p = 1$, $\ell = 0$, $\sigma = 1$, and $\omega = \omega_c$, is given as

$$\begin{aligned} F_{\rm LG}^{(1,0,1)}(B) &= \frac{\sqrt{2}C_{1,0}e^4R^2d\ NA}{4Vm_e^2c\hbar}B^2\left(1-\frac{3}{4}R^2\ NA^2\frac{e^2}{m_e^2c^2}B^2\right) \\ &= F_0^{(1,0,1)}B^2\left(1-\frac{3}{4}R^2\ NA^2\frac{e^2}{m_e^2c^2}B^2\right), \end{aligned} \tag{G.49}$$

which gives the zero point at $B = 0.322$ T. The physical part of B dependence of the induced photocurrent with $p = 1$, $\ell = 2$, $\sigma = -1$, and $\omega = \omega_c$, is also given as

$$\begin{aligned} F_{\rm LG}^{(1,2,-1)}(B) &= -\frac{C_{1,2}e^6R^4d\ NA^3}{8\sqrt{2}Vm_e^4c^3\hbar}B^4\left(3-\frac{5}{4}R^2\ NA^2\frac{e^2}{m_e^2c^2}B^2\right) \\ &= F_0^{(1,2,-1)}B^4\left(3-\frac{5}{4}R^2\ NA^2\frac{e^2}{m_e^2c^2}B^2\right), \end{aligned} \tag{G.50}$$

which gives the zero point at $B = 0.433$ T. We then demonstrate these numerical results of the normalized photocurrent for $p = 1$ in the region $B < 4.5$ T in Fig. G.2.

Furthermore, the physical part of B dependence of the induced photocurrent $\delta j_+^{(p,\ell,\sigma)}(\omega, B)$ for LG-mode OV with $p = 2$, $\ell = 0$, $\sigma = 1$, and $\omega = \omega_c$, is obtained as

$$\begin{aligned} F_{\rm LG}^{(2,0,1)}(B) &= \frac{\sqrt{2}C_{2,0}e^4R^2d\ NA}{4Vm_e^2c\hbar}B^2\left(1-\frac{5}{4}R^2\ NA^2\frac{e^2}{m_e^2c^2}B^2\right) \\ &= F_0^{(2,0,1)}B^2\left(1-\frac{5}{4}R^2\ NA^2\frac{e^2}{m_e^2c^2}B^2\right), \end{aligned} \tag{G.51}$$

which gives the zero point at $B = 0.250$ T. For that with $p = 2$, $\ell = 2$, $\sigma = -1$, and $\omega = \omega_c$, we obtain

$$\begin{aligned} F_{\rm LG}^{(2,2,-1)}(B) &= -\frac{\sqrt{2}C_{2,2}e^6R^4d\ NA^3}{8Vw_0^3m_e^4c^3\hbar}B^4\left(3-\frac{7}{4}R^2\ NA^2\frac{e^2}{m_e^2c^2}B^2\right) \\ &= F_0^{(2,2,-1)}B^4\left(3-\frac{7}{4}R^2\ NA^2\frac{e^2}{m_e^2c^2}B^2\right), \end{aligned} \tag{G.52}$$

which gives the zero point at $B = 0.366$ T. We then demonstrate these numerical results of the normalized photocurrent for $p = 2$ in the region $B < 4.5$ T in Fig. G.3.

From Figs. G.2 - G.3, we find that, for each p, the first vanishing point of $\ell = 0$ is smaller than that of $\ell = 2$. This tendency can be seen in Bessel-mode case as shown in 4.6.

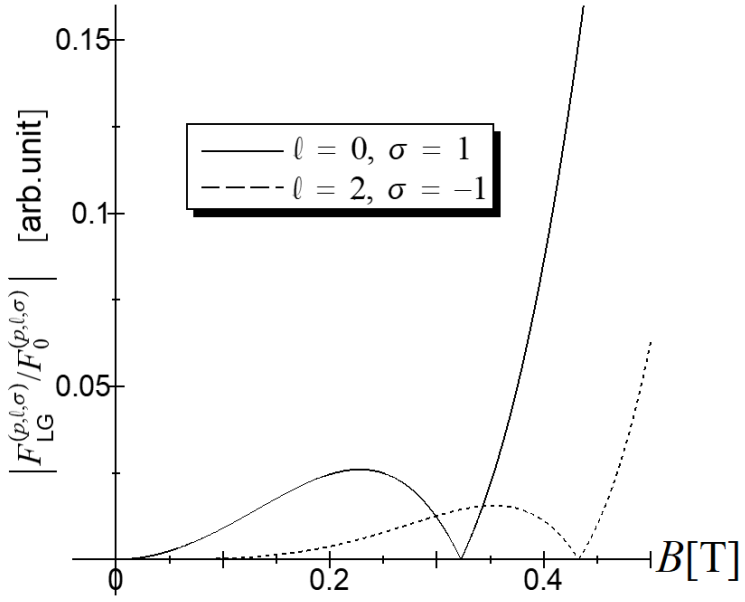

Figure G.2: B-dependence of the amplitude of $F_{\mathrm{LG}}^{(p,\ell,\sigma)}(B)$ for $p = 1$. We used the rest mass of electron $m_e = 9.11 \times 10^{-31}$ kg, elementary charge $e = 1.60 \times 10^{-19}$ C, light speed $c = 3.00 \times 10^{8}$ m/s, and numerical aperture $NA = 0.61$. The wavenumber and beam waist also have B-dependence as $k_c \sim 5.85 \times 10^{2} B$ m^{-1} and $w_0 \sim 5.60 \times 10^{-3} B^{-1}$ m, respectively.

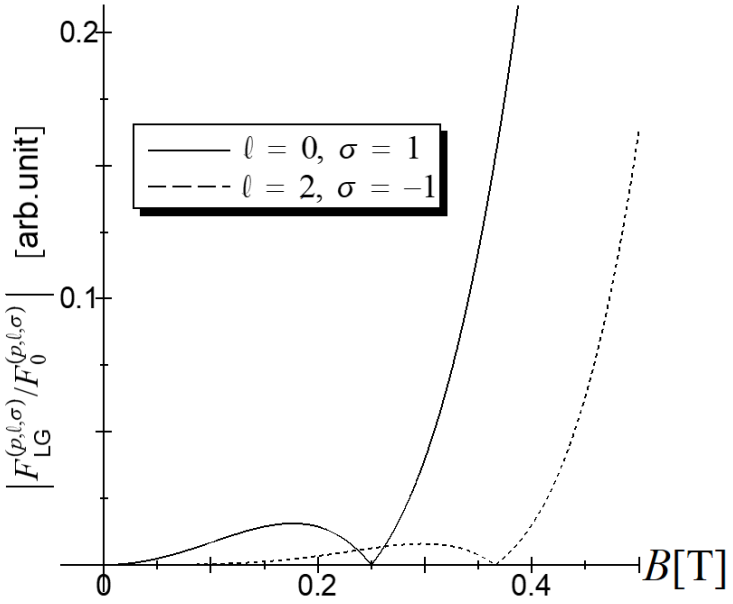

Figure G.3: B-dependence of the amplitude of $F_{\mathrm{LG}}^{(p,\ell,\sigma)}(B)$ for $p = 2$. We used the rest mass of electron $m_e = 9.11 \times 10^{-31}$ kg, elementary charge $e = 1.60 \times 10^{-19}$ C, light speed $c = 3.00 \times 10^8$ m/s, and numerical aperture $NA = 0.61$. The wavenumber and beam waist also have B-dependence as $k_c \sim 5.85 \times 10^2 B$ m^{-1} and $w_0 \sim 5.60 \times 10^{-3} B^{-1}$ m, respectively.

Appendix H

Multipolar Transitions by OV

H.1 Multipolar Transition Hamiltonian

We now generalize our theory discussed within an electric dipole transition to within multipolar transitions. In the main body, we have worked in the cylindrical coordinates, which manifest the symmetry of the optical vortex (OV). However, our final results, of course, are not specific to a particular coordinate system. We can alternatively consider the spherical coordinates and examine the multipole expansion by the vector spherical harmonics (VSH)[74, 75] of current operators in Eq. (4.7). We will then obtain the general expression of the interaction Hamiltonian by using VSH. We will also show that the selection rules for the dipole transitions are consistent with the results obtained without multipole expansion in Eq. (4.22).

First, we give the definition of the VSH as the followings,

$$\begin{aligned}
\mathbf{Y}_{\ell m}(\theta,\phi) &= Y_{\ell m}(\theta,\phi)\,\hat{\mathbf{e}}_r, \\
\mathbf{\Psi}_{\ell m}(\theta,\phi) &= r\boldsymbol{\nabla} Y_{\ell m}(\theta,\phi), \\
\mathbf{\Phi}_{\ell m}(\theta,\phi) &= \mathbf{r}\times\boldsymbol{\nabla} Y_{\ell m}(\theta,\phi),
\end{aligned} \tag{H.1}$$

with a spherical harmonics

$$Y_{\ell m}(\theta,\phi) = (-1)^m \sqrt{\frac{2\ell+1}{4\pi}\frac{(\ell-m)!}{(\ell+m)!}} P_\ell^m(\cos\theta)\,\mathrm{e}^{im\phi}, \tag{H.2}$$

where $P_\ell^m(\cos\theta)$ is an associated Legendre polynomial. We here introduce spherical coordinates (r,θ,ϕ) taken as Fig. 4.1. Then the current can gener-

ally be expanded by VSH as

$$\mathbf{j}(\mathbf{r}) = \sum_{\ell=0}^{\infty} \sum_{m=-\ell}^{\ell} \Big[j_{\ell m}^{(r)}(r)\, \mathbf{Y}_{\ell m}(\theta,\phi) + j_{\ell m}^{(1)}(r)\, \mathbf{\Psi}_{\ell m}(\theta,\phi) + j_{\ell m}^{(2)}(r)\, \mathbf{\Phi}_{\ell m}(\theta,\phi) \Big], \tag{H.3}$$

where we introduced the multipole coefficients $j_{\ell m}^{(r)}(r)$, $j_{\ell m}^{(1)}(r)$, and $j_{\ell m}^{(2)}(r)$, which are defined by[74]

$$\begin{aligned} j_{\ell m}^{(r)}(r) &= \int \mathbf{j}(\mathbf{r}) \cdot \mathbf{Y}_{lm}(\theta,\phi)^*\, d\Omega, \\ j_{\ell m}^{(1)}(r) &= \frac{1}{l(l+1)} \int \mathbf{j}(\mathbf{r}) \cdot \mathbf{\Psi}_{lm}(\theta,\phi)^*\, d\Omega, \\ j_{lm}^{(2)}(r) &= \frac{1}{l(l+1)} \int \mathbf{j}(\mathbf{r}) \cdot \mathbf{\Phi}_{lm}(\theta,\phi)^*\, d\Omega, \end{aligned} \tag{H.4}$$

where Ω is a solid angle.

Next, the vector potential of OV can also be expressed in terms of the spherical coordinates,

$$\mathbf{A}_{\ell,\sigma}^{\mathrm{OV}}(\mathbf{r}) = \boldsymbol{\eta}_\sigma \sqrt{\frac{k_\perp}{2\pi}} \sum_{\ell'=-\infty}^{\infty} i^{\ell'-\sigma} J_\ell(k_\perp r \sin\theta)\, J_{\ell'}(k_z r) \mathrm{e}^{i\ell\phi} \mathrm{e}^{i\ell'\theta}, \tag{H.5}$$

where the polarization vector is expressed in the spherical coordinates,

$$\boldsymbol{\eta}_\sigma = -\sigma \frac{\sin\theta}{\sqrt{2}} \mathrm{e}^{i\sigma\phi} \hat{\mathbf{e}}_r - \sigma \frac{\cos\theta}{\sqrt{2}} \mathrm{e}^{i\sigma\phi} \hat{\mathbf{e}}_\theta - \frac{i}{\sqrt{2}} \mathrm{e}^{i\sigma\phi} \hat{\mathbf{e}}_\phi \quad \text{for } \sigma = \pm 1. \tag{H.6}$$

and we applied Jacobi-Anger expansion (a plane wave expansion)

$$\mathrm{e}^{ik_z r\cos\theta} = \sum_{\ell=-\infty}^{\infty} i^\ell J_\ell(k_z r) \mathrm{e}^{i\ell\theta}. \tag{H.7}$$

We consider the interaction of the current with the OV as a minimal coupling.

The Hamiltonian is given by

$$
\begin{aligned}
H_{\mathrm{int}} &= -\int \mathbf{j}\left(\mathbf{r}\right)\cdot\mathbf{A}_{\ell,\sigma}^{\mathrm{OV}}\left(\mathbf{r}\right)d^{3}\mathbf{r}\\
&= k_{\perp}^{1/2}\sum_{\ell'=-\infty}^{\infty}\sum_{\ell''=0}^{\infty}\sum_{m''=-\ell''}^{\ell''}\delta_{m'',-(\ell+\sigma)}i^{\ell'-\sigma}\left(-1\right)^{m''}\\
&\times\sqrt{\frac{2\ell''+1}{4}\frac{(\ell''-m'')!}{(\ell''+m'')!}}\int drd\theta\ r^{2}J_{\ell'}(k_{z}r)J_{\ell}\left(k_{\perp}r\sin\theta\right)\mathrm{e}^{i\ell'\theta}\\
&\times\Bigg[\sigma j_{\ell''m''}^{(r)}\left(r\right)\sin^{2}\theta P_{\ell''}^{m''}\left(\cos\theta\right)+\sigma j_{\ell''m''}^{(1)}\left(r\right)\cos\theta\sin\theta\frac{\partial P_{\ell''}^{m''}\left(\cos\theta\right)}{\partial\theta}\\
&\quad-m''j_{\ell''m''}^{(1)}\left(r\right)P_{\ell''}^{m''}\left(\cos\theta\right)-i\sigma m''j_{\ell''m''}^{(2)}\left(r\right)\cos\theta P_{\ell''}^{m''}\left(\cos\theta\right)\\
&\quad+ij_{\ell''m''}^{(2)}\left(r\right)\sin\theta\frac{\partial P_{\ell''}^{m''}\left(\cos\theta\right)}{\partial\theta}\Bigg].
\end{aligned}
\tag{H.8}
$$

We here note that the angular momentum conservation $\delta_{m'',-(\ell+\sigma)}$ is provided by integral with respect to the azimuthal angle ϕ. This expression is important to obtain the selection rules via symmetry information of currents in matter.

H.2 Consistency with our results

By applying the expression (H.8) to our model, we will show the consistency with our results. Before this, we try to obtain the general expressions for the dipole transitions, that is, we consider the dipole component of $\mathbf{j}\left(\mathbf{r}\right)$, which carries the azimuthal quantum number $\ell''=1$ in Eq. (H.8).

The radial profile of optical vortex is described by the Bessel function, which depends on the polar angle θ as shown in Eq. (H.5). To perform the integral with respect to θ, we now assume that the current interacts with OV near the optical axis, that is, $k_{\perp}r\sin\theta\ll1$. Then we can approximate the Bessel function as $J_{\ell}\left(k_{\perp}r\sin\theta\right)\sim\left(k_{\perp}r\sin\theta/2\right)^{\ell}/\ell!$. In addition, we note $J_{-\ell}\left(k_{\perp}r\sin\theta\right)=\left(-1\right)^{\ell}J_{\ell}\left(k_{\perp}r\sin\theta\right)$. After some calculations, we then arrive

at six types of allowed transitions,

$$\begin{aligned} H^{\rm dip}_{{\rm int}(\ell=0,\sigma=1)} &= -ik_\perp^{1/2}\frac{\sqrt{6}}{3}\int r^2\mathcal{Q}^{(0)}_{1,-1}(r)\,J_0(k_z r)dr \\ &\quad - ik_\perp^{1/2}\sum_{n=1}^{\infty}\frac{(-1)^n\,6\sqrt{6}}{\mathcal{N}_2(n)}\int r^2\mathcal{Q}^{(n)}_{1,-1}(r)\,J_{2n}(k_z r)dr \\ &\quad - ik_\perp^{1/2}\sum_{n=0}^{\infty}\frac{(-1)^n\,2\sqrt{6}}{\mathcal{N}_1(n)}\int r^2 j^{(2)}_{1,-1}(r)\,J_{2n+1}(k_z r)dr, \end{aligned} \tag{H.9}$$

$$\begin{aligned} H^{\rm dip}_{{\rm int}(\ell=2,\sigma=-1)} &= -ik_\perp^{5/2}\frac{\sqrt{6}}{30}\int r^4\mathcal{P}_{1,-1}(r)\,J_0(k_z r)dr \\ &\quad + ik_\perp^{5/2}\sum_{n=1}^{\infty}\frac{(-1)^n\,15\sqrt{6}}{\mathcal{N}_4(n)}\int r^4\mathcal{P}_{1,-1}(r)\,J_{2n}(k_z r)dr, \end{aligned} \tag{H.10}$$

$$\begin{aligned} H^{\rm dip}_{{\rm int}(\ell=-1,\sigma=1)} &= -k_\perp^{3/2}\sum_{n=0}^{\infty}\frac{(-1)^n\,6\sqrt{3}}{\mathcal{N}_3(n)}\int r^3\mathcal{P}_{1,0}(r)\,J_{2n+1}(k_z r)dr \\ &\quad + k_\perp^{3/2}\frac{\sqrt{3}}{3}\int r^3 j^{(2)}_{1,0}(r)\,J_0(k_z r)dr \\ &\quad + k_\perp^{3/2}\sum_{n=1}^{\infty}\frac{(-1)^n\,6\sqrt{3}}{\mathcal{N}_2(n)}\int r^3 j^{(2)}_{1,0}(r)\,J_{2n}(k_z r)dr, \end{aligned} \tag{H.11}$$

$$\begin{aligned} H^{\rm dip}_{{\rm int}(\ell=1,\sigma=-1)} &= k_\perp^{3/2}\sum_{n=0}^{\infty}\frac{(-1)^n\,6\sqrt{3}}{\mathcal{N}_3(n)}\int r^3\mathcal{P}_{1,0}(r)\,J_{2n+1}(k_z r)dr \\ &\quad + k_\perp^{3/2}\frac{\sqrt{3}}{3}\int r^3 j^{(2)}_{1,0}(r)\,J_0(k_z r)dr \\ &\quad + k_\perp^{3/2}\sum_{n=1}^{\infty}\frac{(-1)^n\,6\sqrt{3}}{\mathcal{N}_2(n)}\int r^3 j^{(2)}_{1,0}(r)\,J_{2n}(k_z r)dr, \end{aligned} \tag{H.12}$$

$$\begin{aligned} H^{\rm dip}_{{\rm int}(\ell=-2,\sigma=1)} &= ik_\perp^{5/2}\frac{\sqrt{6}}{30}\int r^4\mathcal{P}_{1,1}(r)\,J_0(k_z r)dr \\ &\quad - ik_\perp^{5/2}\sum_{n=1}^{\infty}\frac{(-1)^n\,15\sqrt{6}}{\mathcal{N}_4(n)}\int r^4\mathcal{P}_{1,1}(r)\,J_{2n}(k_z r)dr, \end{aligned} \tag{H.13}$$

$$
\begin{aligned}
H^{\mathrm{dip}}_{\mathrm{int}(\ell=0,\sigma=-1)} &= ik_{\perp}^{1/2}\frac{\sqrt{6}}{3}\int r^2\mathcal{Q}^{(0)}_{1,1}(r)\,J_0(k_z r)dr \\
&+ ik_{\perp}^{1/2}\sum_{n=1}^{\infty}\frac{(-1)^n\,6\sqrt{6}}{\mathcal{N}_2(n)}\int r^2\mathcal{Q}^{(n)}_{1,1}(r)\,J_{2n}(k_z r)dr \\
&- ik_{\perp}^{1/2}\sum_{n=0}^{\infty}\frac{(-1)^n\,2\sqrt{6}}{\mathcal{N}_1(n)}\int r^2 j^{(2)}_{1,1}(r)\,J_{2n+1}(k_z r)dr, \qquad \text{(H.14)}
\end{aligned}
$$

where we denoted the combinations of the multipole coefficients as

$$
\begin{aligned}
\mathcal{P}_{\ell m}(r) &= j^{(r)}_{\ell m}(r) - j^{(1)}_{\ell m}(r), \\
\mathcal{Q}^{(n)}_{\ell m}(r) &= j^{(r)}_{\ell m}(r) - \frac{2}{3}\left(2n^2-3\right) j^{(1)}_{\ell m}(r), \qquad \text{(H.15)}
\end{aligned}
$$

and the integer factors as

$$
\begin{aligned}
\mathcal{N}_1(n) &= (2n-1)(2n+3), \\
\mathcal{N}_2(n) &= (2n-3)(2n-1)(2n+1)(2n+3), \\
\mathcal{N}_3(n) &= (2n-3)(2n-1)(2n+3)(2n+5), \\
\mathcal{N}_4(n) &= (2n-5)(2n-3)(2n-1)(2n+1)(2n+3)(2n+5). \qquad \text{(H.16)}
\end{aligned}
$$

We summarize the allowed absorptions as the followings,

$$
(J,\ell,\sigma) = \left\{ \begin{array}{c} (1,0,1) \\ (1,2,-1) \\ (0,-1,1) \\ (0,1,-1) \\ (-1,-2,1) \\ (-1,0,-1) \end{array} \right. . \qquad \text{(H.17)}
$$

In other words, the absorptions in the dipole transition are allowed in case of the optical TAM, $J = 1$, 0, and -1.

Finally, to apply our model, we need to impose further conditions to the current $\mathbf{j}(\mathbf{r})$. The first is that we have considered the current which increases z-component of the electron angular momentum by one, $j_+ = (j_x - ij_y)/\sqrt{2} \propto \mathrm{e}^{-i\phi}$. The reason is because such a current is described by + component of the chiral basis (see Appendix B). The second is that the 2DEG have distributed on the surface $\theta = \pi/2$. Thus, we can guess the form of the current distribution of j_+ as

$$
\mathbf{j}(\mathbf{r}) = j_\phi(r)\,\delta(\cos\theta)\,\mathrm{e}^{-i\phi}\hat{\mathbf{e}}_\phi. \qquad \text{(H.18)}
$$

Then, by using Eq. (H.4), we obtain the multipole coefficients as

$$j_{\ell m}^{(r)}(r) = 0, \tag{H.19}$$

$$\begin{aligned} j_{\ell m}^{(1)}(r) &= \frac{1}{\ell(\ell+1)} \int j_\phi(r)\, \delta(\cos\theta)\, \mathrm{e}^{-i\phi} \frac{1}{\sin\theta} \frac{\partial Y_{\ell m}(\theta,\phi)}{\partial \phi} d\Omega \\ &= \frac{-im}{\ell(\ell+1)} \sqrt{\frac{2\ell+1}{4\pi} \frac{(\ell-m)!}{(\ell+m)!}} j_\phi(r) \\ &\times \int_{-1}^{1} \delta(\cos\theta) \frac{P_\ell^m(\cos\theta)}{\sin\theta} d(\cos\theta) \int_0^{2\pi} \mathrm{e}^{-i(m+1)\phi} d\phi \\ &= 2\pi i \sqrt{\frac{2\ell+1}{4\pi\ell(\ell+1)}} P_\ell^{-1}(0)\, j_\phi(r)\, \delta_{m,-1}, \end{aligned} \tag{H.20}$$

$$\begin{aligned} j_{\ell m}^{(2)}(r) &= \frac{1}{\ell(\ell+1)} \int j_\phi(r)\, \delta(\cos\theta)\, \mathrm{e}^{-i\phi} \frac{\partial Y_{\ell m}(\theta,\phi)}{\partial \theta} d\Omega \\ &= \frac{1}{\ell(\ell+1)} \sqrt{\frac{2\ell+1}{4\pi} \frac{(\ell-m)!}{(\ell+m)!}} j_\phi(r) \\ &\times \int_{-1}^{1} \frac{\partial P_\ell^m(\cos\theta)}{\partial \theta} \delta(\cos\theta)\, d(\cos\theta) \int_0^{2\pi} \mathrm{e}^{-i(m+1)\phi} d\phi \\ &= 2\pi \sqrt{\frac{2\ell+1}{4\pi\ell(\ell+1)}} j_\phi(r) \frac{d}{d\theta} P_\ell^{-1}(\cos\theta)\,|_{\theta=\pi/2} \delta_{m,-1}. \end{aligned} \tag{H.21}$$

In particular, when we confine the case of the dipole transition $\ell = 1$, we obtain

$$\begin{aligned} J_{1,-1}^{(r)}(r) &= 0, \\ J_{1,-1}^{(1)}(r) &= i\sqrt{\frac{3\pi}{8}} j_\phi(r), \\ J_{1.-1}^{(2)}(r) &= 0, \end{aligned} \tag{H.22}$$

which give the two types of allowed transitions from the Hamiltonian (H.9)-

(H.14) as

$$H^{\rm dip}_{{\rm int}(l=0,\sigma=1)} = \sqrt{\pi k_\perp}\int r^2 j_\phi\left(r\right) J_0(k_z r)dr$$
$$-6\sqrt{\pi k_\perp}\sum_{n=1}^{\infty}\frac{(-1)^n\left(2n^2-3\right)}{\mathcal{N}_3\left(n\right)}\int r^2 j_\phi\left(r\right) J_{2n}(k_z r)dr, \tag{H.23}$$

$$H^{\rm dip}_{{\rm int}(l=2,\sigma=-1)} = -\frac{\sqrt{\pi k_\perp^5}}{20}\int r^4 j_\phi\left(r\right) J_0(k_z r)dr$$
$$+\frac{45}{2}\sqrt{\pi k_\perp^5}\sum_{n=1}^{\infty}\frac{(-1)^n}{\mathcal{N}_4\left(n\right)}\int r^4 j_\phi\left(r\right) J_{2n}(k_z r)dr, \tag{H.24}$$

$$H^{\rm dip}_{{\rm int}(l=-2,\sigma=1)} = H^{\rm dip}_{{\rm int}(l=-1,\sigma=1)} = H^{\rm dip}_{{\rm int}(l=0,\sigma=-1)} = H^{\rm dip}_{{\rm int}(l=1,\sigma=-1)} = 0, \tag{H.25}$$

which leads to Eq. (4.22) by seeing the non-zero Hamiltonians, that is,

$$(J,\ell,\sigma) = \left\{ \begin{array}{c} (1,0,1) \\ (1,2,-1) \end{array} \right. . \tag{H.26}$$

Therefore, we proved the consistency with the results without VSH.

In this Appendix, since we have obtained the general expression of the multipolar expanded Hamiltonian of the interaction with optical vertex, we can generalize the spectroscopic selection rules beyond the dipole transition. This is our future work.

Appendix I

Vector Spherical Harmonics

We briefly summarize the definition and the properties of the vector spherical harmonics (VSH).

Definition

We here use the definition by Barrera *et al.*[74],

$$\begin{aligned} \boldsymbol{Y}_{\ell m}(\theta,\phi) &= Y_{\ell m}(\theta,\phi)\,\hat{\mathbf{e}}_r, \\ \boldsymbol{\Psi}_{\ell m}(\theta,\phi) &= r\boldsymbol{\nabla}Y_{\ell m}(\theta,\phi), \\ \boldsymbol{\Phi}_{\ell m}(\theta,\phi) &= \boldsymbol{r}\times\boldsymbol{\nabla}Y_{\ell m}(\theta,\phi), \end{aligned} \tag{I.1}$$

with $\boldsymbol{r} = r\hat{\mathbf{e}}_r$.

Symmetric Property

Symmetric property of VSH with respect to m is given by

$$\begin{aligned} \boldsymbol{Y}_{\ell,-m}(\theta,\phi) &= (-1)^m\,\boldsymbol{Y}^*_{\ell m}(\theta,\phi), \\ \boldsymbol{\Psi}_{\ell,-m}(\theta,\phi) &= (-1)^m\,\boldsymbol{\Psi}^*_{\ell m}(\theta,\phi), \\ \boldsymbol{\Phi}_{\ell,-m}(\theta,\phi) &= (-1)^m\,\boldsymbol{\Phi}^*_{\ell m}(\theta,\phi). \end{aligned} \tag{I.2}$$

Orthogonality

VSH are orthogonal each other,

$$\begin{aligned} \boldsymbol{Y}_{\ell m}(\theta,\phi)\cdot\boldsymbol{\Psi}_{\ell m}(\theta,\phi) &= 0, \\ \boldsymbol{Y}_{\ell m}(\theta,\phi)\cdot\boldsymbol{\Phi}_{\ell m}(\theta,\phi) &= 0, \\ \boldsymbol{\Psi}_{\ell m}(\theta,\phi)\cdot\boldsymbol{\Phi}_{\ell m}(\theta,\phi) &= 0, \end{aligned} \tag{I.3}$$

in addition,

$$\begin{aligned}\boldsymbol{Y}_{\ell m}(\theta,\phi)\cdot\boldsymbol{\Psi}_{\ell' m'}(\theta,\phi)&=0,\\ \boldsymbol{Y}_{\ell m}(\theta,\phi)\cdot\boldsymbol{\Phi}_{\ell' m'}(\theta,\phi)&=0.\end{aligned}\tag{I.4}$$

We also give the orthogonality in Hilbert space as the followings,

$$\begin{aligned}&\int \boldsymbol{Y}^{*}_{\ell' m'}(\theta,\phi)\cdot\boldsymbol{Y}_{\ell m}(\theta,\phi)\,d\Omega=\delta_{\ell\ell'}\delta_{mm'},\\ &\int \boldsymbol{\Psi}^{*}_{\ell' m'}(\theta,\phi)\cdot\boldsymbol{\Psi}_{\ell m}(\theta,\phi)\,d\Omega=\ell(\ell+1)\,\delta_{\ell\ell'}\delta_{mm'},\\ &\int \boldsymbol{\Phi}^{*}_{\ell' m'}(\theta,\phi)\cdot\boldsymbol{\Phi}_{\ell m}(\theta,\phi)\,d\Omega=\ell(\ell+1)\,\delta_{\ell\ell'}\delta_{mm'},\\ &\int \boldsymbol{Y}^{*}_{\ell' m'}(\theta,\phi)\cdot\boldsymbol{\Psi}_{\ell m}(\theta,\phi)\,d\Omega=0,\\ &\int \boldsymbol{Y}^{*}_{\ell' m'}(\theta,\phi)\cdot\boldsymbol{\Phi}_{\ell m}(\theta,\phi)\,d\Omega=0,\\ &\int \boldsymbol{\Psi}^{*}_{\ell' m'}(\theta,\phi)\cdot\boldsymbol{\Phi}_{\ell m}(\theta,\phi)\,d\Omega=0.\end{aligned}\tag{I.5}$$

Divergence of VSH

By introducing the arbitrary radial function $f(r)$, the divergences of VSH are given by

$$\begin{aligned}\boldsymbol{\nabla}\cdot(f(r)\,\boldsymbol{Y}_{\ell m}(\theta,\phi))&=\left(\frac{df(r)}{dr}+\frac{2}{r}f(r)\right)Y_{\ell m}(\theta,\phi),\\ \boldsymbol{\nabla}\cdot(f(r)\,\boldsymbol{\Psi}_{\ell m}(\theta,\phi))&=-\frac{\ell(\ell+1)}{r}f(r)\,Y_{\ell m}(\theta,\phi),\\ \boldsymbol{\nabla}\cdot(f(r)\,\boldsymbol{\Phi}_{\ell m}(\theta,\phi))&=0.\end{aligned}\tag{I.6}$$

Rotation of VSH

Similarly to the divergence, the rotations of VSH are given by

$$\begin{aligned}\boldsymbol{\nabla}\times(f(r)\,\boldsymbol{Y}_{\ell m}(\theta,\phi))&=-\frac{f(r)}{r}\boldsymbol{\Phi}_{\ell m}(\theta,\phi),\\ \boldsymbol{\nabla}\times(f(r)\,\boldsymbol{\Psi}_{\ell m}(\theta,\phi))&=\left(\frac{df(r)}{dr}+\frac{f(r)}{r}\right)\boldsymbol{\Phi}_{\ell m}(\theta,\phi),\\ \boldsymbol{\nabla}\times(f(r)\,\boldsymbol{\Phi}_{\ell m}(\theta,\phi))&=\\ &-\frac{\ell(\ell+1)}{r}f(r)\,\boldsymbol{Y}_{\ell m}(\theta,\phi)-\left(\frac{df(r)}{dr}+\frac{f(r)}{r}\right)\boldsymbol{\Psi}_{\ell m}(\theta,\phi).\end{aligned}\tag{I.7}$$

Laplacian of VSH

Because the gradient of the (scalar) spherical harmonics $Y_{\ell m}(\theta,\phi)$ leads to

$$\boldsymbol{\nabla}\left(f(r)\,Y_{\ell m}(\theta,\phi)\right)=\left(\frac{df(r)}{dr}\right)\boldsymbol{Y}_{\ell m}(\theta,\phi)+\frac{f(r)}{r}\boldsymbol{\Psi}_{\ell m}(\theta,\phi), \tag{I.8}$$

the Laplacian of the scalar spherical harmonics is expressed as

$$\Delta\left(f(r)\,Y_{\ell m}(\theta,\phi)\right)=\left[\frac{1}{r}\frac{d^2}{dr^2}\left(rf(r)\right)-\frac{\ell(\ell+1)}{r^2}f(r)\right]Y_{\ell m}(\theta,\phi). \tag{I.9}$$

By using this, when we collectively denote all three types of VSH as $\boldsymbol{Z}_{\ell m}$, we can see that the Laplacian of VSH is as follows,

$$\Delta\left(f(r)\,\boldsymbol{Z}_{\ell m}(\theta,\phi)\right)=\left[\frac{1}{r^2}\frac{\partial}{\partial r}\left(r^2\frac{\partial f(r)}{\partial r}\right)\right]\boldsymbol{Z}_{\ell m}(\theta,\phi)+f(r)\,\Delta\boldsymbol{Z}_{\ell m}(\theta,\phi). \tag{I.10}$$

In particular, the explicit expressions of $\Delta\boldsymbol{Z}_{lm}$ are as follows,

$$\begin{aligned}
\Delta\boldsymbol{Y}_{\ell m}(\theta,\phi)&=-\frac{1}{r^2}\left\{2+\ell(\ell+1)\right\}\boldsymbol{Y}_{\ell m}(\theta,\phi)+\frac{2}{r^2}\boldsymbol{\Psi}_{\ell m}(\theta,\phi),\\
\Delta\boldsymbol{\Psi}_{\ell m}(\theta,\phi)&=\frac{2}{r^2}\ell(\ell+1)\,\boldsymbol{Y}_{\ell m}(\theta,\phi)-\frac{1}{r^2}\ell(\ell+1)\,\boldsymbol{\Psi}_{\ell m}(\theta,\phi),\\
\Delta\boldsymbol{\Phi}_{\ell m}(\theta,\phi)&=-\frac{1}{r^2}\ell(\ell+1)\,\boldsymbol{\Phi}_{\ell m}(\theta,\phi).
\end{aligned} \tag{I.11}$$

Bibliography

[1] J. H. Poynting. The wave motion of a revolving shaft, and a suggestion as to the angular momentum in a beam of circularly polarised light. *Proceedings of the Royal Society of London. Series A, Containing Papers of a Mathematical and Physical Character*, 82(557):560–567, 1909.

[2] R. A. Beth. Direct detection of the angular momentum of light. *Physical Review*, 48:471–471, Sep 1935.

[3] R. A. Beth. Mechanical detection and measurement of the angular momentum of light. *Physical Review*, 50:115–125, Jul 1936.

[4] L. Allen, M. W. Beijersbergen, R. J. C. Spreeuw, and J. P. Woerdman. Orbital angular momentum of light and the transformation of laguerre-gaussian laser modes. *Physical Review A*, 45:8185–8189, Jun 1992.

[5] A. Mair, A. Vaziri, G. Weihs, and A. Zeilinger. Entanglement of the orbital angular momentum states of photons. *Nature*, 412(6844):313–316, 2001.

[6] J. Durnin. Exact solutions for nondiffracting beams. i. the scalar theory. *Journal of the Optical Society of America A*, 4(4):651–654, Apr 1987.

[7] D. L. Andrews, editor. *Structured Light and Its Applications*. Academic Press, Burlington, 2008.

[8] D. L. Andrews and M. Babiker, editors. *The Angular Momentum of Light*. Cambridge University Press, 2012.

[9] S. Franke-Arnold. Optical angular momentum and atoms. *Philosophical Transactions of the Royal Society A: Mathematical, Physical and Engineering Sciences*, 375(2087):20150435, 2017.

[10] S. M. Barnett, M. Babiker, and M. J. Padgett. Optical orbital angular momentum. *Philosophical Transactions of the Royal Society A: Mathematical, Physical and Engineering Sciences*, 375(2087):20150444, 2017.

[11] J. Durnin, J. J. Miceli, and J. H. Eberly. Diffraction-free beams. *Physical Review Letters*, 58:1499–1501, Apr 1987.

[12] G. Indebetouw. Nondiffracting optical fields: some remarks on their analysis and synthesis. *Journal of the Optical Society of America A*, 6(1):150–152, Jan 1989.

[13] A. Vasara, J. Turunen, and A. T. Friberg. Realization of general nondiffracting beams with computer-generated holograms. *Journal of the Optical Society of America A*, 6(11):1748–1754, Nov 1989.

[14] A. J. Cox and D. C. Dibble. Nondiffracting beam from a spatially filtered fabry–perot resonator. *Journal of the Optical Society of America A*, 9(2):282–286, Feb 1992.

[15] C. Paterson and R. Smith. Higher-order bessel waves produced by axicon-type computer-generated holograms. *Optics Communications*, 124(1):121 – 130, 1996.

[16] J. Arlt and K. Dholakia. Generation of high-order bessel beams by use of an axicon. *Optics Communications*, 177(1):297 – 301, 2000.

[17] N. E. Andreev, S. S. Bychkov, V. V. Kotlyar, L. Ya. Margolin, Lev. N. Pyatnitskii, and P. G. Serafimovich. Formation of high-power hollow bessel light beams. *Quantum Electronics*, 26(2):126–130, Feb 1996.

[18] T.A. King, W. Hogervorst, N.S. Kazak, N.A. Khilo, and A.A. Ryzhevich. Formation of higher-order bessel light beams in biaxial crystals. *Optics Communications*, 187(4):407 – 414, 2001.

[19] B. Amos and P. Gill. Optical tweezers. *Measurement Science and Technology*, 6(2):248, Feb 1995.

[20] H. He, M. E. J. Friese, N. R. Heckenberg, and H. Rubinsztein-Dunlop. Direct observation of transfer of angular momentum to absorptive particles from a laser beam with a phase singularity. *Physical Review Letters*, 75:826–829, Jul 1995.

[21] M. E. J. Friese, J. Enger, H. Rubinsztein-Dunlop, and N. R. Heckenberg. Optical angular-momentum transfer to trapped absorbing particles. *Physical Review A*, 54:1593–1596, Aug 1996.

[22] M. E. J. Friese, T. A. Nieminen, N. R. Heckenberg, and H. Rubinsztein-Dunlop. Optical alignment and spinning of laser-trapped microscopic particles. *Nature*, 394(6691):348–350, 1998.

[23] J. Hamazaki, R. Morita, K. Chujo, Y. Kobayashi, S. Tanda, and T. Omatsu. Optical-vortex laser ablation. *Optics express*, 18(3):2144–2151, Feb 2010.

[24] M. F. Andersen, C. Ryu, P. Cladé, V. Natarajan, A. Vaziri, K. Helmerson, and W. D. Phillips. Quantized rotation of atoms from photons with orbital angular momentum. *Physical Review Letters*, 97:170406, Oct 2006.

[25] G. F. Quinteiro and P. I. Tamborenea. Theory of the optical absorption of light carrying orbital angular momentum by semiconductors. *EPL (Europhysics Letters)*, 85(4):47001, Feb 2009.

[26] J. Wätzel, A S. Moskalenko, and J. Berakdar. Photovoltaic effect of light carrying orbital angular momentum on a semiconducting stripe. *Optics express*, 20:27792–9, 12 2012.

[27] M. B. Farías, G. F. Quinteiro, and P. I. Tamborenea. Photoexcitation of graphene with twisted light. *The European Physical Journal B*, 86(10):432, Oct 2013.

[28] K. Sakai, K. Nomura, T. Yamamoto, and K. Sasaki. Excitation of multipole plasmons by optical vortex beams. *Scientific Reports*, 5:8431, Feb 2015.

[29] K. Shintani, K. Taguchi, Y. Tanaka, and Y. Kawaguchi. Spin and charge transport induced by a twisted light beam on the surface of a topological insulator. *Physical Review B*, 93:195415, May 2016.

[30] H. Fujita and M. Sato. Ultrafast generation of skyrmionic defects with vortex beams: Printing laser profiles on magnets. *Physical Review B*, 95:054421, Feb 2017.

[31] M. Babiker, C. R. Bennett, D. L. Andrews, and L. C. Dávila Romero. Orbital angular momentum exchange in the interaction of twisted light with molecules. *Physical Review Letters*, 89:143601, Sep 2002.

[32] S. M. Lloyd, M. Babiker, and J. Yuan. Interaction of electron vortices and optical vortices with matter and processes of orbital angular momentum exchange. *Physical Review A*, 86:023816, Aug 2012.

[33] C. T. Schmiegelow, J. Schulz, H. Kaufmann, T. Ruster, U. G. Poschinger, and F. Schmidt-Kaler. Transfer of optical orbital angular momentum to a bound electron. *Nature Communications*, 7:12998, Oct 2016.

[34] A. Afanasev, C. E. Carlson, C. T. Schmiegelow, J. Schulz, F. Schmidt-Kaler, and M. Solyanik. Experimental verification of position-dependent angular-momentum selection rules for absorption of twisted light by a bound electron. *New Journal of Physics*, 20(2):023032, Feb 2018.

[35] M. Solyanik-Gorgone, A. Afanasev, C. E. Carlson, C. T. Schmiegelow, and F. Schmidt-Kaler. Excitation of e1-forbidden atomic transitions with electric, magnetic, or mixed multipolarity in light fields carrying orbital and spin angular momentum. *Journal of the Optical Society of America B*, 36(3):565–574, Mar 2019.

[36] K. Shigematsu, K. Yamane, R. Morita, and Y. Toda. Coherent dynamics of exciton orbital angular momentum transferred by optical vortex pulses. *Physical Review B*, 93:045205, Jan 2016.

[37] W. Kohn. Cyclotron resonance and de haas-van alphen oscillations of an interacting electron gas. *Physical Review*, 123:1242–1244, Aug 1961.

[38] N. Zettili. *Quantum Mechanics: Concepts and Applications*. Wiley, 2009.

[39] H. T. Takahashi, I. Proskurin, and J. Kishine. Landau level spectroscopy by optical vortex beam. *Journal of the Physical Society of Japan*, 87(11):113703, 2018.

[40] T. Thonhauser, D. Ceresoli, D. Vanderbilt, and R. Resta. Orbital magnetization in periodic insulators. *Physical Review Letters*, 95:137205, Sep 2005.

[41] T. Yoda, T. Yokoyama, and S. Murakami. Orbital edelstein effect as a condensed-matter analog of solenoids. *Nano Letters*, 18(2):916–920, 2018.

[42] O. Matula, A. G. Hayrapetyan, V. G. Serbo, A. Surzhykov, and S. Fritzsche. Atomic ionization of hydrogen-like ions by twisted photons: angular distribution of emitted electrons. *Journal of Physics B: Atomic, Molecular and Optical Physics*, 46(20):205002, Oct 2013.

[43] U. D. Jentschura and V. G. Serbo. Generation of high-energy photons with large orbital angular momentum by compton backscattering. *Physical Review Letters*, 106:013001, Jan 2011.

[44] J. E. Greivenkamp. *Field Guide to Geometrical Optics*. Field Guide Series. SPIE Press, 2004.

[45] K. v. Klitzing, G. Dorda, and M. Pepper. New method for high-accuracy determination of the fine-structure constant based on quantized hall resistance. *Physical Review Letters*, 45:494–497, Aug 1980.

[46] D. C. Tsui, H. L. Stormer, and A. C. Gossard. Two-dimensional magnetotransport in the extreme quantum limit. *Physical Review Letters*, 48:1559–1562, May 1982.

[47] L. D. Landau and L. M. Lifshitz. *Quantum Mechanics Non-Relativistic Theory*. Butterworth-Heinemann, 3rd edition, Jan 1981.

[48] C. Kittel. *Introduction to Solid State Physics*. Wiley, 8th edition, 2004.

[49] I. S. Gradshteyn and I. M. Ryzhik. *Table of integrals, series, and products*. Elsevier/Academic Press, Amsterdam, 7th edition, 2007.

[50] I. D. Vagner, V. M. Gvozdikov, and P. Wyder. Quantum mechanics of electrons in strong magnetic field. *HIT Journal of Science and Engineering A*, 3:5–55, Mar 2006.

[51] C. Cohen-Tannoudji, B. Diu, and F. Laloë. *Quantum mechanics*. Wiley, New York, NY, 1977. Trans. of : Mécanique quantique. Paris : Hermann, 1973.

[52] P. Lederer and M. O. Goerbig. Introduction to the quantum hall effects, Api 2006.

[53] C. G. Darwin. The diamagnetism of the free electron. *Mathematical Proceedings of the Cambridge Philosophical Society*, 27(1):86–90, 1931.

[54] D. Yoshioka. *The Quantum Hall Effect*. Physics and astronomy online library. Springer, 2002.

[55] H. T. Takahashi, I. Proskurin, and J. Kishine. Selection Rules for Optical Vortex Absorption by Landau-quantized Electrons. *arXiv e-prints*, page arXiv:1904.03083, Apr 2019.

[56] R. Kubo. Statistical-mechanical theory of irreversible processes. i. general theory and simple applications to magnetic and conduction problems. *Journal of the Physical Society of Japan*, 12(6):570–586, 1957.

[57] T. Ando. Theory of cyclotron resonance lineshape in a two-dimensional electron system. *Journal of the Physical Society of Japan*, 38(4):989–997, 1975.

[58] J. D. Jackson. *Classical electrodynamics*. Wiley, New York, NY, 3rd edition, 1999.

[59] H.A. Lorentz. The fundamental equations for electromagnetic phenomena in ponderable bodies deduced from the theory of electrons. *Koninklijke Nederlandse Akademie van Wetenschappen Proceedings Series B Physical Sciences*, 5:254–266, Jan 1902.

[60] H. Fujita, Y. Tada, and M. Sato. Accessing electromagnetic properties of matter with cylindrical vector beams. *New Journal of Physics*, 21(7):073010, Jul 2019.

[61] J. Turunen, A. Vasara, and A. T. Friberg. Holographic generation of diffraction-free beams. *Applied Optics*, 27(19):3959–3962, Oct 1988.

[62] R. M. Herman and T. A. Wiggins. Production and uses of diffractionless beams. *Journal of the Optical Society of America A*, 8(6):932–942, Jun 1991.

[63] D. McGloin and K. Dholakia. Bessel beams: Diffraction in a new light. *Contemporary Physics*, 46(1):15–28, 2005.

[64] M.W. Beijersbergen, R.P.C. Coerwinkel, M. Kristensen, and J.P. Woerdman. Helical-wavefront laser beams produced with a spiral phaseplate. *Optics Communications*, 112(5):321 – 327, 1994.

[65] V. Bazhenov, M. Vasnetsov, and M. Soskin. Laser beams with screw dislocations in their wavefronts. *JETP Letters*, 52:429–431, Jan 1990.

[66] N. R. Heckenberg, R. McDuff, C. P. Smith, H. Rubinsztein-Dunlop, and M. J. Wegener. Laser beams with phase singularities. *Optical and Quantum Electronics*, 24(9):S951–S962, Sep 1992.

[67] P. Phillips. *Advanced Solid State Physics*. Cambridge University Press, 2nd edition, 2012.

[68] T. Ando and Y. Uemura. Theory of quantum transport in a two-dimensional electron system under magnetic fields. i. characteristics of level broadening and transport under strong fields. *Journal of the Physical Society of Japan*, 36(4):959–967, 1974.

[69] T. Ando, A. B. Fowler, and F. Stern. Electronic properties of two-dimensional systems. *Reviews of Modern Physics*, 54:437–672, Apr 1982.

[70] W. van der Wel, E. G. Haanappel, J. E. Mooij, C. J. P. M. Harmans, J. P. André, G. Weimann, K. Ploog, C. T. Foxon, and J. J. Harris. Selection criteria for AlGaAs/GaAs heterostructures in view of their use as a quantum hall resistance standard. *Journal of Applied Physics*, 65(9):3487–3497, 1989.

[71] W. Li, D. R. Luhman, D. C. Tsui, L. N. Pfeiffer, and K. W. West. Observation of reentrant phases induced by short-range disorder in the lowest landau level of $Al_xGa_{1-x}As/Al_{0.32}Ga_{0.68}As$ heterostructures. *Physical Review Letters*, 105:076803, Aug 2010.

[72] J. J. Sakurai. *Modern quantum mechanics*. Addison-Wesley, Reading, MA, Revised edition, 1994.

[73] G. F. Quinteiro and P. I. Tamborenea. Electronic transitions in disk-shaped quantum dots induced by twisted light. *Physical Review B*, 79:155450, Apr 2009.

[74] R. G. Barrera, G. A. Estevez, and J. Giraldo. Vector spherical harmonics and their application to magnetostatics. *European Journal of Physics*, 6(4):287–294, Oct 1985.

[75] C. Cohen-Tannoudji, J. Dupont-Roc, and G. Grynberg. *Photons and Atoms: Introduction to Quantum Electrodynamics*. Wiley, 1989.